



**Silesian
University
of Technology**

DOCTORAL THESIS

Experimental and numerical study on ammonia fueled compression ignition engine

Author:

**Ebrahim NADIMI
KARAMJAVAN, MSc.**

Supervisor:

**Dr hab. inż, Grzegorz
PRZYBYŁA, prof. PŚ**

Scientific Discipline: Environmental Engineering, Mining and Energy

**Department of Thermal Technology
Faculty of Energy and Environmental Engineering**

April, 2024

Author:

Ebrahim Nadimi Karamjavan, MSc.

Silesian University of Technology

Faculty of Energy and Environmental Engineering

Department of Thermal Technology

ul. Konarskiego 22, 44-100 Gliwice, Poland

e-mails: enadimi@polsl.pl and Ebrahim.nadimi@gmail.com

ORCID: [0000-0003-3338-5288](https://orcid.org/0000-0003-3338-5288)

Supervisor:

Dr hab. inż, Grzegorz Przybyła, prof. PŚ

Professor at Silesian University of Technology

Head of Internal Combustion Engines and Automotive Engineering Laboratory

Faculty of Energy and Environmental Engineering

Department of Thermal Technology

ul. Konarskiego 22, 44-100 Gliwice, Poland

e-mail: grzegorz.przybyla@polsl.pl

Abstract

Ammonia is currently receiving more interest as a carbon-free alternative fuel for internal combustion engines. A promising energy carrier, easy to store and transport, being liquid, and has zero carbon-based emissions which makes ammonia a green fuel to decarbonize internal combustion engines and reduce greenhouse gas emissions. This thesis explores the development and use of ammonia with pilot diesel in dual fuel compression ignition engine, by retrofitting a single-cylinder diesel engine for experimental and numerical analyses. Hence, the first part of the thesis involves experimental development and the procedure of utilizing ammonia as a primary fuel with biodiesel in a dual-fuel mode. Thus, a single-cylinder diesel engine was retrofitted to introduce gaseous ammonia into the intake manifold, and then a pilot dose of biodiesel was injected into the cylinder to initiate combustion of the premixed ammonia-air mixture. The effects of various ammonia mass flow rates with a constant biodiesel dose on engine performance and emissions were investigated. In a subsequent study, the impacts of substituting diesel fuel with gaseous ammonia in a dual fuel engine were examined. The effects of various ammonia diesel ratios on combustion, emissions, and engine performance were tested. Additionally, a developed 1D model was utilized to analyze the performance of the dual fuel engine. The second part of the thesis discusses the development of two injection systems for the direct injection of liquid ammonia and biodiesel in a dual direct injection engine. The effects of liquid ammonia and ammonia energy share were investigated. In addition, various ammonia injection timings were studied to improve ammonia/biodiesel combustion and reduce emissions. Furthermore, a CFD model was developed and validated with experimental data to study ammonia sprays, combustion characteristics, and emissions formation. Finally, the impacts of the biodiesel injector configuration and its number of nozzles were explored. Hence, the number of nozzles in the biodiesel injector was blocked by welding in various configurations to improve injection and engine performance. Moreover, different injection timings of biodiesel were tested to determine the optimal injection timing for biodiesel in the dual direct injection engine. The main findings showed that a maximum of 84.2% of input energy can be provided by gaseous ammonia in port injection. Increasing the ammonia energy share changed the combustion mode from diffusion to premixed combustion resulting in a short combustion duration. Although ammonia significantly reduced CO_2 , CO , and particulate matter emissions, it also increased NO_x emissions and unburned ammonia (14800 ppm) in the port injection strategy. The results of dual direct injection strategy showed that higher ammonia energy share significantly reduced the local cylinder temperature due to the strong cooling effects of ammonia, therefore, a maximum ammonia energy share of 50% was achieved. Direct injection of liquid ammonia reduced unburned ammonia by 10813 ppm compared to port injection. Moreover, the optimal injection timing for ammonia and biodiesel was determined at -10 and -16 CAD, respectively. Finally, since biodiesel was used as pilot fuel with lower injected mass, blocking three nozzles of the original six-nozzle injector increased indicated efficiency and reduced CO and NH_3 emissions.

Acknowledgements

I want to express my heartfelt gratitude to the individuals who have played a significant role in supporting and guiding me throughout my PhD journey.

First and foremost, I extend my deepest gratitude to my esteemed supervisor, Professor Grzegorz Przybyła, for his unwavering support, insightful mentorship, and collaborative leadership throughout this journey.

I extend my heartfelt gratitude to the ACTIVATE Team for their exceptional collaborative efforts. I am deeply appreciative for the valuable partnerships and meaningful experiences we have shared during this journey. I am also grateful to my esteemed co-authors for their invaluable guidance, support, advice, and contributions.

I gratefully acknowledge the financial support of the Norway and Poland Grants provided to the ACTIVATE project, titled "Ammonia as carbon free fuel for internal combustion engine driven agricultural vehicle" (Contract NO. NOR/POLNOR/ACTIVATE/0046/2019-00) operated by the National Center for Research and Development (NCBR) Poland <https://AmmoniaEngine.org/>. Also, I would like to acknowledge all used software for providing licenses.

I am incredibly thankful for my family, who have always been my unwavering pillar of support and encouragement.

List of publications

This thesis consists of four published articles which are listed below. The full text of the papers can be find in the Appendix A.

- I. **Ebrahim Nadimi**, Przybyła G, Emberson D, Løvås T, Ziółkowski Ł, Adamczyk W. *Effects of using ammonia as a primary fuel on engine performance and emissions in an ammonia/biodiesel dual-fuel CI engine*. International Journal of Energy Research. 2022 Sep;46(11):15347-61. [1]
DOI: [10.1002/er.8235](https://doi.org/10.1002/er.8235)
IF=4.6 (2022)
- II. **Ebrahim Nadimi**, Przybyła G, Lewandowski M, Adamczyk W. *Effects of ammonia on combustion, emissions, and performance of the ammonia/diesel dual-fuel compression ignition engine*. Journal of the Energy Institute. 2023 Apr 1;107:101158. [2]
DOI: [10.1016/j.joei.2022.101158](https://doi.org/10.1016/j.joei.2022.101158)
IF=5.7 (2023)
- III. **Ebrahim Nadimi**, Przybyła G, Løvås T, Peczkis G, Adamczyk W. *Experimental and numerical study on direct injection of liquid ammonia and its injection timing in an ammonia-biodiesel dual injection engine*. Energy. 2023 Oct. 7:129301. [3]
DOI: [10.1016/j.energy.2023.129301](https://doi.org/10.1016/j.energy.2023.129301)
IF=8.9 (2023)
- IV. **Ebrahim Nadimi**, Przybyła G, Løvås T, Adamczyk W. *Effects of biodiesel injector configuration and its injection timing on performance, combustion and emissions characteristics of liquid ammonia dual direct injection engine*. Journal of the Energy Institute. 2024 Mar 19:101605. [4]
DOI: [10.1016/j.joei.2024.101605](https://doi.org/10.1016/j.joei.2024.101605)
IF=5.7 (2024)

The author of this thesis has co-authored in two published papers that are directly related to the thesis topic and the ammonia-fueled engine. The details of these papers are provided below:

- a. Kuta K, **Ebrahim Nadimi**, Przybyła G, Żmudka Z, Adamczyk W. *Ammonia CI engine aftertreatment systems design and flow simulation*. Combustion Engines, vol. 190, no. 3, 2022, pp. 3-10. [5]
DOI: [10.19206/CE-143158](https://doi.org/10.19206/CE-143158)
- b. Proniewicz M, Petela K, Szłek A, Przybyła G, **Ebrahim Nadimi**, Ziółkowski Ł, Løvås T, Adamczyk W. *Energy and exergy assessments of a diesel-, biodiesel-, and ammonia-fueled compression ignition engine*. International Journal of Energy Research. 2023 Aug 14;2023. [6]
DOI: [10.1155/2023/9920670](https://doi.org/10.1155/2023/9920670)

CRedit authorship contribution statement

The author and co-authors contribution to each paper was provided in the section of "CRedit authorship contribution statement " in each corresponding paper in the Appendix A. However, the author contribution for each paper was the following:

- I. **Ebrahim Nadimi:** Conceptualization, Methodology, Software, Validation, Formal analysis, Investigation, Experiment, Data Curation, Figures, Original draft, Writing - Review & editing. [1]
- II. **Ebrahim Nadimi:** Conceptualization, Methodology, Software, Validation, Formal analysis, Investigation, Experiment, Data Curation, Figures, Original draft, Writing - review & editing. [2]
- III. **Ebrahim Nadimi:** Conceptualization, Methodology, Software, Validation, Formal analysis, Investigation, Experiment, Data Curation, Visualization, Figures, Original draft, Writing - review & editing. [3]
- IV. **Ebrahim Nadimi:** Conceptualization, Methodology, Software, Validation, Investigation, Experiment, Data Curation, Visualization, Original draft, Writing - review & editing. [4]

Contents

Abstract	v
Acknowledgements	vii
List of publications	ix
CRedit authorship contribution	xi
1 Introduction	1
1.1 Background	1
1.2 Motivation and objectives	2
1.3 Thesis outline	3
2 Paper I: Experimental development and port injection of ammonia	5
2.1 Experimental development	5
2.1.1 Emissions measurements	5
2.1.2 Test rig	5
2.1.3 Gaseous ammonia port injection fuel line	7
2.2 Paper I	7
2.2.1 Scope of the study and tests	8
2.2.2 Results and Conclusions	8
3 Paper II: Port injection of ammonia with diesel and 1D model	11
3.1 One dimensional (1D) modeling of the engine	11
3.1.1 AVL BOOST	11
3.1.2 Combustion Model	11
3.1.3 Heat transfer model	13
3.1.4 Emission formation	13
3.2 1D model of the engine	14
3.2.1 1D model of port injection of gaseous ammonia	14
3.2.2 Validation of 1D model	16
3.3 Paper II	17
3.3.1 Scope of the study and experiment	17
3.3.2 Main findings	18
3.4 Conclusions for the next steps	19
4 Paper III: Direct injection of liquid ammonia and CFD model	21
4.1 Direct injection of liquid ammonia	21
4.1.1 Injection system for both fuels	21
4.2 Injectors	22
4.3 CFD	23
4.3.1 Designing full geometry of engine	23
4.3.2 CFD models	24
4.4 Paper III	25

4.4.1	Scope of the study and tests	25
4.4.2	Experiments producer	25
4.4.3	Conclusions	26
5	Paper IV: Biodiesel injector configurations	29
5.1	Scope	29
5.2	Biodiesel injector configurations	29
5.3	Paper IV	32
5.3.1	Operating conditions and studied parameters	32
5.3.2	Selected findings	32
6	Summary and conclusions	35
	References	39
	A	41
	Appendix A	41
A.1	Paper I	41
A.2	Paper II	57
A.3	Paper III	70
A.4	Paper IV	84

List of Figures

2.1	Emissions measurement equipment: a) FTIR, b) SMG200M PM device, and c) Capelec gas analyzer.	6
2.2	Test rig for port injection of gaseous ammonia with pilot ignition of biodiesel	6
2.3	The intake manifold with mounted elements for introducing gaseous ammonia	7
3.1	Energy balance in cylinder [16]	12
3.2	One dimensional model of the engine in the AVL BOOST.	14
3.3	Vibe curve to model combustion and heat release in the cylinder, and influence of m shape parameter	15
3.4	AVL BOOST 1D model of ammonia port injection engine	16
3.5	Validation of 1D model with experimental data at 1700 rpm, $\dot{m}_f = 0.082 \frac{g}{s}$, idle.	17
4.1	Ammonia injection (left) and biodiesel injection control system (right)	21
4.2	Diagram of the concept of connection of ammonia fuel line components [28].	22
4.3	Photo of the engine head and location of GDI and biodiesel injectors on engine head	23
4.4	The the engine full geometry for CFD	23
4.5	Repairing engine geometry in CONVERGE	24
5.1	Biodiesel injector: a) open nozzle b) welded nozzle.	29
5.2	Different configuration of welded biodiesel injector and their corresponding CFD sprays: a) 3a, b) 3b, and C) 1 nozzle	30
5.3	Various configurations of biodiesel spray and welded nozzles along with GDI injector and ammonia spray.	31
5.4	GDI injector a) before and b) after working in diesel engine	31
6.1	Liquid ammonia-biodiesel fueled prototype agriculture tractor	37

List of Abbreviations

ICE	Internal Combustion Engine	CI	Compression Ignition
SI	Spark Ignition	CR	Compression Ratio
TDC	Top Dead Center	BDC	Bottom Dead Center
BTDC	Before Top Dead Center	ATDC	After Top Dead Center
BBDC	Before Bottom Dead Center	ABDC	After Bottom Dead Center
IVO	Inlet Valve Opening	IVC	Inlet Valve Closing
EVO	Exhaust Valve Opening	EVC	Exhaust Valve Closing
BSFC	Brake Specific Fuel Consumption	rpm	Rotation Per Minute
GDI	Gasoline Direct Injection	MFB	Mass Fraction Burned
CD	Combustion Duration	BTE	Brake Thermal Efficiency
CAD	Crank Angle Degree	LHV	Lower Heating Value
SOI	Start Of Injection	SOC	Start Of Combustion
HRR	Heat Release Rate	GWP	Global Warming Potential
COV	Coefficient Of Variation	PRR	Pressure Rise Rate
AES	Ammonia Energy Share	ITE	Indicated Thermal Efficiency
ISFC	Indicated Specific Fuel Consumption	ID	Injection Duration
AMR	Adaptive Mesh Refinement	GHG	GreenHouse Gases
DI	Direct Injection	Bio	Biodiesel
ABDI	Ammonia Biodiesel Direct Injection	FTIR	Fourier-Transform Infrared spectroscopy
IMEP	Indicated Mean Effective Pressure	CFD	Computational Fluid Dynamics
SCR	Selective Catalytic Reduction	EGT	Exhaust Gas Temperature
ECU	Electronic Control Unit	PM	Particulate Matter

Chapter 1

Introduction

1.1 Background

Fossil fuels, greenhouse gas (GHG) emissions, and their effects on climate change are the primary reasons to prevent internal combustion engines (ICE) from utilizing fossil fuels. ICEs also produce harmful emissions, such as nitrogen oxides (NO_x), hydrocarbons (HC), Particulate Matter (PM) and carbon monoxide (CO), and exceeding the threshold limit for these hazardous gases has harmful health effects. Nevertheless, ICEs are widely used in the transportation sector, such as heavy-duty vehicles, producing a significant amount of carbon dioxide (CO_2) emission. To combat these worldwide challenges, the legitimately binding international agreement on climate change, the 2015 Paris Agreement provided a global framework for reducing greenhouse gases in the next decades. Hence, the European Union countries have an aim to decrease the emissions of greenhouse gases by 55% by 2030 [7]. Therefore, ICEs must be decarbonized by replacing them either with electric motors or using alternative green fuels. Electrical Vehicles (EVs), which can be battery type or hydrogen (H_2) fuel cell, are more feasible for light-duty vehicles. However, the majority heavy-duty engine manufacturers will still use diesel engines because of the challenges of batteries such as energy density and charging duration [8].

Therefore, alternative carbon-free fuels, such as ammonia (NH_3) and hydrogen, are a good way to replace fossil fuels and stop the emission of carbon dioxide. However, the big problem with hydrogen is storing in the high pressure at a reasonable cost because of the extremely low density of gaseous hydrogen. Among all green fuels such as ethanol [9], methanol [10], and methyl ester [11], ammonia is currently attracting a lot of interest as a potential alternative to fossil fuels [12, 13, 14]. It is a good hydrogen carrier (17.8% by mass), is liquid and easy to store under low pressure, and is also one of the most produced chemicals in the world. Additionally, ammonia already has a great established infrastructure for distribution, production, and handling, as it is used as fertilizer in the agriculture industry. However, the practical usage of liquid ammonia as fuel for ICE requires many technical and operational difficulties to be surmounted.

Ammonia has different characteristics from common fossil fuels. However, the challenges in using ammonia as fuel in ICE are high ignition energy and temperature, low flame speed, and low adiabatic flame temperature compared to diesel fuel. Furthermore, the Lower Heat Value (LHV) of ammonia is around 60% lower than diesel fuel. Nevertheless, the sociometric mixture of ammonia/air has almost the same amount of energy compared to the sociometric mixture of diesel/air [15].

1.2 Motivation and objectives

The motivation for this thesis comes from the urgent need to address the environmental challenges posed by conventional fossil fuels, particularly in the context of ICEs. Furthermore, the significant impact of greenhouse gas emissions on climate change requires a shift toward renewable and carbon-free energy sources. Hence, ammonia has emerged as a promising green fuel due to its carbon-free nature and hydrogen carrier to utilize in the Compression Ignition (CI) engine. Therefore, the main objective of this thesis is to develop an ammonia fueled CI engine by retrofitting the single cylinder diesel engine. Then, experimentally and numerically investigating the use of ammonia in CI engine, focusing on dual fuel combustion. Also, addressing challenges of ammonia such as ammonia slip and NO_x . The overarching goal is to enhance combustion, reduce emissions, and improve the performance of ammonia-fueled CI engine compared to traditional diesel engine. Hence, the following research and objectives were formulated to achieve the thesis goals:

- The experimental development for using ammonia as primary fuel and biodiesel or diesel as a secondary pilot fuel in a CI engine.
- Developing and investigating two different approaches for utilizing ammonia by retrofitting a single-cylinder diesel engine. The first strategy involves the introduction of gaseous ammonia into the intake manifold, while the second strategy is direct injection of liquid ammonia into the cylinder in dual injection engine.
- Testing the impacts of replacing diesel fuel with ammonia to the maximum possible substitution in the CI engine. Therefore, engine performance and emission characteristics are experimentally studied for various ammonia-diesel ratios and compared with pure diesel mode.
- Investigation of injection parameters for both liquid ammonia and biodiesel. Therefore, injection timing of ammonia and biodiesel are studied to optimize engine performance and reduce emissions.
- Since biodiesel is employed as pilot fuel with low injected mass, the number of nozzles in biodiesel injector are blocked to improve injection and thus reduce emissions.
- Development of a 1D model to analyze ammonia-fueled CI engine.
- The development and validation of a CFD model for both pure biodiesel and ammonia biodiesel CI engine. The CFD model is developed to study ammonia spray and combustion, as well as to predict local temperature and emissions such as CO_2 , CO , NO_x , and NH_3 .

1.3 Thesis outline

The thesis consists of four published articles, each contributing to the experimental and numerical study of an ammonia-fueled compression ignition engine. Thus, this thesis serves as a guide for the four papers. **Chapter 1** provides background by highlighting the potential of ammonia as a carbon-neutral alternative to traditional fossil fuels. It establishes the global context, motivation, and objectives of the work. **Chapter 2** outlines the modification of a single-cylinder diesel engine to use gaseous ammonia as the primary fuel with pilot ignition of biodiesel in a dual fuel engine. It investigates the impact of varying ammonia mass flow rates on engine performance and emissions at constant biodiesel doses and different engine loads. **Chapter 3** discusses the experimental development for port injection of gaseous ammonia, exploring the impacts of replacing diesel fuel with ammonia in a dual-fuel engine and studying the effects of various ammonia/diesel ratios on combustion emissions and engine performance. Additionally, it discusses 1D model development of the engine. **Chapter 4** focuses on the development of the direct injection of liquid ammonia with biodiesel and explains the dual direct injection system. It examines the effects of the injection timing of ammonia and Ammonia Energy Share (AES) on combustion, emissions, and engine performance through experimental and CFD analysis. Moreover, it describes the CFD model case setup. **Chapter 5** aims to investigate the influence of the biodiesel injector configuration, injection timing, and its number of nozzles on the performance, combustion, and emissions characteristics of the liquid ammonia-biodiesel dual direct injection engine. Furthermore, the last sections of **Chapters 2, 3, 4, and 5** explain and summarize the corresponding papers in the Appendix A. Hence, paper I, II, III, and IV can be found in the Appendix A.1, A.2, A.3, and A.4, respectively. Finally, **Chapter 6** summarizes key findings of the thesis.

Chapter 2

Paper I: Experimental development and port injection of ammonia

2.1 Experimental development

Investigating the performance, emissions, and combustion of an ammonia-fueled engine requires a well-equipped test rig. Therefore, the test rig was designed and constructed in a way that allows for extensive research on engines fueled by ammonia, biodiesel, and diesel. The measured data includes exhaust species concentration, in-cylinder pressure, engine speed, fuel and air mass flow rates, and PM levels. The test rig consists of various components such as the ammonia fueling system, electric motor, coupling shaft, National Instrument, gas analyzer, Fourier-transform infrared spectroscopy (FTIR), temperature sensors and air and fuel flow measurement devices. The construction and development of each part of the test rig, as well as equipment selection, will be discussed in the following sections.

2.1.1 Emissions measurements

A sample of exhaust gas was analyzed using FTIR, Capelec gas analyzer, and SMG200M PM device. The FTIR is a Gasmeter DX4000 gas analyzer that is operated by Calcmeter software. The Calcmeter can simultaneously analyze gas components in wet and corrosive gas streams, and it has various spectrum libraries in different ranges to determine the concentration of each species. The FTIR has an accuracy of less than 2%. FTIR can measure H_2O , CO_2 , CO , N_2O , NO , NO_2 , SO_2 , NH_3 , HCl (Hydrogen chloride), HF (Hydrogen fluoride), CH_4 , C_2H_6 (Ethane), C_2H_4 (Ethylene), C_3H_8 (Propane), C_6H_{14} (Hexane), $CHOH$ (Formaldehyde) and O_2 . Furthermore, PM was measured using SMG200M with a precision of 3% and particle sizes in the range of $0.04\mu m$ to $10\mu m$ under normal conditions (1 atm and $0^\circ C$). The additional Capelec gas analyzer measured the dry exhaust gas for CO , CO_2 , HC , O_2 and lambda. Emissions measurement devices are shown in figure 2.1.

2.1.2 Test rig

A single-cylinder CI engine has been retrofitted to operate with port injection of gaseous ammonia and then will be installed in the tractor for using in the agricultural sector. Gaseous ammonia was introduced into the port near the inlet valve, through the pipe inserted into the intake manifold, and the mass flow of ammonia was measured using a Coriolis flow meter. A surge tank has been installed in the intake manifold to measure the constant air mass flow rate, also to avoid backflow



FIGURE 2.1: Emissions measurement equipment: a) FTIR, b) SMG200M PM device, and c) Capelec gas analyzer.

of ammonia from the intake manifold to the environment. The temperature of the port, exhaust gas, and ambient as well as the air and ammonia mass flow rate were monitored by LabVIEW software and National Instruments hardware. The engine has been coupled by the vibration damping shaft to the electric motor to adjust the engine load and speed for the test. Also, the electrical parameters such as generated electric power on the electric motor and estimated torque were indicated by the system. The in-cylinder pressure was measured with a resolution of 1024 measuring points per one shaft revolution and for 100 consecutive cycles using a piezoelectric pressure transducer. An encoder with 0.35 CAD resolution was installed on the engine shaft to sample the electrical signal from the pressure transducer to identify the piston position at TDC. The photo of the test rig is shown in Figure 2.2.

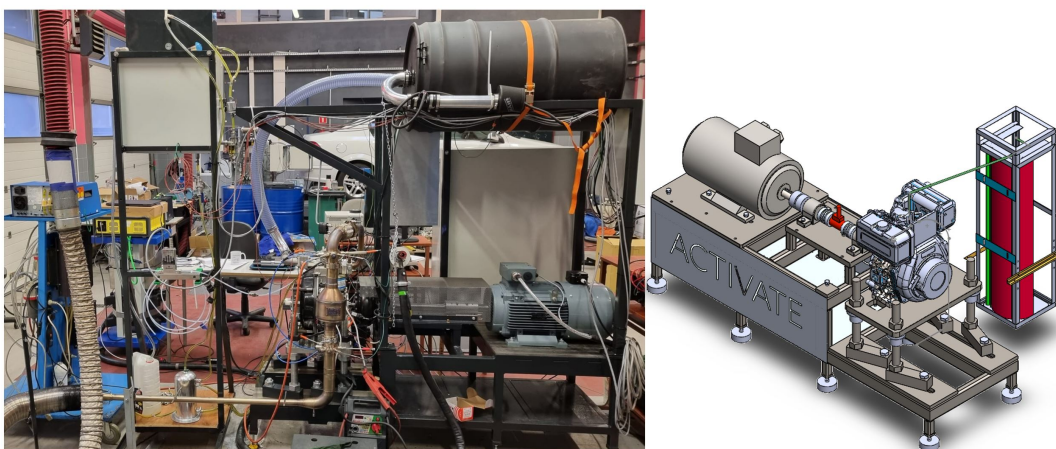


FIGURE 2.2: Test rig for port injection of gaseous ammonia with pilot ignition of biodiesel

2.1.3 Gaseous ammonia port injection fuel line

The engine intake manifold was equipped with a custom-designed block to facilitate the installation of an ammonia pipeline, a temperature sensor, and a pressure transducer. The PTFE pipe was placed inside the intake manifold and secured by attaching the block. The installation of the ammonia line, disassembled block along with its position near the inlet valve, are illustrated in Figure 2.3. Then, the ammonia tank was connected to the block using piping, a control valve, and a Coriolis flow meter.

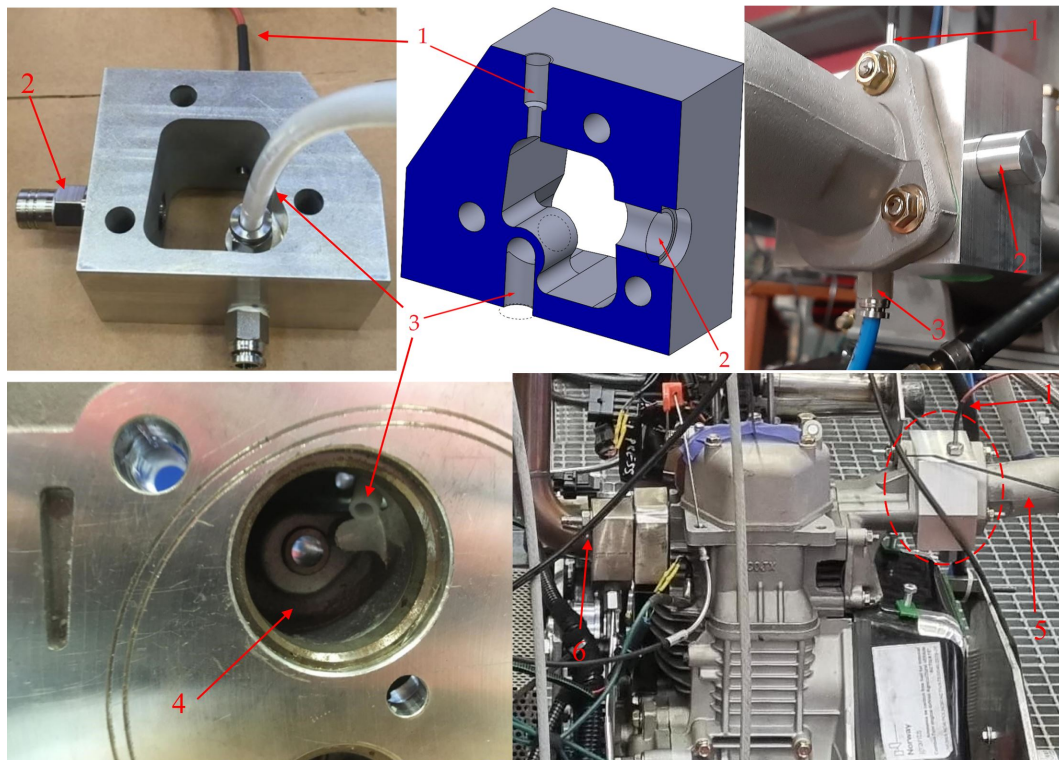


FIGURE 2.3: The intake manifold with mounted elements for introducing gaseous ammonia

The elements highlighted in Figure 2.3 are as follows: 1- thermocouple nest allowing for inserting thermocouples head into flows core, 2- hole and plug for pressure sensor, 3- ammonia gas connector, 4- intake valve channel, 5- intake manifold, 6- exhaust port.

2.2 Paper I

The attached paper in Appendix A.1 entitled "Effects of using ammonia as a primary fuel on engine performance and emissions in an ammonia/biodiesel dual-fuel CI engine" is result of experimental development of the ammonia-fueled engine and the ammonia use strategy. In this paper, a comprehensive study has been carried out to investigate the effects of using ammonia as the main fuel with biodiesel in dual fuel mode. In this paper, a single-cylinder diesel engine was retrofitted to allow for introducing gaseous ammonia into the intake manifold while using biodiesel

for pilot ignition. The strategy of using ammonia with biodiesel as secondary fuel is proposed to run the engine with the lowest possible biodiesel at low load, and then ammonia is introduced to obtain higher loads. Therefore, the effects of various ammonia mass flows with two constant pilot doses on combustion, emissions, and engine performance are investigated and compared with original engine operation fueled with pure biodiesel.

2.2.1 Scope of the study and tests

The paper I demonstrates the use of ammonia as a potential carbon-free fuel with biodiesel in the CI engine in dual fuel mode. An experimental carried out to investigate the impacts of different ammonia and biodiesel load contributions on ammonia/biodiesel combustion, engine performance, and emissions. Therefore, the engine is run first with two different pilot doses of biodiesel at low loads; then ammonia is introduced into the intake port to obtain higher loads. Therefore, the engine was initially run on biodiesel at various loads to determine the baseline. The approach to introduce ammonia into the port is defined in this way in which the engine is operated with biodiesel at low load and with a constant biodiesel mass flow rate, and then ammonia is injected to increase torque and power. In first test, the biodiesel load contribution was 10%, i.e., the engine has been operated with biodiesel and the measured load and biodiesel mass flow rate were 10% and $\dot{m}_{bio} = 0.107 \text{ g/s}$, respectively. Then, the ammonia mass flow is increased to obtain higher loads at the same operating point as the biodiesel baseline. The second test is similar to the test one, but with the difference that the engine was run with biodiesel at a low load of 3.5% with constant $\dot{m}_{bio} = 0.082 \text{ g/s}$. With increasing ammonia mass flow, ammonia load contribution and ammonia energy share have been increased. The maximum input AES is 59.1% and 69.4% at full load for test one with $\dot{m}_{bio} = 0.107 \text{ g/s}$, and test two with $\dot{m}_{bio} = 0.082 \text{ g/s}$, respectively.

The main scopes of this study are summarized as follows:

- The test bench has been built for gaseous ammonia operation.
- A strategy for using ammonia with biodiesel has been proposed.
- Comparison of port injection of gaseous ammonia with pure biodiesel operations at various loads.
- The ammonia biodiesel dual fuel CI engine has been experimentally investigated.

2.2.2 Results and Conclusions

The results of this paper shows that 69.4% of the input energy of biodiesel can be replaced by ammonia, but increasing the mass flow rate of ammonia slightly decreases the brake thermal efficiency. Moreover, increasing the ammonia load contribution significantly reduced the emissions of CO_2 , CO , and HC but increased the emission of NO . It was found that ammonia delayed the start of combustion by 2.6 CAD compared to pure biodiesel due to the low in-cylinder temperature and the high resistance of ammonia to autoignition. However, the combustion duration of biodiesel/ammonia decreased 19 CAD compared to pure biodiesel operation at full load, as most of the heat was released during the premixed combustion phase.

The main conclusions drawn from this study are summarized as follows:

- Increasing ammonia energy share decreases the exhaust gas temperature. Therefore, the exhaust gas temperature was reduced by 100 K when the AES was 69.4%.
- Increasing ammonia load contribution increases the peak of in-cylinder pressure, e.g. in-cylinder pressure increased by 11.15 bar compared to biodiesel at full load. Moreover, ammonia also increases the peak of the pressure rise rate diagram.
- Ammonia increases the peak of the HRR and decreases the diffusion combustion phase in the HRR diagram. Therefore, as more ammonia is introduced into the intake manifold, the combustion mode changes from diffusion to pre-mixed combustion.
- The maximum 69.4% of the input energy is provided by ammonia in reasonable operation.
- A higher ammonia contribution to the engine load delays the SOC and decreases the combustion duration.
- Significant reduction in CO_2 , CO , and HC emissions in the ammonia/biodiesel-fueled engine compared to pure biodiesel operation. Therefore, CO_2 decreases by 510 g/kWh and CO reduces by 30.1 g/kWh.

Chapter 3

Paper II: Port injection of ammonia with diesel and 1D model

3.1 One dimensional (1D) modeling of the engine

3.1.1 AVL BOOST

AVL BOOST is a software for simulating engine cycles and gas exchange, designed to create detailed models of engines and vehicles. It allows the modeling of various components, such as cylinders, air cleaners, catalysts, turbochargers, valves, and advanced junction models. It also models heat transfer, flow, combustion and emissions. By one-dimensional, it simulates steady-state operating conditions and transient cycles across a wide range of engine speeds and loads. The 1D engine model allows for the obtaining of numerical outputs at different locations of the systems providing data such as pressure, temperature, and air/fuel ratio at any specific measuring point within the model [16].

3.1.2 Combustion Model

Two methods are used to model combustion in the cylinder. The first method is called the "target pressure curve 2 zone", in this model, the measured in-cylinder pressure profiles are used to calculate the mass fraction of burned fuel and heat release profile [16]. In the second method, the Vibe function is used for the second procedure. This method proposed by Vibe aims to model the combustion process by using the first laws of thermodynamics and the rate of heat release. Hence, The Vibe two-zone model was used for the combustion modeling process. In this method, the combustion zone in the cylinder is divided between unburned and burnt gas regions in this model [17]. The first law of thermodynamics is applied to the burnt and unburned regions to calculate the gas temperature for each region [18, 19]:

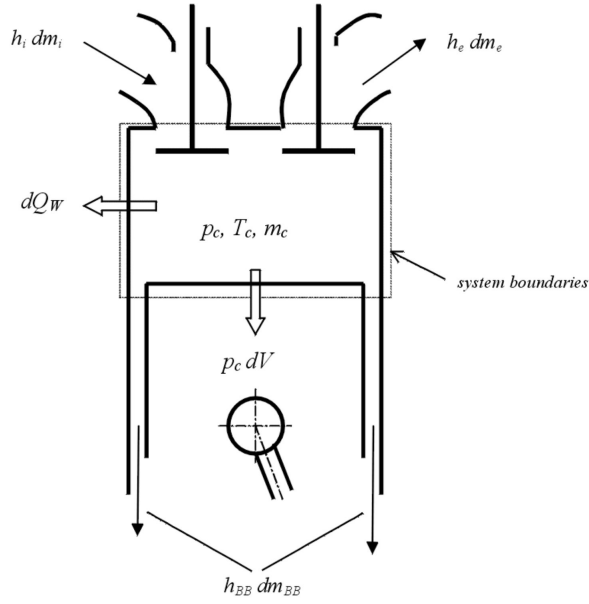


FIGURE 3.1: Energy balance in cylinder [16]

First law for the burned zone (index b):

$$\frac{dm_b u_b}{d\alpha} = -P_c \frac{dV_b}{d\alpha} + \frac{dQ_F}{d\alpha} - \sum \frac{dQ_{wb}}{d\alpha} + h_u \frac{dm_b}{d\alpha} - h_{BB,b} \frac{dm_{BB,b}}{d\alpha} \quad (3.1)$$

And for the unburned zone (index u):

$$\frac{dm_u u_u}{d\alpha} = -P_c \frac{dV_u}{d\alpha} - \sum \frac{dQ_{wu}}{d\alpha} - h_u \frac{dm_B}{d\alpha} - h_{BB,u} \frac{dm_{BB,u}}{d\alpha} \quad (3.2)$$

The terms $\frac{dm_b u_b}{d\alpha}$, $P_c \frac{dV_b}{d\alpha}$, and $\frac{dQ_F}{d\alpha}$ denote the internal energy change in the cylinder, work by piston, and fuel input chemical energy, respectively. Also, $\sum \frac{dQ_{wb}}{d\alpha}$, $h_u \frac{dm_b}{d\alpha}$, and $h_{BB,b} \frac{dm_{BB,b}}{d\alpha}$ are heat losses from the combustion chamber, enthalpy transfer from unburnt to burned zone and enthalpy blow-by loss in the cylinder which is taken into account and calculated by the BOOST model [16]. In the above equations Eq. 3.1, and Eq. 3.2, the volume of the burned and unburned zone is equal to the cylinder volume as well as the changes of each zone volume are equal to the cylinder volume change.

$$V_b + V_u = V_c \quad (3.3)$$

$$\frac{dV_b}{d\alpha} + \frac{dV_u}{d\alpha} = \frac{dV_c}{d\alpha} \quad (3.4)$$

The integral of Vibe curve since the start of ignition calculates the mass of the burnt fuel at each time setup and expressed as follows [20]:

$$m_{b,f} = \int \frac{dm_{b,f}}{d\alpha} d\alpha = 1 - e^{-a \left(\frac{\alpha - \alpha_0}{\Delta\alpha} \right)^{m+1}} \quad (3.5)$$

where a , α_0 , $\Delta\alpha$, and m denote the vibe parameter ($a = 6.9$), Start Of Combustion (SOC), combustion duration, and m shape parameter, respectively.

3.1.3 Heat transfer model

The heat transfer to the combustion chamber walls, namely, the the cylinder head, piston, and cylinder liner, is determined by using the following Newton's law of cooling equation [16]:

$$Q_{wi} = A_{wi} \times h_w \times (T_c - T_{wi}) \quad (3.6)$$

where Q_{wi} , A_{wi} , and T_{wi} are heat transfer, surface area, and temperature of cylinder head, liner, and piston, respectively. The liner wall temperature difference between BDC and TDC is taken into account by given $T_{L,BDC}$ and $T_{L,TDC}$ and defined as follows:

$$T_L = T_{L,TDC} \times \frac{1 - e^{-c \cdot z}}{z \cdot c} \quad (3.7)$$

Where c is $\ln\left(\frac{T_{L,TDC}}{T_{L,BDC}}\right)$ and z is the piston position related to full stroke. The heat transfer coefficient (h_w) is calculated using the following Woschni model [21]:

$$h_w = 130 \times D^{-0.2} \cdot P_c^{0.8} \cdot T_c^{-0.53} \cdot \left[C_1 \cdot c_m + C_2 \cdot \frac{V_D \cdot T_{c,1}}{P_{c,1} \cdot V_{c,1}} (P_c - P_{c,o}) \right]^{0.8} \quad (3.8)$$

Where [16]:

- D : Cylinder bore [m]
- P_c : Cylinder pressure [bar]
- T_c : Cylinder gas temperature [K]
- c_m : Mean piston speed [m/s]
- c_u : Circumferential velocity
- V_D : Displacement per cylinder [m³]
- $T_{c,1}$: Temperature in the cylinder IVC [K]
- $P_{c,1}$: Pressure in the cylinder at IVC [bar]
- $P_{c,o}$: Cylinder pressure of the motored engine [bar]
- $C_1 = 2.28 + 0.308c_u / c_m$
- $C_2 = 0.00324$

3.1.4 Emission formation

In 1D model, NO_x formation is determined through Zeldovich mechanism. Pattas and Hafner [22] developed the NO_x production model known as Zeldovich mechanism [23]. Moreover, the rate of CO formation is calculated based on Onorati et al.[24] with two reactions. The soot formation was model based on Schubiger et al [25].

3.2 1D model of the engine

The engine 1D model is shown in Figure 3.2 was simulated using AVL BOOST software. This model includes the engine (E1), single cylinder (C1), Inlet (SB1) and outlet (SB2) boundary conditions, measurement points 1 and 2 (MP1, MP2), and the lines representing pipes. For this model, data for setting cylinder covers the basic dimensions of the cylinder like bore, stroke, compression ratio, conrod length, piston pin offset, firing order, plus information on the combustion characteristics, heat transfer, and valve/port specifications for the attached pipes. Therefore, the cylinder dimensions and inlet and exhaust valves lift profiles from our measurements of the engine have been used to set the 1D model. As initialization, the cylinder conditions, pressure, temperature, and gas composition at the end of the high pressure at exhaust valve opening were set. Furthermore, the initial conditions for the calculation of the cylinder have been specified.

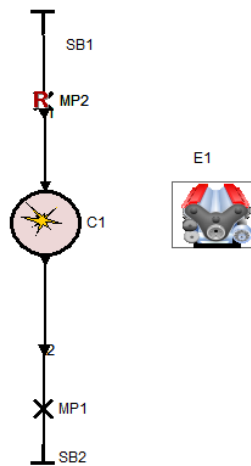


FIGURE 3.2: One dimensional model of the engine in the AVL BOOST.

The heat release rate in the engine cylinder was modeled using the Vibe function. Vibe function is often used to approximate the heat release characteristics of the engine. Figure 3.3 illustrates the approximation of a heat release profile of a diesel engine using a vibration function for different values of the ' m ' shape parameter (0.4, 0.6, 0.8, and 1). The shape parameter determines the speed of combustion and heat release. For different values of m , the vibe diagram and burned fuel mass fraction are calculated and presented in this figure. The start of combustion, combustion duration, and m shape parameter will be obtained by a least square fit of the measured heat release curve. However, for accurate modeling of the double peak heat release in the cylinder, since there are two peaks in the heat release diagram, the first peak due to premixed burning and the second peak due to diffusion combustion. Therefore, two vibe functions will be specified for the modeling.[5]

3.2.1 1D model of port injection of gaseous ammonia

The 1D model was developed to simulate the ammonia-fueled engine by using AVL BOOST software. The model covers all test bench elements as can be seen in Figure 3.4. In this model, E1, CL1, C1, and CAT are engine, air cleaner, cylinder, and

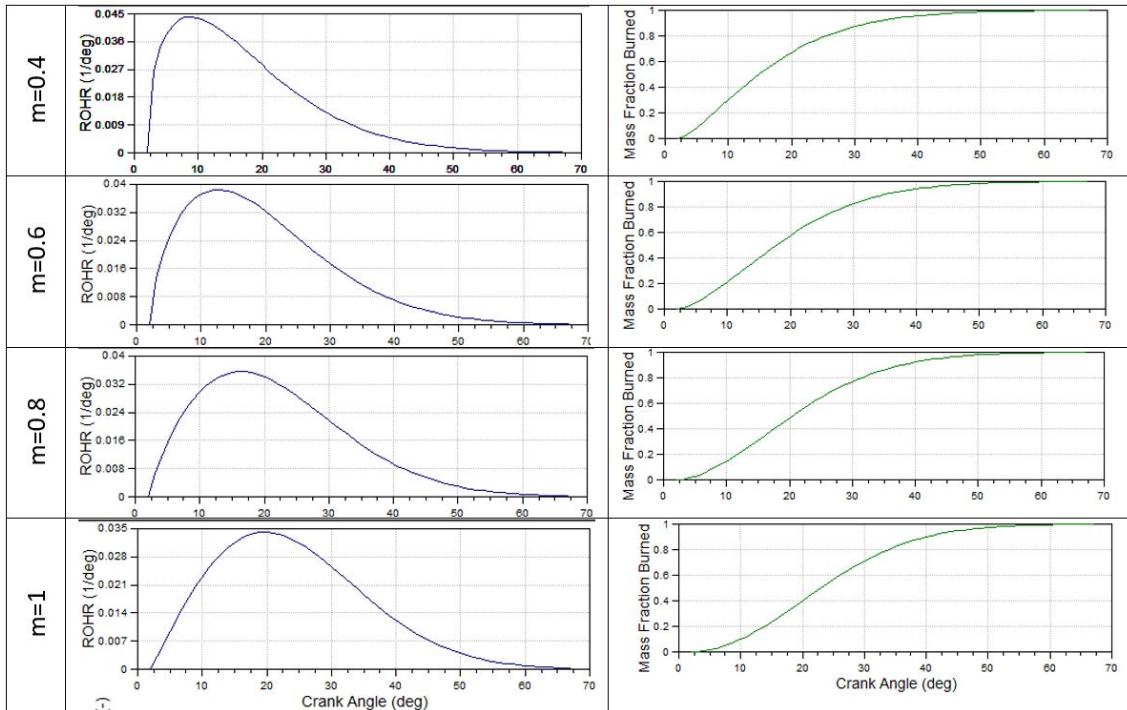


FIGURE 3.3: Vibe curve to model combustion and heat release in the cylinder, and influence of m shape parameter

aftertreatment systems, respectively. Moreover, seven measurement points (MP) are set to measure thermophysical properties of the flow inside the pipes. Ammonia is continuously introduced into the pipe through the injector I1. For this model, the measured experimental data were applied to setup each element, for example, engine friction (FMEP), valves lift profile, and flow coefficient through the valves were determined and used in the model.

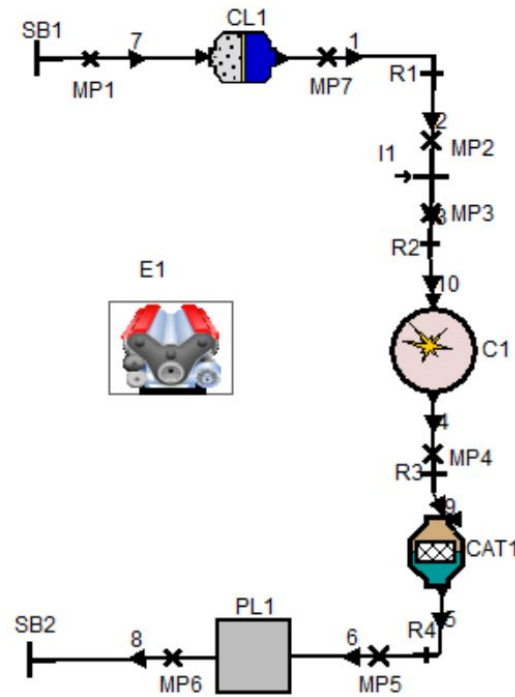


FIGURE 3.4: AVL BOOST 1D model of ammonia port injection engine

3.2.2 Validation of 1D model

For ensuring the accuracy of the 1D results, the numerically modeled pressure profile is compared with the experimentally measured one at the same operating condition. Figure 3.5 illustrates the simulated in-cylinder pressure for the motored and combustion operation along with the measured pressure traces. By comparing the two pressure traces, it can be seen that the equations which were used for modeling fluid flow, combustion, and heat transfer are accurate. Therefore, the results of the 1D model for the modeling of ammonia fueled engine is reliable.

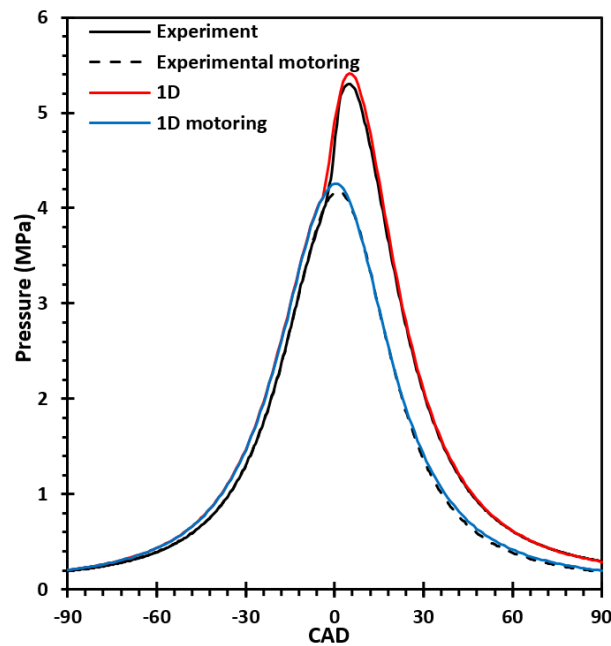


FIGURE 3.5: Validation of 1D model with experimental data at 1700 rpm, $\dot{m}_f = 0.082 \frac{\text{g}}{\text{s}}$, idle.

3.3 Paper II

The paper II in Appendix A.2, titled "Effects of ammonia on combustion, emissions, and performance of the ammonia/diesel dual fuel compression ignition engine" investigates how replacing diesel with ammonia in a dual fuel engine impacts combustion, emissions, greenhouse gases (GHG) and performance. Therefore, this paper aims to illustrate the impacts of replacing diesel fuel with gaseous ammonia in an ammonia/diesel dual fuel engine. Hence, the effects of various ammonia diesel ratios on emissions and engine performance were experimentally investigated. CO_2 equivalent GHG emissions are evaluated over 100 years to show the effectiveness of ammonia in reducing GHG emissions considering the emission of N_2O . Additionally, a developed 1D model is used to analyze the combustion characteristics of ammonia and diesel.

3.3.1 Scope of the study and experiment

The utilization of ammonia in CI engines still presents notable research gaps. Ammonia is known for its carbon-free emission, yet nitrogen oxides are an issue besides NO and NO_2 which cumulatively known as NO_x , N_2O is particular concern as it can be emitted from ammonia-diesel combustion and has nearly 300 times larger greenhouse effects than CO_2 on the 100-year time scale. Considering the emissions by the greenhouse effect, it can offset the reduction of CO_2 . Furthermore, unburned ammonia on itself can be another challenge for dual-fuel diesel ammonia engines. This paper investigate the impacts of replacing diesel fuel with gaseous ammonia to the maximum possible substitution in the CI engine under full loads conditions and engine speed of 1200 rpm. Engine performance and emission characteristics are experimentally studied for various ammonia-diesel ratios. Moreover, 1D model is

used to calculate the combustion characteristics indicators. Therefore, ignition delay, combustion phasing and duration are determined for different ammonia diesel ratios. Furthermore, unburned ammonia and N_2O emissions are discussed.

The test was carried out to determine the maximum diesel that can be replaced with ammonia. In addition, the impact of the ammonia energy share on engine performance, combustion, and emissions characteristics was examined. Since ammonia has a low flame speed and a high minimum required ignition energy [26, 27], low engine speed fixed at 1200 rpm and full load were chosen for all operating conditions. The first operating point (OP1) regarded as the reference was taken at those conditions fueled with pure diesel. Subsequently, the mass flow of diesel is reduced and gaseous ammonia is aspirated to the intake port close to the inlet valve according to the AES values in Table 3.1 (Table 3 in Paper II in Appendix A.2), to achieve the same power as in the case of pure diesel. Therefore, 9 operating points have been tested. The maximum amount of diesel fuel that could be replaced with ammonia was $AES = 84.2\%$ in OP9 and for a higher value of AES, the engine could not run.

TABLE 3.1: Overview of the operating points conditions (Table 3 in Paper II in Appendix A.2).

NO.	\dot{m}_{diesel}	\dot{m}_{NH_3}	\dot{m}_{air}	Y_{NH_3}	AES	T_{port}	T_{Ex}	P_i	AFR_{sto}	λ
	g/s	g/s	g/s	-	%	$^{\circ}C$	$^{\circ}C$	kW	kg/kg	-
OP1	0.220	0	4.27	0	0	33.6	460	3	14.59	1.35
OP2	0.186	0.074	4.25	0.286	14.90	31.3	450.6	3.05	12.15	1.36
OP3	0.152	0.135	4.25	0.470	27.94	28.1	399.2	3	10.58	1.41
OP4	0.127	0.162	4.25	0.561	35.85	26.6	387.7	2.95	9.80	1.51
OP5	0.103	0.212	4.21	0.674	47.44	26.0	373.5	3	8.84	1.52
OP6	0.09	0.249	4.15	0.735	54.81	24.9	370.6	3.06	8.32	1.48
OP7	0.076	0.279	4.03	0.786	61.62	24.8	357.7	3.06	7.89	1.45
OP8	0.040	0.338	3.97	0.894	78.73	23.6	335.4	2.98	6.96	1.51
OP9	0.030	0.364	3.88	0.924	84.16	22.5	328	3.03	6.71	1.47

3.3.2 Main findings

The results of PaperII show 84.2% of input energy can be provided by ammonia meanwhile indicated thermal efficiency is increased by increasing the diesel substitution. Moreover, increasing the ammonia energy share changed the combustion mode from diffusion combustion in pure diesel operation to premixed combustion in dual fuel mode. Therefore, the combustion duration and the combustion phasing decreased by 6.8 CAD and 32 CAD, respectively. Although ammonia significantly reduced CO_2 , CO , and particulate matter emissions, it also increased NO_x emissions and unburned ammonia (14800 ppm). Furthermore, it is important to note that in order to effectively reduce greenhouse gas emissions, diesel must be replaced with more than 35.9% ammonia, as ammonia combustion produces N_2O at a level of 90 ppm, which offsets the reduction in CO_2 emissions.

The main results are summarized as follows:

- The maximum 84.2% of input energy was provided by ammonia. As more ammonia was introduced into the intake port, ITE increased by around 5.6 percent point at the highest AES compared to pure diesel. It also reduced the exhaust gas temperature by $132^{\circ}C$.

- Since ammonia has a lower γ than air, the compression pressure decreases by increasing the ammonia mass flow. However, ammonia increases the peak of in-cylinder pressure. Furthermore, it also increases dramatically the peak of pressure rise rate to 9.5bar/deg for AES of 61.6%, which is 76.5% higher than only the diesel case due to premixed combustion.
- Ammonia delayed the SOC by around 7.2CAD at the highest diesel substitution due to the low compression pressure and consequently in-cylinder temperature. Higher ammonia ratio also reduced diffusion combustion phase and increased premixed combustion mode at the highest AES.
- By substituting diesel fuel, carbon-based emissions were markedly reduced, but NO , NO_2 and N_2O emissions increased. However, a significant amount of unburned ammonia was measured that further investigation is needed to reduced ammonia emission.
- Ammonia significantly reduced the CO_2 emission from 705g/kWh to 103g/kWh , but it also produced N_2O emission, which has 298 times GHG effects. The GHG emissions decreased when more than 35.9% of diesel was replaced. GHG emissions decreased significantly from 727g/kWh for only diesel operation to 243g/kWh for the highest AES.
- The ammonia-fueled CI engine significantly reduced GHG emissions by 3 times over 100 years scale.

3.4 Conclusions for the next steps

In papers I and II gaseous ammonia was introduced into the intake manifold and pilot fuel was injected into the cylinder through the engine's old injection system and injector. Therefore, the injection parameters of diesel, such as injection timing and injection pressure can not be controlled. Since diesel was used as pilot ignition in low doses, it became necessary to optimize the injection parameters in order to enhance combustion and engine performance. As a result of using the engine's old injection system which lacked control over diesel fuel injection, led to high emissions of CO and PM , as well as reduced engine efficiency. In addition, introducing gaseous ammonia into intake manifold caused significant amount of ammonia emissions. However, direct injection of liquid ammonia could considerably reduce these emissions.

Therefore, in the next step, two common rail injection systems for ammonia and biodiesel will be used to optimize injection parameters for both fuels. Moreover, different diesel injector configurations and number of nozzles will be investigated. In addition, the CFD model of the ammonia biodiesel fueled engine will be developed.

Chapter 4

Paper III: Direct injection of liquid ammonia and CFD model

4.1 Direct injection of liquid ammonia

4.1.1 Injection system for both fuels

The ammonia fuel system was specifically designed and constructed for high pressure injection. Ammonia was stored in the ammonia tank under low pressure around 8 bar. Since the GDI pump did not work with liquid ammonia to feed high pressure ammonia to GDI injector, a nitrogen gas tank was used to pressurize the ammonia tank to 100 bar. However, the nitrogen gas can pressurized ammonia between 50 and 150 bar. The liquid ammonia is then transferred to the common rail at a pressure of 100 bar. The final concept of the manual and solenoid valves locations is illustrated in Figure 4.2. Two distinct injection systems, with their own Electronic Control Unit (ECU), are employed for the injection of ammonia and biodiesel. This allows the control of injection timing parameters such as Start of Injection (SOI), main dose, injection pressure, and split injection for both fuels. The common rail injection system with its own ECU to control biodiesel injection timing with a separate ECU and injection system for ammonia. These two injection systems were used to optimize the injection of both fuels. Figure 4.1 displays a view of the dialog window of the ECU management program used to control the common rail injector, as well as the corresponding window for the ammonia injector program of ECU.

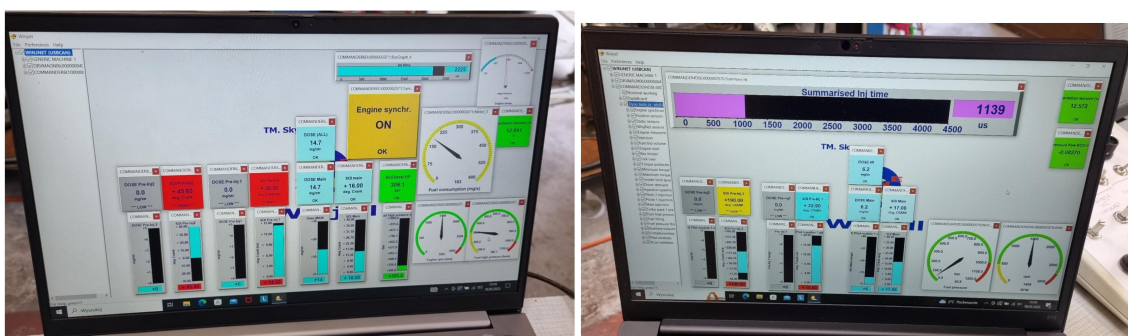


FIGURE 4.1: Ammonia injection (left) and biodiesel injection control system (right)

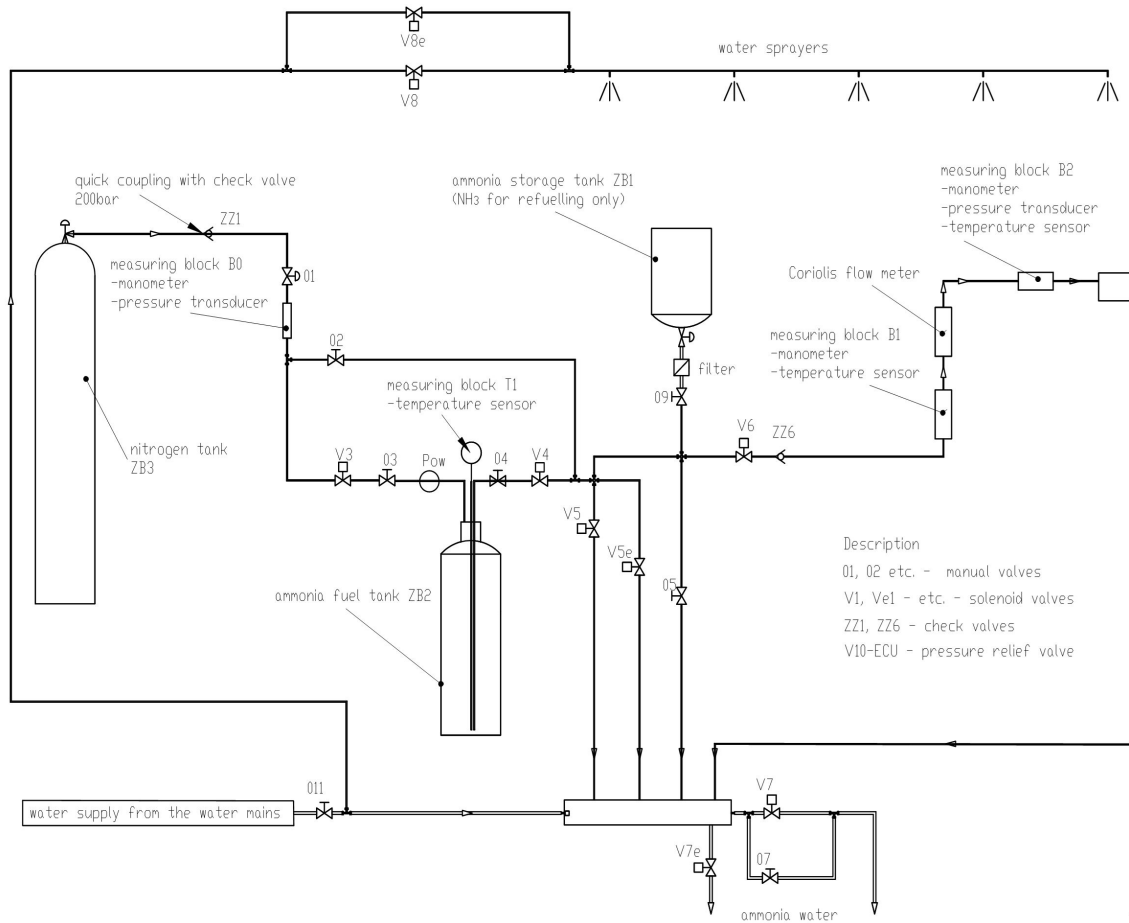


FIGURE 4.2: Diagram of the concept of connection of ammonia fuel line components [28].

4.2 Injectors

For direct injection of ammonia and biodiesel, BOSCH injectors have been selected from the automotive market. Therefore, the injector OSEF 83F02 328480 model is used for diesel/biodiesel, and the GDI injector 0 261 500 172 model is used for ammonia. Considering the modified cylinder head geometry and limited space in the engine head, the GDI injector was used for direct ammonia injection and installed in the center of the engine head. While biodiesel injector angularity inserted to cylinder as can be seen in Figure 4.3. The GDI injector derived from a four cylinder spark ignition engine with a maximum power of about 45 kW per cylinder which may face challenges in supplying an adequate dose of ammonia due to differences in the LHV of ammonia compared to gasoline. Consequently, future investigations needed to adjust the injection strategy and configurations.

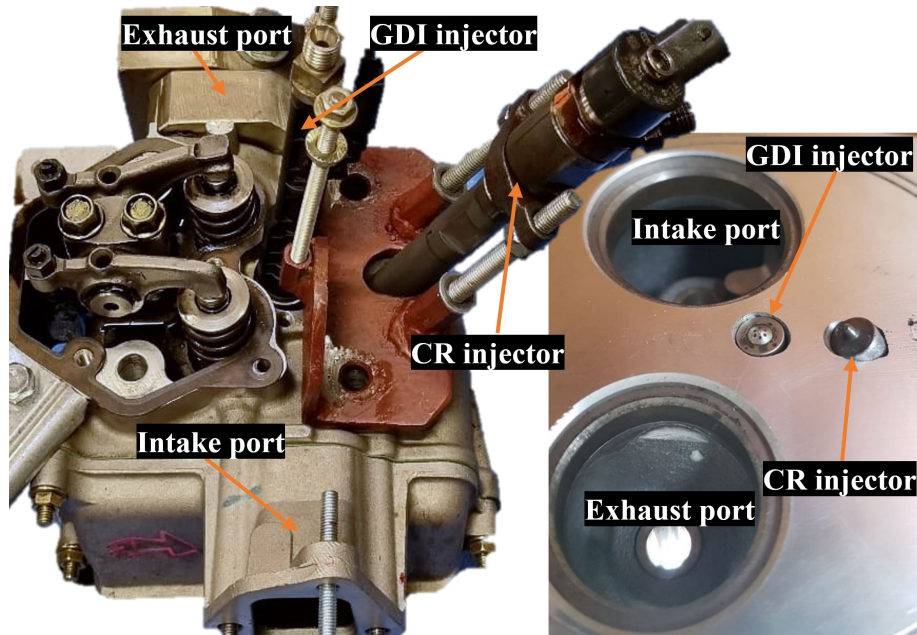


FIGURE 4.3: Photo of the engine head and location of GDI and biodiesel injectors on engine head

4.3 CFD

4.3.1 Designing full geometry of engine

The full engine geometry has been designed in SolidWorks and ANSYS SpaceClaim. The geometry includes the intake port, exhaust manifold, crevice and inlet and exhaust valves. The geometry was prepared according to the CONVERGE requirement such as valves positions and connection with port and engine head. The geometry will be imported in CONVERGE as a CAD file. The CAD geometry of engine for CFD simulation is shown in figure 4.4.

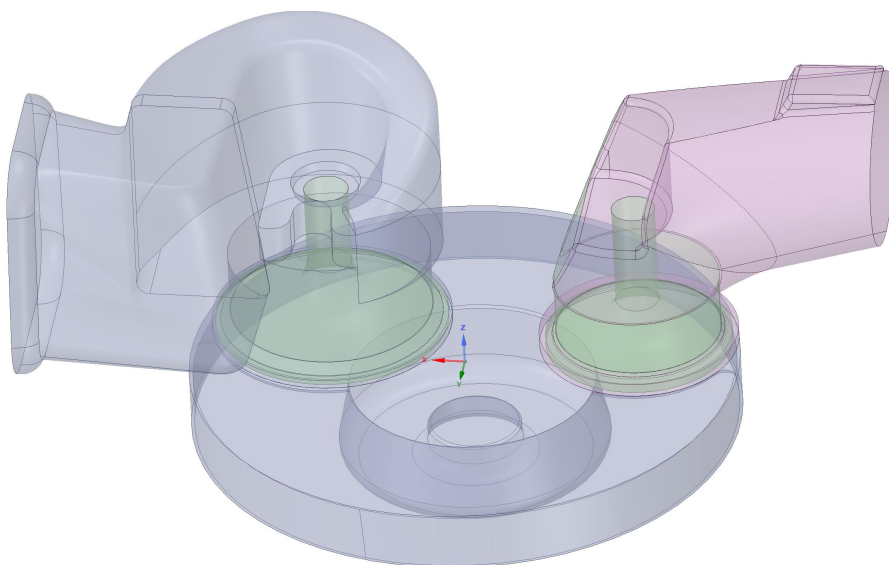


FIGURE 4.4: The the engine full geometry for CFD

Imported CAD geometry needs to be repaired using CONVERGE tools. Various cleaning and refining processes are utilized to clean the geometry. The Coarsen tool is applied to reduce the surface triangle density in overly refined areas of the geometry, ensuring an efficient simulation. The Boolean tools perform boolean operations between different parts of the geometry, while Healing efficiently repairs defects in the surface geometry [29]. Figure 4.5 displays the repaired CAD geometry in CONVERGE.

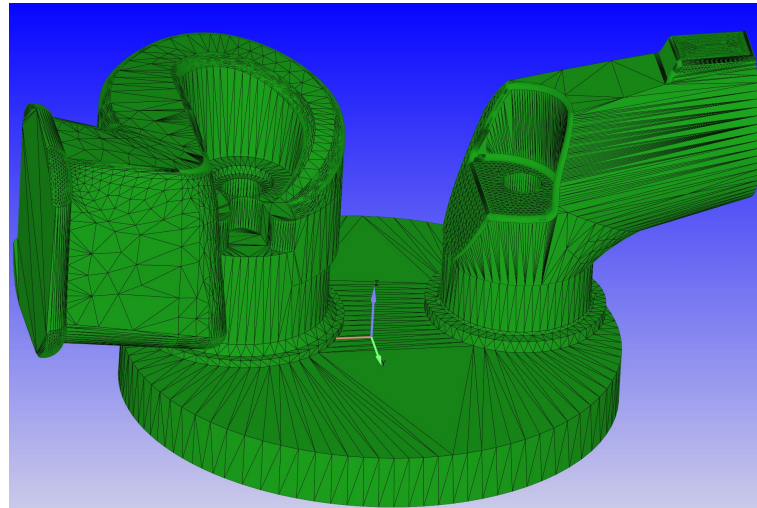


FIGURE 4.5: Repairing engine geometry in CONVERGE

4.3.2 CFD models

The detailed description of CFD simulation is provided in Section 3, "Numerical methods", of Paper III in Appendix A.3. Therefore, it covers boundary conditions, grid generation, spray, turbulence, combustion, and validation discussions. The following is a summary of the model used in the CFD simulation:

- Transient RANS
- RNG $k - \varepsilon$ turbulence model
- SAGE combustion
- Spray: Lagrangian solver
- Blob injection drop distribution (solid cone)
- Non-flash boiling spray
- Spray angle and injection parameters
- Spray break-up: (KH-RT) model
- Droplet collisions: The No Time Counter (NTC) method; dynamic drag model
- Evaporation: Frossling correlation with boiling

- Turbulent dispersion: O'Rourke approach
- O'Rourke and Amsden heat transfer model

4.4 Paper III

The paper III in Appendix A.3 entitled "**Experimental and numerical study on direct injection of liquid ammonia and its injection timing in an ammonia-biodiesel dual injection engine**" shows results of direct injection of liquid ammonia and CFD model. In this paper, experimental and CFD studies have been carried out to investigate the effects of direct injection of liquid ammonia, ammonia injection strategy (injection timing) and input AES on sprays, mixing process, combustion, ignition, engine performance and emission characteristics in the dual-fuel ammonia/biodiesel mode. The primary focus of this paper is to explore the possibilities of direct liquid ammonia injection within a dual direct injection engine. It highlights the importance of ammonia spray and optimizing injection timing to reduce emissions and improve combustion efficiency.

4.4.1 Scope of the study and tests

Based on previous chapters and the literature review, ammonia was applied in CI engines in the gaseous phase through introducing into the intake manifold. However, this can lead to high ammonia emissions in dual fuel CI engines due to unsuccessful flame propagation and uncontrolled combustion. Hence, combustion, emissions, and engine performance can be improved by injecting liquid ammonia directly into the cylinder. Therefore, in this work, the effects of liquid ammonia direct injection as well as AES with using biodiesel as pilot fuel are studied and compared with pure biodiesel operation. In addition, various ammonia injection timings are investigated in order to improve ammonia combustion and then reduce emissions. A CFD model is developed and validated with experimental data to study ammonia spray and combustion, as well as to predict local temperature and emissions.

The key areas addressed in this research include:

- The ammonia-biodiesel dual direct injection engine are studied.
- Various strategies for injecting liquid ammonia and its impacts on combustion, engine performance, and emissions are investigated.
- Enchanting the performance of the dual fuel engine by optimizing the injection timing of ammonia
- Addressing the source of ammonia emission for direct injection and port injection strategies.
- Developing a CFD model for dual direct injection engine to study ammonia spray, combustion, and emissions formation.

4.4.2 Experiments producer

In Paper III, all tests have been carried out on a retrofitted single-cylinder CI engine. The test rig, engine specifications, and equipment are similar to those in our previous work on port injection of gaseous ammonia [1, 2, 5, 6]. However, the ammonia

fueling system and injectors were changed for the direct injection of liquid ammonia and biodiesel. Since biodiesel is used as a pilot fuel, three of the six holes in the biodiesel injector were welded to inject a low amount of biodiesel under high pressure and with a long injection duration. The GDI injector was used without any modifications for the injection of ammonia. Two separate injection systems were used to adjust the injections of ammonia and biodiesel under different injection timings, pressures, or split injections.

In Paper III, two cases were designed to study ammonia biodiesel dual direct injection CI engine. Since liquid ammonia has a higher heat of evaporation and high mass flow due to low LHV compared to fossil fuels, it can reduce the in-cylinder temperature resulting in unsuccessful operation of the engine. Therefore, Case 1 investigates the effects of biodiesel substitution with liquid ammonia. The engine first runs with pure biodiesel at partial load that IMEP is 5.7 bar at a speed of 1500 rpm as a baseline for comparison. As the ammonia emission increases with higher loads, therefore, the engine is operated under a partial load condition. Thereupon, biodiesel is replaced by ammonia to achieve different AESs. For test case 1, the start of injections of ammonia and biodiesel are kept at -15 and -16 CAD, respectively, as shown in Table 1 from Appendix A.3. However, a higher AES above 50% caused a striking amount of unburned ammonia and hydrocarbons and a drop in power. Therefore, a maximum AES of 50% was achieved during the test for direct injection of liquid ammonia. Furthermore, case 2 investigates the impacts of the ammonia injection timing, while the biodiesel injection timing, the biodiesel and the ammonia injection durations, and both fuel mass flow rates are kept constant. Therefore, the start of injection of ammonia in -25, -20, -15, and -10 CAD are tested in case 2.

4.4.3 Conclusions

The results of Paper III showed higher AES significantly reduced the local cylinder temperature due to the strong cooling effects of ammonia, therefore, a maximum AES of 50% was achieved. Increasing AES to 50% decreased combustion duration and combustion phasing by 26.2 and 4.4 CAD, respectively. However, it deteriorated the indicated thermal efficiency by 1.3 percent point compared to pure biodiesel. Furthermore, retarding ammonia injection from -25 to -10 CAD significantly reduced NO_x , CO, and ammonia emissions by 31.4%, 39.6%, and 31.3%, respectively. Ultimately, the optimal operating condition was suggested when ammonia was injected at -10 CAD and biodiesel at -16 CAD with AES of 50%.

The main conclusions can be summarized below:

- The injection of liquid ammonia significantly reduced the local and average in-cylinder temperature during injection due to the strong cooling effects of ammonia compared to pure biodiesel operation. When AES is 50%, combustion only occurs when ammonia is injected between -25 to -10 CAD.
- Increasing liquid ammonia energy share slightly increased the ITE by 0.7 percent point and reached 38.5% for AES of 40% compared to only biodiesel operation. However, it then decreased to 36.5% when AES is 50% due to incomplete combustion.
- Ammonia notably reduced combustion duration by 26.2 CAD compared to pure biodiesel at the highest AES. Furthermore, the early injection of ammonia at -25 CAD delayed the start of combustion by 3.6 CAD relative to when it was injected at -10 CAD. Because, as ammonia is injected before biodiesel, it

reduces the in-cylinder temperature during biodiesel injection, resulting in a longer ignition delay.

- Liquid ammonia energy share diminished CO_2 and CO emissions by 47.4% and 51.2% when AES is 50% and SOI_{NH_3} is -15 CAD compared to pure biodiesel. Additionally, direct injection of ammonia significantly reduced ammonia emissions by approximately three times compared to the port injection strategy.
- Shifting the ammonia injection from -25 to -10 CAD markedly reduced all emissions when AES is 50%. Hence, NO_x , CO , and ammonia emissions decreased by 31.4%, 39.6%, and 31.3%, respectively, due to the improvement in ammonia combustion.

Chapter 5

Paper IV: Biodiesel injector configurations

5.1 Scope

The process of biodiesel injection and its related parameters have a significant impact on biodiesel evaporation, atomization and air/fuel mixing and consequently its combustion with ammonia. Since biodiesel is used as a pilot fuel with low injection mass, conducting a study on the number of nozzles and their orientations contributes to gain a deeper understanding of the combustion process. In this regard, the number of holes in the common rail injector is welded in various configurations to ensuing effective injection and combustion of biodiesel with liquid ammonia in the engine. This chapter aims to explore the influence of the number of nozzles on the performance, combustion, and emissions characteristics of liquid ammonia biodiesel dual direct injection engine. Furthermore, previous findings in Chapter 4 and Paper III revealed that late injection of ammonia at -10 CAD is the optimal injection timing of liquid ammonia [3]. Thus, the interaction of ammonia spray with biodiesel spray, as well as the cooling effect of ammonia spray, can significantly affect engine performance and emissions. Therefore, this chapter determines the optimal injection timing for biodiesel.

5.2 Biodiesel injector configurations

As biodiesel is used as a pilot fuel along with ammonia, the injected dose of biodiesel is lower compared to using biodiesel alone for the same operating point. Consequently, various configurations of biodiesel injector nozzles are blocked by using laser welding techniques to achieve longer injection duration. Figure 5.1 shows the welded nozzles of the injector before and after welding.

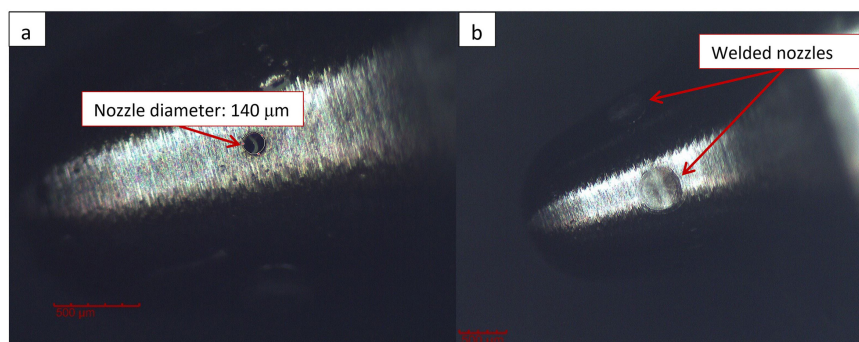


FIGURE 5.1: Biodiesel injector: a) open nozzle b) welded nozzle.

Therefore, the biodiesel spray of the injector from the experiment and CFD for injector with a) 3a, b) 3b, and C) 1 nozzle can be seen in Figure 5.2.

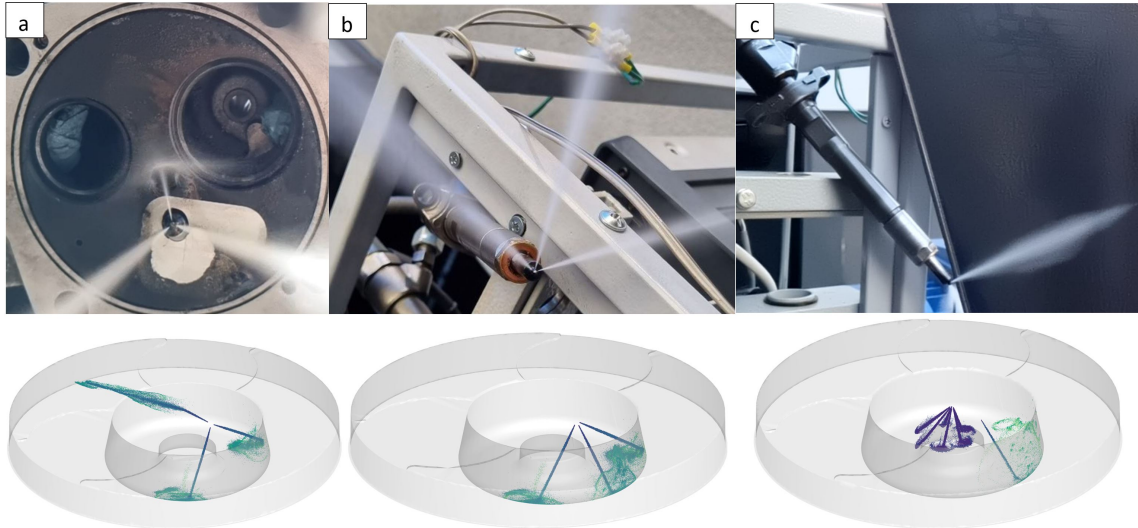


FIGURE 5.2: Different configuration of welded biodiesel injector and their corresponding CFD sprays: a) 3a, b) 3b, and C) 1 nozzle

The approach used for closing the nozzle hole of the injector is in this way that three of them are welded in two different configurations and spray orientations. Then, 4 and 5 nozzles are welded. Therefore, five different injectors with 6, 3a, 3b, 2, and 1 nozzle are studied, as can be seen in Figure 5.3. The welded and open nozzles in the biodiesel injector are shown in this figure along with biodiesel and ammonia sprays from CONVERGE. Also, the GDI injector nozzles and the locations of both GDI and biodiesel injectors on the engine head are fixed for all five configurations of injectors.

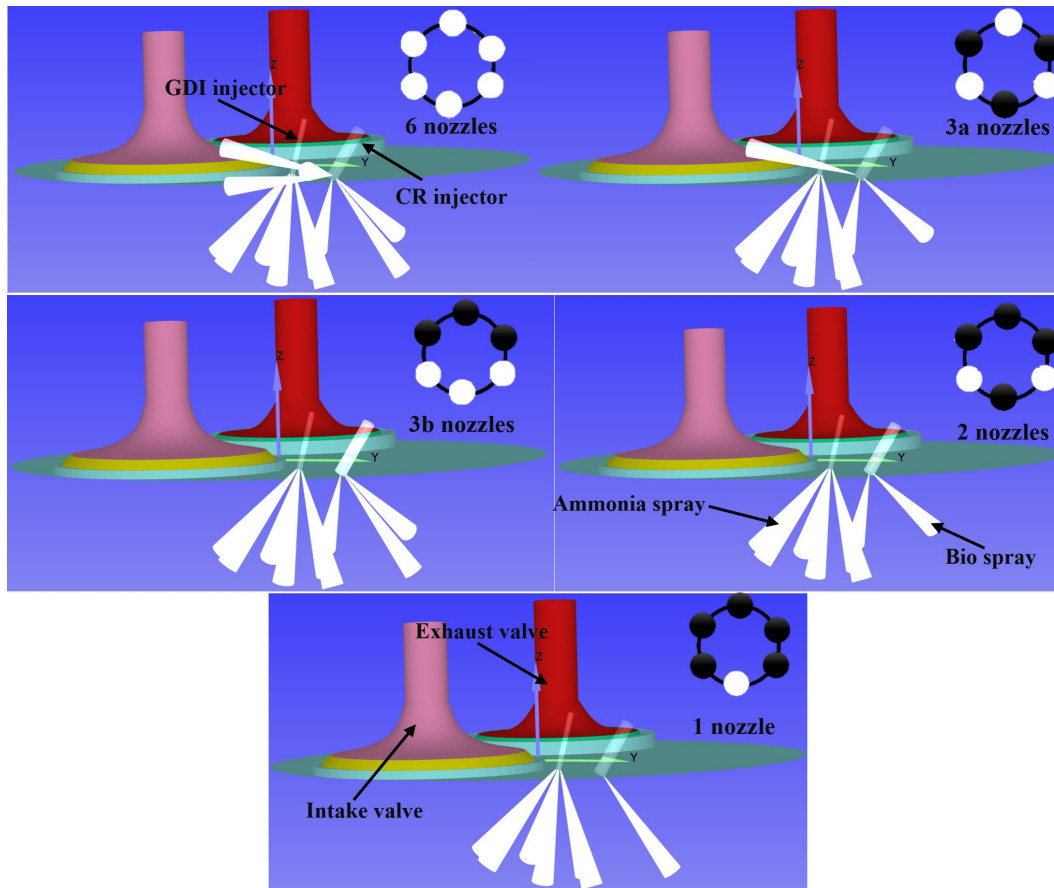


FIGURE 5.3: Various configurations of biodiesel spray and welded nozzles along with GDI injector and ammonia spray.

In paper III, the injector with 3a nozzles was used. However, one of the biodiesel sprays was directed towards the engine head and impacted the GDI injector as shown in Figure 5.2a. This resulted in increased emissions, reduced efficiency, and negative effects on the GDI injector functionality. Hence, Figure 5.4 illustrates the soot deposit in the GDI injector, leading to the closure of its nozzles. Therefore, using the CR injector with three nozzles on one side (Figure 5.2b) can prevent this deposit, result in decreasing emissions and enhancing engine performance.

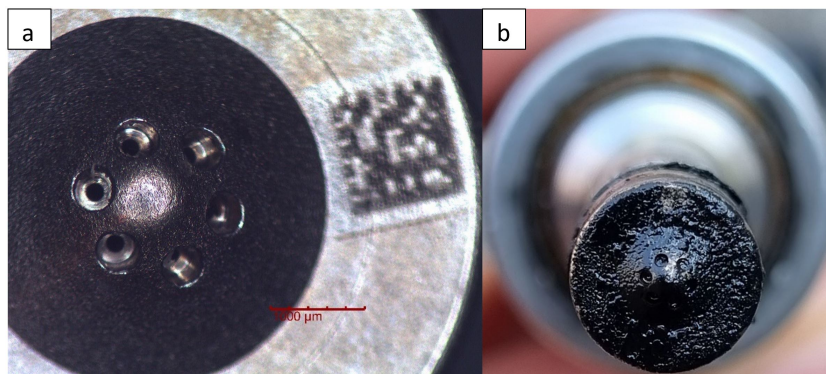


FIGURE 5.4: GDI injector a) before and b) after working in diesel engine

5.3 Paper IV

The paper IV in Appendix A.4 titled "Effects of biodiesel injector configuration and injection timing on the performance, combustion, and emissions characteristics of a liquid ammonia direct injection engine" presents results of biodiesel injector configurations and its injection timings. This study investigates the influence of the biodiesel injector configuration and its number of nozzles on the performance, combustion and emissions characteristics of the liquid ammonia-biodiesel dual direct injection engine. Therefore, the number of holes in the biodiesel injector was welded in various configurations for further improving injection. Furthermore, various injection timings of biodiesel were tested, ranging from -24 to -14 CAD, while the ammonia injection timing was kept at -10 CAD with AES of 50%.

5.3.1 Operating conditions and studied parameters

The paper IV investigates the biodiesel injector with fewer nozzles and its injection timing to achieve efficient combustion, improved engine performance, and reduce emissions. The research focuses on the following areas:

- Assessing the biodiesel injector with fewer nozzles.
- Optimization of the common rail injector configuration to enhance engine performance.
- CFD study of dual direct injection CI engine.
- Study of biodiesel injection timing in dual injection mode.
- Effects of blocking injector nozzles on CO , N_2O , CO_2 , NH_3 emissions.
- Analysis of the source of emission formation, including PM, CO , N_2O , and NH_3 .

5.3.2 Selected findings

By welding three nozzles from the original six-nozzle CR injector, the highest pressure peak and the highest indicated thermal efficiency were achieved. This new injector not only improved the combustion but also substantially reduced the emissions when compared to the original CR injector. The impact of injection timing was addressed through retarding injection timing from -24 to -14 CAD, revealing an improvement in combustion. Emissions were also analyzed, with decreasing the number of nozzles in the biodiesel injector leading to a longer injection duration, promoting the formation of a lean mixture during combustion, which significantly reduced CO emissions and resulted in a noticeable reduction in ammonia emissions. Furthermore, this reduction in the number of nozzles reduced NO_x emissions.

The main findings of this research are summarized as follows:

- The highest ITE and low emissions were achieved when biodiesel was injected at -16 CAD.

- When ammonia energy share is 50%, blocking three nozzles of the original six-nozzle injector results in a remarkable 29.2% reduction in ammonia emissions compared to the original injector. It also reduces CO emission from 26.9 to 8.9 g/kWh.
- The lowest N_2O emissions (115.0 ppm) at the earliest SOI of biodiesel -24 CAD.
- The number of biodiesel injector nozzles significantly impacts engine performance. By welding three nozzles from the original six-nozzle CR injector (3b nozzle), the highest pressure peak at 66.4 bar and the highest ITE of 39.7% were achieved, indicating the most effective combustion of liquid ammonia with biodiesel.

Chapter 6

Summary and conclusions

Ammonia is currently receiving more interest as a carbon-free alternative fuel for internal combustion engines. A promising energy carrier, easy to store and transport, being liquid, and non-carbon-based emissions which make ammonia a green fuel to decarbonize internal combustion engines and reduce greenhouse gas emissions. This thesis aims to experimentally and numerically study the use of ammonia as a primary fuel with pilot ignition of biodiesel in compression ignition engine. Two strategies were tested for the ammonia-fueled engine. In the first strategy, a single-cylinder diesel engine was retrofitted to introduce gaseous ammonia into the intake manifold, followed by the injection of a pilot dose of biodiesel into the cylinder to initiate combustion of the premixed ammonia-air mixture using the engine's existing injection system. In the second approach, the diesel engine was modified to install two common rail injection systems, allowing for the direct injection of liquid ammonia along with biodiesel as a pilot fuel into the cylinder. Moreover, a CFD model was developed and validated with experimental data to study ammonia/biodiesel sprays, ammonia cooling effects, combustion characteristics, and emissions formation. In addition, a developed 1D model is used to analyze the ammonia-fueled engine.

In the initial tests by using the first strategy, the engine was operated with biodiesel in low load and with a constant biodiesel mass flow rate, and then gaseous ammonia was introduced into the intake port to increase torque and power. The effects of various ammonia mass flow with two constant pilot doses of biodiesel on combustion, emissions, and engine performance were investigated and compared with respective pure biodiesel operations.

Subsequent work was carried out using the first strategy, testing the impacts of replacing diesel fuel with ammonia to the maximum possible diesel substitution in the compression ignition engine under full load conditions. Engine performance and emission characteristics are experimentally studied for various ammonia-diesel ratios in dual fuel mode. Furthermore, CO_2 equivalent greenhouse gas emissions were discussed to show the effectiveness of ammonia in reducing CO_2 equivalent emissions by considering N_2O emission.

The second part of the thesis focuses on the development of two injection systems for the direct injection of liquid ammonia and biodiesel. By using the second strategy, the effects of liquid ammonia injection and ammonia energy share on combustion, emissions, and engine performance were investigated and compared with pure biodiesel operation. Moreover, various ammonia injection timings were studied to improve ammonia/biodiesel combustion and reduce emissions. The CFD model was used to study ammonia spray and its combustion with biodiesel, flame propagation, and emissions formation, as well as to address unburned ammonia.

The final work investigated the influence of the biodiesel injector configuration

and its number of nozzles on the performance, combustion, and emissions characteristics of the liquid ammonia-biodiesel dual direct injection engine. Therefore, the number of holes in the biodiesel injector was welded in various configurations to improve injection, since biodiesel was used as a pilot fuel with less injected mass. Furthermore, various injection timings of biodiesel were tested.

The key findings of this thesis can be summarized as follows:

- A maximum AES of 84.2% was achieved by introducing gaseous ammonia into the intake manifold with the pilot ignition of diesel fuel.
- Increasing AES reduced CO_2 and CO emissions, but it led to an increase in ammonia emissions and NO_x .
- Increasing the AES resulted in a longer ignition delay time and a shorter combustion duration.
- The ammonia-diesel fueled engine significantly reduced greenhouse gas emissions by 3 times over 100 years scale at highest AES.
- Direct injection of liquid ammonia strategy significantly reduced ammonia emission compared to introducing gaseous ammonia to the intake manifold.
- Maximum AES of 50% was achieved for direct injection of liquid ammonia with biodiesel in reasonable engine operation.
- Direct injection of liquid ammonia significantly reduced the local and average in-cylinder temperature during injection as a result of the strong cooling effects of ammonia.
- The optimal injection timing for ammonia and biodiesel is -10 CAD for ammonia and -16 CAD for biodiesel. Therefore, liquid ammonia should be injected after biodiesel and close to TDC.
- Welding three out of the six nozzles of the biodiesel injector was shown to increase efficiency and reduce emissions.

In the end, the research and results of this thesis were used to develop and optimize the ammonia fueled compression ignition engine for powering the prototype agriculture tractor which was developed as part of the ACTIVATE project. The photo of ammonia fueled tractor is presented in figure 6.1.



FIGURE 6.1: Liquid ammonia-biodiesel fueled prototype agriculture tractor

References

- [1]E. Nadimi et al. "Effects of using ammonia as a primary fuel on engine performance and emissions in an ammonia/biodiesel dual-fuel CI engine". In: *International Journal of Energy research* (2022).
- [2]E. Nadimi et al. "Effects of ammonia on combustion, emissions, and performance of the ammonia/diesel dual-fuel compression ignition engine". In: *Journal of the Energy Institute* (2022).
- [3]Ebrahim Nadimi et al. "Experimental and numerical study on direct injection of liquid ammonia and its injection timing in an ammonia-biodiesel dual injection engine". In: *Energy* 284 (2023), p. 129301.
- [4]Ebrahim Nadimi et al. "Effects of biodiesel injector configuration and its injection timing on performance, combustion and emissions characteristics of liquid ammonia dual direct injection engine". In: *Journal of the Energy Institute* (2024), p. 101605.
- [5]Kacper Kuta et al. "Ammonia CI engine aftertreatment systems design and flow simulation". In: *Combustion Engines* 61 (2022).
- [6]Mateusz Proniewicz et al. "Energy and Exergy Assessments of a Diesel-, Biodiesel-, and Ammonia-Fueled Compression Ignition Engine". In: *International Journal of Energy Research* 2023 (2023).
- [7]Genovaitė Liobikienė and Mindaugas Butkus. "The European Union possibilities to achieve targets of Europe 2020 and Paris agreement climate policy". In: *Renewable Energy* 106 (2017), pp. 298–309.
- [8]PK Senecal and Felix Leach. "Diversity in transportation: Why a mix of propulsion technologies is the way forward for the future fleet". In: *Results in Engineering* 4 (2019), p. 100060.
- [9]T Venugopal et al. "Experimental study of hydrous ethanol gasoline blend (E10) in a four stroke port fuel-injected spark ignition engine". In: *International journal of energy research* 37.6 (2013), pp. 638–644.
- [10]Chunhua Sun et al. "Experimental study of effects of exhaust gas recirculation and combustion mode on combustion, emission, and performance of DME-methanol-fueled turbocharged common-rail engine". In: *International Journal of Energy Research* 46.3 (2022), pp. 2385–2402.
- [11]BK Venkanna and C Venkataramana Reddy. "Direct injection diesel engine performance, emission, and combustion characteristics using diesel fuel, nonedible honne oil methyl ester, and blends with diesel fuel". In: *International Journal of Energy Research* 36.13 (2012), pp. 1247–1261.
- [12]Agustin Valera-Medina et al. "Ammonia for power". In: *Progress in Energy and Combustion Science* 69 (2018), pp. 63–102.
- [13]A Valera-Medina et al. "Review on ammonia as a potential fuel: from synthesis to economics". In: *Energy & Fuels* 35.9 (2021), pp. 6964–7029.
- [14]Agung Tri Wijayanta et al. "Liquid hydrogen, methylcyclohexane, and ammonia as potential hydrogen storage: Comparison review". In: *International Journal of Hydrogen Energy* 44.29 (2019), pp. 15026–15044.
- [15]Aaron J Reiter and Song-Charng Kong. "Demonstration of compression-ignition engine combustion using ammonia in reducing greenhouse gas emissions". In: *Energy & Fuels* 22.5 (2008), pp. 2963–2971.
- [16]AVL Boost. "2-Theory". In: *AVL List GmbH* 769 (2013).
- [17]Şehmus Altun et al. "Exhaust emissions of methanol and ethanol-unleaded gasoline blends in a spark ignition engine". In: (2013).

- [18]Georg Noske. *A quasi-dimensional model to describe the combustion process in the gasoline engine*. VDI-Verlag, 1988.
- [19]Simeon Iliev. "A comparison of ethanol and methanol blending with gasoline using a 1-D engine model". In: *Procedia Engineering* 100 (2015), pp. 1013–1022.
- [20]Ii Vibe. *Combustion and Cycle Process in Combustion Engines German translation from Russian by Dr. Joachim Heinrich, published under the title: Brennverlauf und Kreisprozess von Verbrennungsmotorenby*. 1970.
- [21]Gerhard Woschni. *A universally applicable equation for the instantaneous heat transfer coefficient in the internal combustion engine*. Tech. rep. SAE Technical paper, 1967.
- [22]Konstantin Pattas and G H "a fner. "Nitric oxide formation during gasoline engine combustion". In: *MOTORTECHN. Z.* 34.12 (1973).
- [23]Craig T Bowman. "Kinetics of pollutant formation and destruction in combustion". In: *Progress in energy and combustion science* 1.1 (1975), pp. 33–45.
- [24]Angelo Onorati, Giancarlo Ferrari, and G D'Errico. "1D unsteady flows with chemical reactions in the exhaust duct-system of SI engines: predictions and experiments". In: *SAE Transactions* (2001), pp. 738–752.
- [25]Raffael A Schubiger, Konstantinos Boulouchous, and Meinrad K Eberle. "Ruß-formation and oxidation during diesel engine combustion". In: *MTZ motor technology magazine* 63.5 (2002), pp. 342–353.
- [26]Stefano Frigo and Roberto Gentili. "Analysis of the behaviour of a 4-stroke Si engine fuelled with ammonia and hydrogen". In: *International Journal of Hydrogen Energy* 38.3 (2013), pp. 1607–1615.
- [27]James J MacKenzie and William H Avery. *Ammonia fuel: the key to hydrogen-based transportation*. Tech. rep. Inst. of Electrical and Electronics Engineers, Piscataway, NJ (United States), 1996.
- [28]ACTIVATE Project. 2020-2023. URL: <https://ammoniaengine.org/>.
- [29]Keith J Richards, Peter K Senecal, and Eric Pomraning. "CONVERGE 3.0". In: *Convergent Science, Madison, WI* (2021).

Appendix A

A.1 Paper I



Received: 7 March 2022 | Revised: 23 May 2022 | Accepted: 29 May 2022

DOI: 10.1002/er.8235

RESEARCH ARTICLE

INTERNATIONAL JOURNAL OF
ENERGY RESEARCH WILEY

Effects of using ammonia as a primary fuel on engine performance and emissions in an ammonia/biodiesel dual-fuel CI engine

Ebrahim Nadimi¹ | Grzegorz Przybyła¹ | David Emberson² |
Terese Løvås² | Łukasz Ziółkowski¹ | Wojciech Adamczyk¹ ¹Department of Thermal Technology, Faculty of Energy and Environmental Engineering, Silesian University of Technology, Gliwice, Poland²Department of Energy and Process Engineering, Norwegian University of Science and Technology, NTNU, Trondheim, Norway**Correspondence**Ebrahim Nadimi, Department of Thermal Technology, Faculty of Energy and Environmental Engineering, Silesian University of Technology, Gliwice, Poland.
Email: enadimi@polsl.pl**Funding information**

POLNOR, Grant/Award Number: NOR/POLNOR/ACTIVATE/0046/2019-00; AVL List

Summary

Ammonia is a promising alternative fuel that can replace current fossil fuels. Hydrogen carrier, zero carbon base emissions, liquid unlike hydrogen, and can be produced using renewable resources, making ammonia a future green fuel for the internal combustion engine. This study aims to show the procedure of utilizing ammonia as a primary fuel with biodiesel in a dual-fuel mode. Hence, a single-cylinder diesel engine was retrofitted to inject ammonia into the intake manifold, and then a pilot dose of biodiesel is sprayed into the cylinder to initiate combustion of the premixed ammonia-air mixture. The effects of various ammonia mass flow rates with a constant biodiesel dose on engine performance and emissions were investigated. Furthermore, a one-dimensional model has been developed to analyze the combustion of ammonia and biodiesel. The results reveal that 69.4% of the biodiesel input energy can be replaced by ammonia but increasing the ammonia mass flow rate slightly decreases the brake thermal efficiency. Moreover, increasing the ammonia load contribution significantly reduced the emissions of CO_2 , CO , and HC but increased the emission of NO . It was found that ammonia delayed the start of combustion by 2.6CAD compared with pure biodiesel due to the low in-cylinder temperature and the high resistance of ammonia to autoignition. However, the combustion duration of biodiesel/ammonia decreased 19CAD compared with only biodiesel operation at full load, since most of the heat was released during the pre-mixed combustion phase.

Highlights

- Ammonia biodiesel dual-fuel CI engine has been investigated experimentally.
- Maximum 69.4% of the input energy is provided by ammonia in reasonable operation.
- Higher ammonia contribution in the engine load delays the SOC and decreases the combustion duration.

This is an open access article under the terms of the [Creative Commons Attribution](#) License, which permits use, distribution and reproduction in any medium, provided the original work is properly cited.

© 2022 The Authors. *International Journal of Energy Research* published by John Wiley & Sons Ltd.

- Significant reduction in CO_2 , CO , and HC emissions in the ammonia-/bio-diesel-fueled engine.

KEYWORDS

ammonia, biodiesel, CI engine, dual fuel, emissions

1 | INTRODUCTION

Fossil fuels, greenhouse gases, and their effects on climate change are required to be replaced by renewable energy sources to slow down the emission of carbon dioxide. To combat these worldwide challenges, the legitimately binding international agreement on climate change, the 2015 Paris Agreement provided a global framework for reducing greenhouse gases in the next decades. Hence, the European Union countries have an aim to decrease the emissions of greenhouse gases by 55% by 2030.¹ Therefore, alternative carbon-free fuels, such as ammonia and hydrogen, are a good way to replace fossil fuels and stop the emission of carbon dioxide. However, the big problem with hydrogen is storing in the high pressure at a reasonable cost because of the extremely low density of gaseous hydrogen. Among all green fuels such as ethanol,² methanol,³ and methyl ester,⁴ ammonia (NH_3) is currently attracting a lot of interest as a potential alternative to fossil fuels.⁵⁻⁷ It is a good hydrogen carrier (17.8% by mass), is liquid and easy to store under low pressure, and is also one of the most produced chemicals in the world. Additionally, ammonia already has a great established infrastructure for distribution, production, and handling, as it is used as fertilizer in the agriculture industry. However, the practical usage of liquid ammonia as fuel for internal combustion engine (ICE) requires many technical and operational difficulties to be surmounted. Ammonia has different characteristics from common fossil fuels. High resistance to auto ignition, low flame speed, and corrosivity are challenges of ammonia that make it even harder to apply in ICE.⁸⁻¹⁰ The beginning of using ammonia as fuel goes back to 1943 in Belgium due to a shortage of diesel fuel during World War Two.¹¹ Subsequently, in the 1960s, the possibility of applying ammonia to ICE was examined, providing primary guidance concerning ammonia as a fuel in ICE.¹²⁻¹⁵

In recent years, researchers have been working to overcome the challenges of using ammonia as fuel for both CI and spark ignition (SI) engines. However, a new review paper¹⁶ shows that most research is currently concentrated in SI engines because ammonia is more favorable for use in SI engines. Schönborn¹⁷ by zero-dimensional chemical kinetic calculation estimated the minimum required Compression Ratio (CR) of 27 to ignite pure ammonia in the CI

engine. Grannell et al.¹⁸ investigated mixtures of gasoline and gaseous ammonia in the SI engine in varied ammonia/gasoline ratios, as well as various CR. Their findings revealed that a significant portion of gasoline can be substituted with ammonia. Nevertheless, they suggested a CR of 10:1 for the ammonia gasoline dual-fuel SI engine. Salek et al.¹⁹ numerically studied the impact of adding 10% of ammonia on engine performance and emissions in a wide range of engine speeds for the SI engine using AVL BOOST software. The results show that 10% of ammonia injection reduces the in-cylinder temperature by 50 K, resulting in a significant reduction in NO_x emissions by 50% throughout the different engine speeds. Furthermore, the needed minimum octane number of gasoline for avoiding knock was decreased by the injection of 10% ammonia, indicating that the injection of ammonia could clearly have an effect on engine failure. Nevertheless, it imposed some negative effects on reducing BSFC and increasing HC and CO emissions. Yapicioglu and Dincer²⁰ conducted experimental research on injecting ammonia in SI engine. The primary objective of this study is to utilize ammonia to reduce carbon emissions. Based on their findings, introducing ammonia reduced the gasoline engine's CO_2 emission. In addition, it resulted in a significantly reduction of engine energy and exergy efficiency. The recent paper carried out by Mounaim-Rousselle et al.²¹ provides new information on operation limits in ammonia-fueled gasoline direct injection (GDI) SI engine, especially to find the lowest possible load limit when the engine is fed with pure ammonia. However, they extended the operating limitations by adding less than 10% of hydrogen to ammonia. Although the ammonia-fueled engine does not produce carbon-based emissions, it can emit high NO_x emissions. However, their results show that adding 10% of H_2 to ammonia significantly decreases NO_x emissions up to 40%. Lhuillier et al.²² experimentally investigated engine performance, emissions, and combustion characteristics of an SI engine fueled with premixed ammonia, hydrogen, and air mixtures. They tested mixtures of gaseous ammonia with different portions of hydrogen as well as various equivalence ratios. Their results illustrate that the higher hydrogen fraction in the stoichiometry mixture decreases the indicated efficiency, but the efficiency increases when the equivalence ratio decreases. Moreover, when the equivalence ratio is raised above stoichiometry, the unburned ammonia rises significantly. Sechul et al.²³

experimentally studied ammonia blended with natural gas in the SI engine. According to their findings, CO_2 emissions were reduced by almost 28% when natural gas was replaced with ammonia for more than 50% of the volume portion. However, considering combustion efficiency and emissions, the air/fuel ratio reached a high limit around lambda 1.5. As mentioned above, using only ammonia in CI engines requires high CR; hence, ammonia can be utilized as a secondary fuel with a small dose of diesel or biodiesel to ignite combustion in a dual-fuel mode without considerable modification in the engine.²⁴ Reiter and Kong²⁵ investigated the impacts of injecting gaseous ammonia into the intake manifold on the emissions and combustion characteristics of the CI engine. They tested different ratios of ammonia/diesel to obtain constant power in the operating range of 40% to 60% of the input energy provided by ammonia to achieve the optimal fuel efficiency. Their experimental results show that when the ammonia energy contributes to more than 60% of the total energy, the NO emissions rise significantly, but soot emissions decreased for a higher ammonia ratio. Their other similar work²⁶ proved that engine operation was successful for 95% of energy supplied by ammonia; however, the unburned NH_3 was significantly higher due to unsuccessful combustion. Nevertheless, reasonable efficiency can be achieved if 80% of the total energy is supplied by ammonia.

A novel combustion strategy for using ammonia in CI engine has been suggested by Lee and Song²⁷ to reduce NO emissions. Parametric research has been performed to validate and evaluate the characteristics of the ammonia-fueled engine by applying the suggested combustion strategy. They discussed engine operation characteristics according to the ammonia dose, start of injection (SOI) timing, and NO emissions. Their findings indicate that for constant amount of ammonia and diesel fuel, NO production is a strong function of SOI instead of the load of the engine. Hence, NO emission was reduced from 8500 ppm to 3040 ppm by changing the SOI timing. Recently, Yousefi et al.²⁸ investigated the impacts of the ammonia energy fraction with diesel injection timing on engine performance and emissions. Their results reveal that the NO_x emissions decreased by 58.8% when the ammonia energy percentage was increased from 0 to 40%. However, it increased the N_2O emission, which has a higher greenhouse effect.

In recent years, there has been renewed enthusiasm for utilizing ammonia as a primary fuel for ICE. Nevertheless, it is evident from the above literature review that there is a significant research gap in ammonia-/biodiesel-fueled CI engine. Comprehensive research has to be done to effectively utilize ammonia while reducing emissions in the diesel engine. Therefore, in this paper, a strategy of using ammonia with biodiesel as a secondary fuel is proposed to operate with the lowest possible biodiesel and high amount of ammonia in different loads with reasonable operation. For the first

time, ammonia with biodiesel dual-fuel CI engine has been studied. Hence, the effects of various ammonia mass flows with two constant pilot doses of biodiesel on combustion, emissions, and engine performance are investigated and compared with pure biodiesel operation. Additionally, a 1D model is built and developed to analyze ammonia with biodiesel combustion characteristics.

2 | TEST RIG AND EXPERIMENTAL SETUP

2.1 | Test rig

The tests were performed on a single-cylinder 4-stroke Lifa diesel engine C186F with forced air cooling system. The engine's main specifications are listed in Table 1. The engine has been retrofitted to operate with port injection of ammonia and then will be installed in the tractor for use in the agricultural sector. Gaseous ammonia at 2 bar was injected into the port near the inlet valve, through the pipe inserted into the intake manifold, and the mass flow of ammonia was measured using a Coriolis flow meter. A surge tank has been installed in the intake manifold to measure the constant air mass flow rate, and also to avoid the backflow of ammonia from the intake manifold to the environment. The temperature of the port, exhaust gas, and ambient as well as the air and ammonia mass flow rate were monitored by LabVIEW software and National Instruments hardware. The engine has been coupled by the vibration damping shaft to the

TABLE 1 Engine main specifications

Engine information	Valves	Units
Engine type	4 stroke, CI	
Number of cylinders	1	
Bore × Stroke	86 × 70	mm × mm
Compression ratio	16.5:1	
Maximum power (3500 rpm)	6.4	kW
Piston shape	ω bowl	
IVO	14	BTDC
IVC	45	ABDC
EVO	50	BBDC
EVC	16	ATDC
SOI	15.5	BTDC
Injection pressure	200	bar
Intake temperature	10	°C
Intake pressure	93.19	kPa
Engine speed	1500	rpm

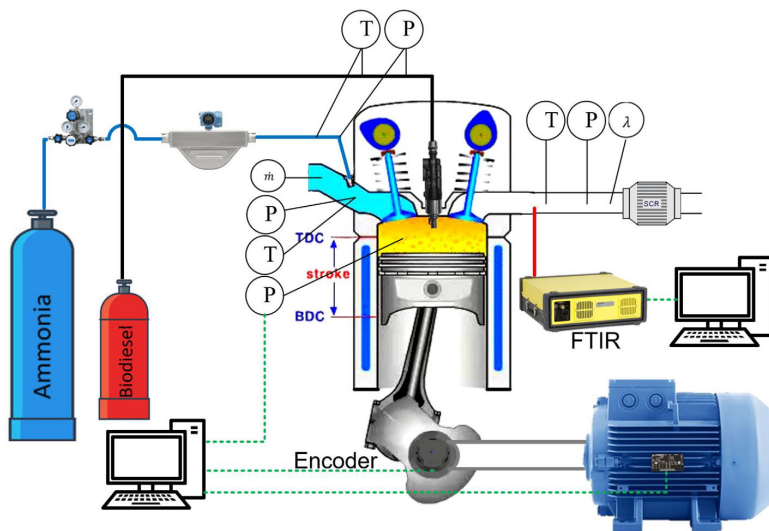


FIGURE 1 Schematic of the experiment for the ammonia biodiesel dual-fuel engine. P and T represent the measurement points of pressure and temperature, respectively

electric motor to adjust the engine load and speed for the test. The in-cylinder pressure was measured with a resolution of 1024 measuring points per one shaft revolution and for 100 consecutive cycles using a piezoelectric pressure transducer. An encoder with 0.35 CA resolution was installed on the engine shaft to sample the electrical signal from the pressure transducer to identify the piston position at TDC. A sample of the exhaust gas was analyzed using Fourier transform infrared spectroscopy (FTIR), gas analyzer, and particulate matter (PM). The FTIR is a Gasetm DX4000 gas analyzer, which is operated by Calcmnet software. The Calcmnet can simultaneously analyze 50 gas components in wet and corrosive gas streams, and it has various spectrum libraries in different ranges to determine the concentration of each species. However, the ammonia concentration was beyond the measurement ranges, so it is not available. The FTIR has an accuracy of less than 2%. Furthermore, the PM measurement device has a precision of less than $\pm 3\%$ and measures particle sizes from 0.04 to 10 μm with particle mass concentrations up to 250 mg/m^3 under normal conditions and dry exhaust gas. Each parameter was measured every second for 5 min in the steady-state running engine for each operating point.

2.2 | Experiment procedure

Figure 1 illustrates the schematic of the test. In this figure, P and T show the measuring points for pressure and temperature. In all tests, the rotational speed has been fixed at 1500 rpm. The engine has been operated with biodiesel at different loads to determine the baseline. The approach

for ammonia port injection is defined in this way that the engine is operated with biodiesel in low load and with constant biodiesel mass flow rate, and then ammonia is injected to increase torque and power. Hence, Table 2 presents the procedure of the two sets of ammonia and biodiesel tests. In the first test, biodiesel load contribution (BLC) was 10%, ie, the engine has been operated with biodiesel and the measured load and biodiesel mass flow rate were 10% and $\dot{m}_{\text{bio}} = 0.107\text{g}/\text{s}$, respectively. Then, the ammonia mass flow is increased to obtain higher loads at the same operating point as the biodiesel baseline. The second test is similar to the test one, but with this difference that the engine was run with biodiesel at a low load of 3.5% with constant $\dot{m}_{\text{bio}} = 0.082\text{g}/\text{s}$. By increasing the ammonia mass flow, ammonia load contribution (ALC), and ammonia energy contribution (AEC), which is defined in Equation (1), have been increased since the biodiesel mass flow rate and the BLC were constant in the two sets of tests. The maximum input AEC is 59.1% and 69.4% at full load for test one with $\dot{m}_{\text{bio}} = 0.107\text{g}/\text{s}$, and test two with $\dot{m}_{\text{bio}} = 0.082\text{g}/\text{s}$, respectively. However, reducing the biodiesel mass flow lower than $\dot{m}_{\text{bio}} = 0.082\text{g}/\text{s}$ to replace it with more ammonia to obtain higher input AEC causes a significant amount of ammonia slip. The exhaust gas sample is interred to FTIR, gas analyzer, and PM measurement before SCR.

2.3 | One-dimensional model and data analysis

One-dimensional (1D) model of ammonia/biodiesel dual-fuel engine was built and developed using the AVL

TABLE 2 Ammonia/biodiesel tests conditions

NO.	BLC	ALC	Load	\dot{m}_{bio}	\dot{m}_{NH_3}	w_{NH_3}	\dot{m}_{air}	AEC	
Unit	%	%	%	g/s	g/s	kg/kg	g/s	%	
Set 1	1	10.0	10.0	20	0.107	0.045	0.29	6.47	17.1
	2	10.0	25.3	35	0.107	0.100	0.48	6.25	32.2
	3	10.0	37.1	47	0.107	0.141	0.56	6.16	40.0
	4	10.0	48.8	59	0.107	0.186	0.63	5.97	46.6
	5	10.0	60.6	71	0.107	0.227	0.67	5.83	51.0
	6	10.0	78.2	88	0.107	0.293	0.73	5.63	57.2
	7	10.0	90.0	100	0.107	0.327	0.75	5.44	59.1
Set 2	8	3.5	16.5	20	0.082	0.107	0.56	6.36	40.0
	9	3.5	31.8	35	0.082	0.157	0.65	6.13	49.2
	10	3.5	43.6	47	0.082	0.213	0.72	6.02	55.6
	11	3.5	55.3	59	0.082	0.260	0.76	5.94	60.7
	12	3.5	67.1	71	0.082	0.293	0.78	5.69	65.0
	13	3.5	84.7	88	0.082	0.361	0.81	5.47	67.1
	14	3.5	96.5	100	0.082	0.398	0.82	5.27	69.4

TABLE 3 Biodiesel properties

Property	Value	Unit
Name	Bioester	-
C	75.33	kg/kg
H	13.97	kg/kg
O	10.7	kg/kg
Molecular weight	200	kg/kmol
LHV	37.4	MJ/kg
Cetane number	51.0	-
Density	860	kg/m ³
Cold point	-3	°C
Flash point	101	°C
Stoichiometric air/fuel ratio	12.96	-

BOOST software. In addition, the AVL Burn utility was used for post-processing of the measured data, analyzing the pressure profile, and calculating the net heat release rate (HRR). The HRR has been determined from the measured pressure trace through the inverse procedure. Additionally, the combustion timing indicators have been calculated by mass fraction burned (MFB). Hence, the MFB diagram, combustion duration (CD), start of combustion (SOC), and the location of MFB 10%, 50%, 90% (CA10, CA50, and CA90) have been calculated using AVL software. In this study, the SOC refers to the location of the rising point on the MFB curve in the Vibe function.²⁹

Biodiesel fuel (Bioester B100) was provided by Orlen Poludnie company in Poland. The LHV of biodiesel was measured at 37.400 MJ/kg; however, the ammonia LHV is 18.6 MJ/kg.³⁰ The elementary analysis and properties

of biodiesel are listed in Table 3. In this work, the AEC is defined as the ratio of the ammonia input energy to the total input energy in the dual-fuel model in Equation (1).

$$AEC = \frac{\dot{m}_{NH_3} \times LHV_{NH_3}}{\dot{m}_{bio} LHV_{bio} + \dot{m}_{NH_3} LHV_{NH_3}} \quad (1)$$

The friction power of the electric motor at 1500 rpm has been measured, and it is about 0.52 kW. The torque and power are calculated after subtracting the friction power. Therefore, the brake thermal efficiency (BTE) of the engine is defined as follows:

$$BTE = \frac{P_b}{\dot{m}_{bio} \times LHV_{bio} + \dot{m}_{NH_3} \times LHV_{NH_3}} \quad (2)$$

The concentrations of each species were measured during 5 min of steady-state operation in molecules per million in ppm unit and then recalculated according to Equation (3) in 5% of O₂ since the concentration of each species varies for different loads.³¹ Additionally, the brake-specific emission in g/kW.h units is calculated.

$$(X_i)_{5\%O_2} = (X_i)_m \left[\frac{20.9\% - 5\%}{20.9\% - (O_2)_m} \right] \quad (3)$$

Where (X_i)_m and (O₂)_m are the measured concentration of each species and the measured concentration of O₂, respectively.

The equivalent brake-specific fuel consumption is defined in Equation (4) in dual-fuel engine.³²

$$BSFC = \frac{\dot{m}_{bio} + \dot{m}_{NH_3} \frac{LHV_{NH_3}}{LHV_{bio}}}{P_b} \quad (4)$$

Measurement uncertainty has been evaluated through statistical analysis. The SD of the emissions and data obtained from the test rig were calculated using the Equation (5)^{33,34}:

$$SD = \sqrt{\frac{\sum_{i=1}^n (X_i - \bar{X})^2}{(n-1)}} \quad (5)$$

where X_i and \bar{X} are the measured and mean values, respectively, and n is the number of measurements.

Therefore, uncertainty (U) is defined by^{33,34}:

$$U = \frac{SD}{\sqrt{n}} \quad (6)$$

Furthermore, the coefficient of variation (COV) of 100 continuous cycles for IMEP, P_{max} , and α_{max} was obtained. Therefore, $COV_{P_{max}}$ and $COV_{\alpha_{max}}$ were less than 1% for all tests. However, COV_{IMEP} was less than 2% and 4% for biodiesel and ammonia/biodiesel operations, respectively.

3 | RESULTS

3.1 | Effects of ammonia on engine performance

As mentioned above, the ammonia injection strategy was carried out in such a way that the engine is operated first with only biodiesel at $\dot{m}_{bio} = 0.107\text{g/s}$ in 10% load and secondly at $\dot{m}_{bio} = 0.082\text{g/s}$ in 3.5% load. Hereafter, the ammonia mass flow is increased to obtain the same loads as biodiesel. The maximum power ($P_{b_{max}}$) of the engine at 100% of the load is 3.190 kW, of which 2.356 and 2.576 kW of $P_{b_{max}}$ are provided by ammonia for the tests set 1 and set 2, respectively. The mass flow of ammonia was increased to obtain the same power as only biodiesel tests; however, the brake efficiency of the dual-fuel mode is slightly lower compared with the baseline, as shown in Figure 2. The BTE increases with increasing load and reaches 32.27% at load 88% after that decreased to 31.89% at full load for the biodiesel test. This decline in BTE at full load is due to the high amount of unburned hydrocarbons such as HC, CO, and soot together with high exhaust gas temperature (Figure 3). However, ammonia by decreasing the emission of unburned hydrocarbons

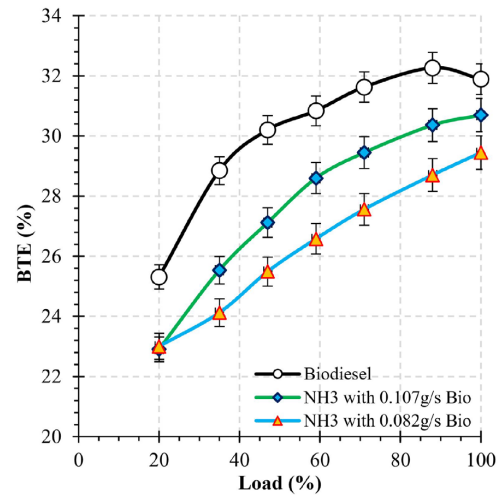


FIGURE 2 Brake thermal efficiency of the ammonia-/biodiesel-fueled engine compared along with biodiesel

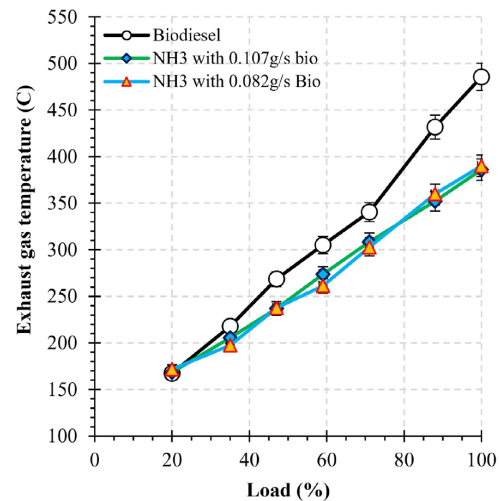


FIGURE 3 Effects of ammonia on exhaust gas temperature compared with biodiesel

obtains a BTE of 30.69% at full load in set 1 test. Moreover, the increase in BTE at higher loads is due to a decrease in the ratio between friction losses and the engine indicated work, resulting in a decrease in the friction power contribution to brake power. Figure 2 also shows that by reducing the biodiesel mass flow rate from $\dot{m}_{bio} = 0.107\text{g/s}$ to $\dot{m}_{bio} = 0.082\text{g/s}$ to obtain a higher ALC, decreases the BTE due to unsuccessful combustion of ammonia with biodiesel, causing a high amount of unburned NH_3 .

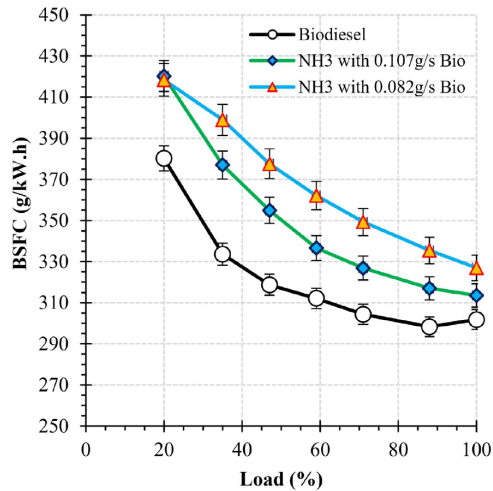


FIGURE 4 Brake-specific fuel consumption of the ammonia/biodiesel with the biodiesel tests corresponds to the engine load

As can be observed in Figure 3, the exhaust gas temperature of the biodiesel test is higher compared with the dual ammonia/biodiesel tests. For example, EGT is reduced by 100 from 485 K for biodiesel to 385 K for ammonia/biodiesel tests at full load due to the lower in-cylinder temperature during the combustion stroke since the in-cylinder temperature of ammonia-/biodiesel-fueled engine is lower than the biodiesel.³⁵ Moreover, the CD of ammonia/biodiesel combustion is lower than that of biodiesel at higher loads, which will be discussed in the next section. Therefore, less heat is released during the expansion stroke, resulting in a temperature drop in the working medium and ultimately a lower exhaust temperature in ammonia/biodiesel operation compared with pure biodiesel, as can be observed in Figure 3. The SCR is activated around 300°C,³⁶ therefore it is only active in higher loads.

Figure 4 illustrates the equivalent BSFC for ammonia/biodiesel tests along with only biodiesel under various loads. The BSFC of ammonia/ biodiesel is higher relative to biodiesel operation due to the lower LHV of the ammonia/biodiesel mixture, since LHV_{NH_3} is considerably lower compared with LHV_{bio} (Equation 4). However, the BSFC difference between ammonia-/biodiesel-fueled engine with only biodiesel at 20% of the load is approximately 10.0% due to the ineffective burning of the lean ammonia/air mixture at low loads.³⁷ Nevertheless, this difference will decrease with increasing load. Hence, the BSFC of set 1, set 2, and biodiesel tests are 300.2, 313.5, and 326.8 g/kW.h, respectively.

3.2 | Effects of ammonia on in-cylinder parameters

Figure 5 shows in-cylinder pressure profiles vs load for each operating point. The pressure traces for the biodiesel test on different loads along with the pressure profiles of the full load of set 1 and set 2 are presented in Figure 5A. The location of rapid rise in pressure is constant with increasing load in the pure biodiesel operation, and the pressure curves are also overlapped in the starting of the high pressure. This is due to the fixed start of biodiesel injection at $-15.5CAD$. It was observed that ammonia/biodiesel combustion generally has higher in-cylinder pressure than biodiesel. For example, the peak of the pressure for biodiesel is 76.64 bar and increased to 82.89 bar (8.1% increase) and 87.79 bar (14.5% increase) for set 1 and set 2 at full load, respectively. This is mainly due to ignition delay and the higher premixed ratio compared with biodiesel, as can be seen in the HRR profile in Figure 7A. HRR diagram of the diesel engine normally has four steps, which are ignition delay, premixed combustion, diffusion combustion, and late combustion, sequentially, according to Heywood.³⁸ However, the evaporation phase of the pilot biodiesel in the premixed air-ammonia is very short compared with the only biodiesel operation in which a high amount of ammonia causes one peak in the HRR diagram, and most of the heat is released in premixed combustion. Hence, the location of the peak of the pressure leads to the advance by increasing the ALC, as can be seen in Figure 5B,C. Furthermore, the pressure rise rate profiles are presented in Figure 6 for 20% and 100% loads. The peak of PRR is 5.4 bar/deg at full loads for the biodiesel test. However, it increases to 6.9 bar/deg for the same operating point at maximum AEC. The maximum PRR of ammonia/biodiesel is higher than pure biodiesel operation due to ignition delay and changing combustion mode from diffusion in pure biodiesel to the premixed combustion in dual-fuel mode, resulting in higher engine noise. However, the peak of PRR of ammonia biodiesel engine is lower than that of pure biodiesel at 20% of load. The flame propagation of ammonia/biodiesel in low loads is slower than the pure biodiesel due to the lean mixture, since the laminar flame speed of ammonia is slower in the lean mixture but faster in the stoichiometric condition.³⁹

MFB and HRR at 20% and 100% of the loads for ammonia/biodiesel along with biodiesel test are shown in Figure 7. HRR curves revealed that when more ammonia is injected into the intake manifold, the HRR peak increases. There are mainly two reasons: first, the higher amount of ammonia increases the peak of the in-cylinder pressure. Second, propagation of the premixed ammonia-air flame increases the HRR peak in the premixed

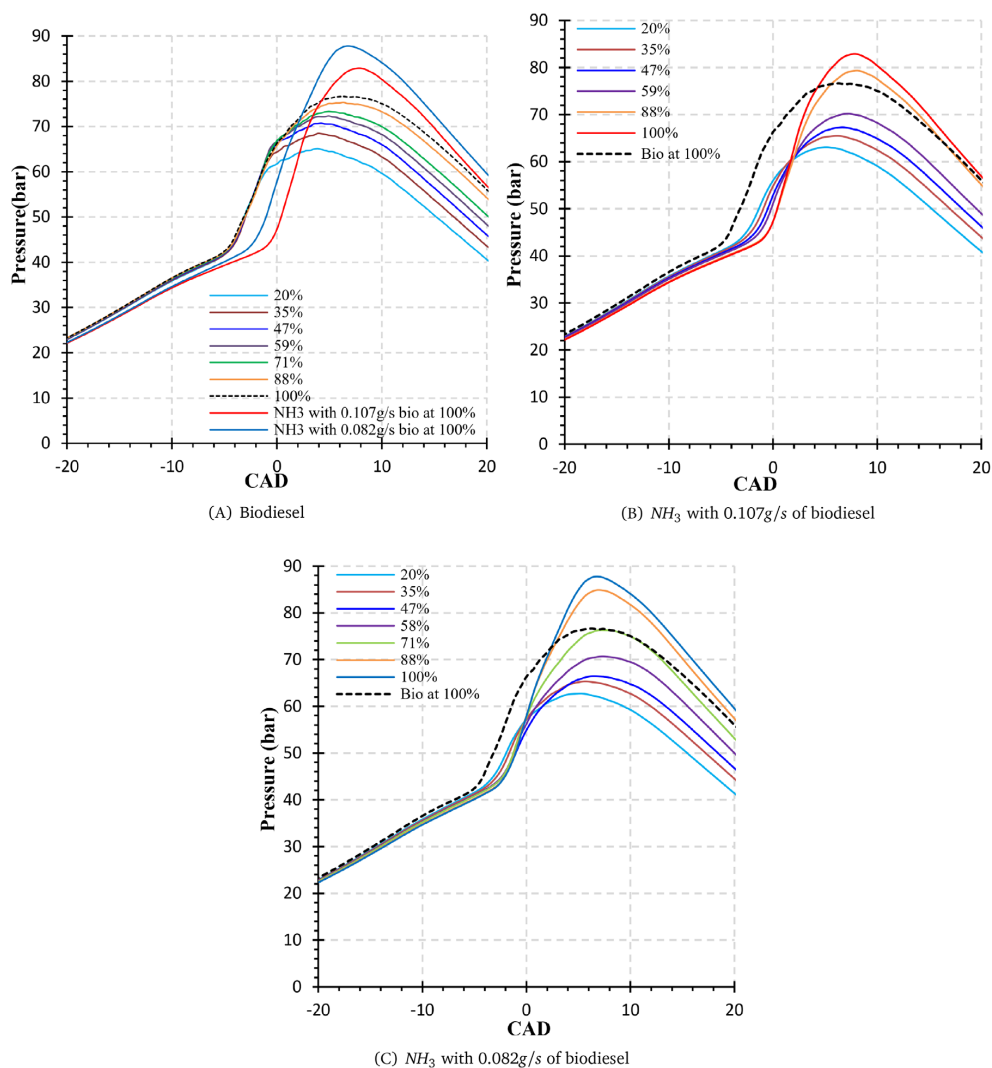


FIGURE 5 In-cylinder pressure profiles for each set of data

combustion phase in the HRR curve. Therefore, a higher ammonia ratio changed the combustion mode from diffusion mode to premixed combustion. Although pure biodiesel ignition starts in advance, the combustion of ammonia/biodiesel is finished earlier than only biodiesel for high loads, as can be observed in Figures 7B and 8C.

The indicators of ammonia with pilot biodiesel combustion are shown in Figure 8. SOC increases slightly from -5.83CAD to -5.24CAD by increasing the load for the pure biodiesel test. However, the minimum energy required to ignite the ammonia-air mixture is higher.⁴⁰ Therefore, biodiesel is first injected and then evaporated, providing energy to initiate the combustion of premixed ammonia-air. Therefore, ammonia with biodiesel in

dual-mode combustion has a longer delay in SOC, as can be observed in Figure 8A,B. SOC is delayed from -5.24CAD in pure biodiesel operation at full load to -1.43CAD and -2.55CAD for biodiesel/ammonia combustion in $\dot{m}_{\text{bio}} = 0.107\text{g/s}$ and $\dot{m}_{\text{bio}} = 0.082\text{g/s}$ tests, respectively, in the same operating point. Figure 8D shows the CA50-CA10 that is related to flame propagation. Thus, the flame propagation of ammonia/biodiesel in low loads is slower than that in the pure diesel case due to the lean mixture as well as the low flame speed of ammonia in lean condition. However, the ammonia flame propagates faster than pure biodiesel in higher loads because combustion mode is changed from the diffusion combustion in pure biodiesel to the premixed

combustion in dual-fuel mode. Moreover, the laminar flame speed of ammonia increases from the lean mixture to the stoichiometric condition.³⁹

CD is defined as the difference between CA90 and CA10. The CD of ammonia/biodiesel combustion has slightly increased for higher load, unlike biodiesel. However, the CD of biodiesel combustion increases as the load increases due to the high biodiesel mass flow rate and diffusion combustion. Therefore, premixed ammonia air burns earlier than pure biodiesel at high load as a result of the higher premixed ratio. Furthermore, the CA90 curve is presented in Figure 8E for set 1 and set

2 together with the biodiesel test. It can be observed that increasing the mass flow rate of pure biodiesel enhanced CA90, for example, 90% of pure biodiesel has been burned at 40.6CAD. It can be concluded that ammonia/biodiesel burns slower than only biodiesel at lower loads, but the CD of pure biodiesel is higher at high loads.

3.3 | Effects of ammonia on emissions

In this section, the influence of various ammonia mass flows with constant biodiesel flow ($\dot{m}_{bio} = 0.107\text{g/s}$ and $\dot{m}_{bio} = 0.082\text{g/s}$) will be discussed. The concentration of each species has been calculated in 5% O_2 to show the exhaust gas composition with the same level of dilution by air, and it should be noted that for each test the excess air was different. As more biodiesel is replaced by ammonia, it significantly reduces CO_2 , as shown in Figure 9. This can be expected since NH_3 has a carbon-free nature. The concentration of CO_2 in the biodiesel test is approximately 10.6% for different loads, however, it dramatically reduced to 2.48% for set 2 at full load, as can be observed in Figure 9B. Although CO_2 decreased significantly, it also produced N_2O around 60 ppm which has a global warming potential (GWP) of 298 times that of CO_2 over a 100-year timescale. Thus, 60 ppm of N_2O is equivalent to 1.7% of CO_2 in terms of GWP. Therefore, the CO_2 emission decreased from 10.6 to 4.26%, considering the equivalent GWP.

As discussed before, ammonia decreases the in-cylinder temperature. Hence, unsuccessful combustion at 20% of load due to low in-cylinder temperature causes a high amount of unreacted species such as NO , CO , and

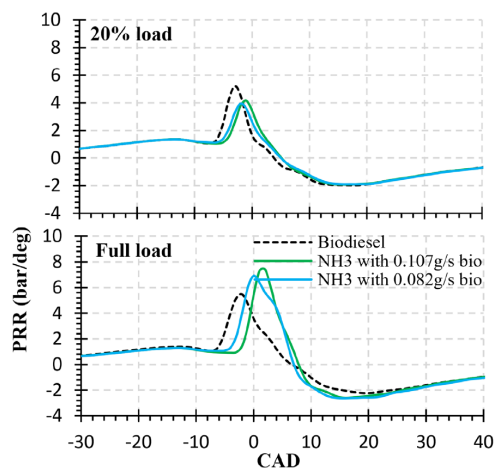


FIGURE 6 Pressure rise rate curves for loads of 20% and 100% in set 1, set 2, and biodiesel

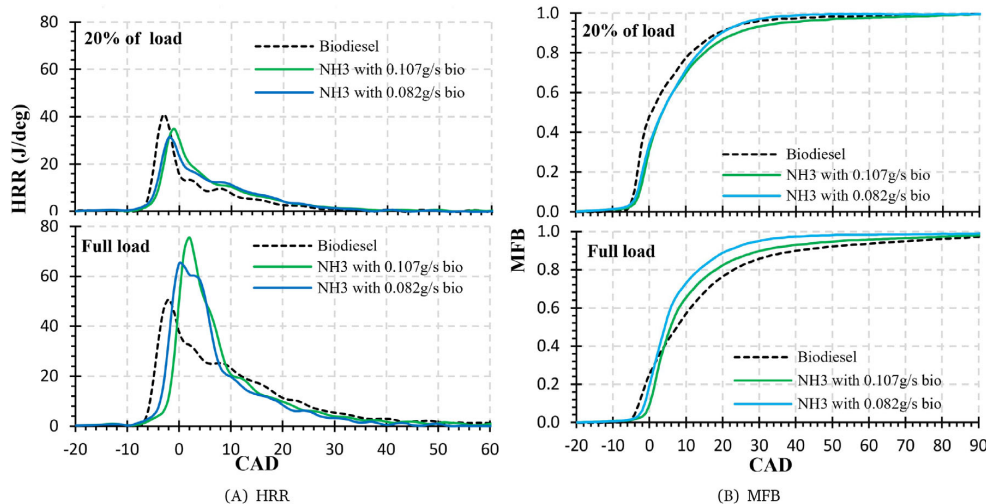


FIGURE 7 Mass fraction burned and heat release rate profiles for loads of 20% and 100% for each test (set 1, set 2, and biodiesel)

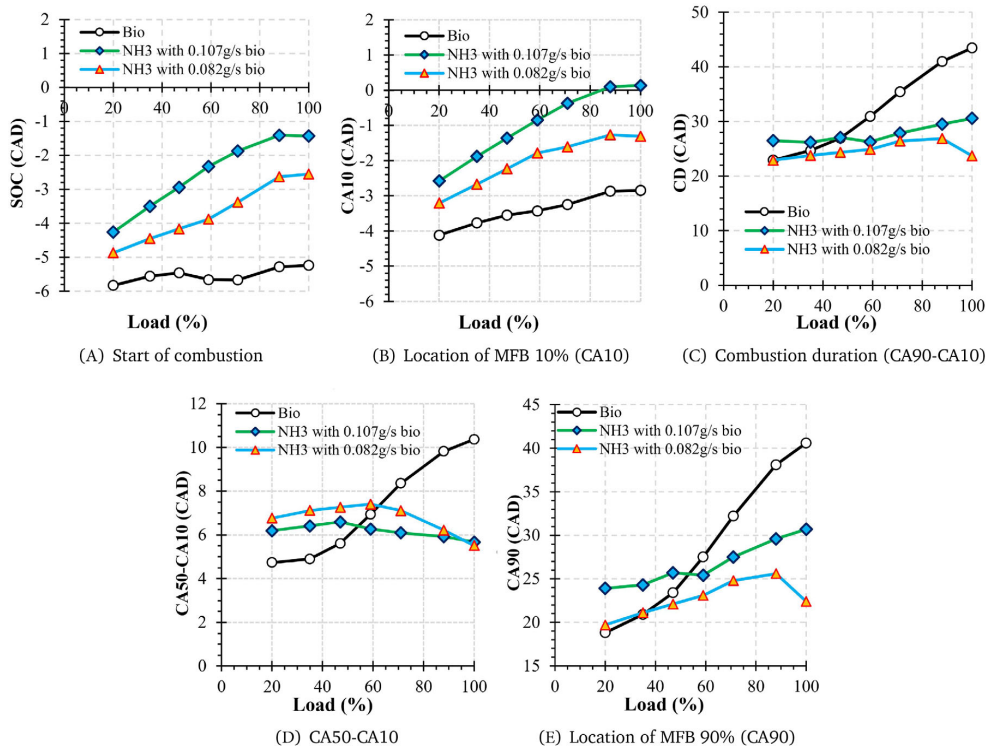


FIGURE 8 Ammonia/biodiesel and biodiesel combustion analysis indicators

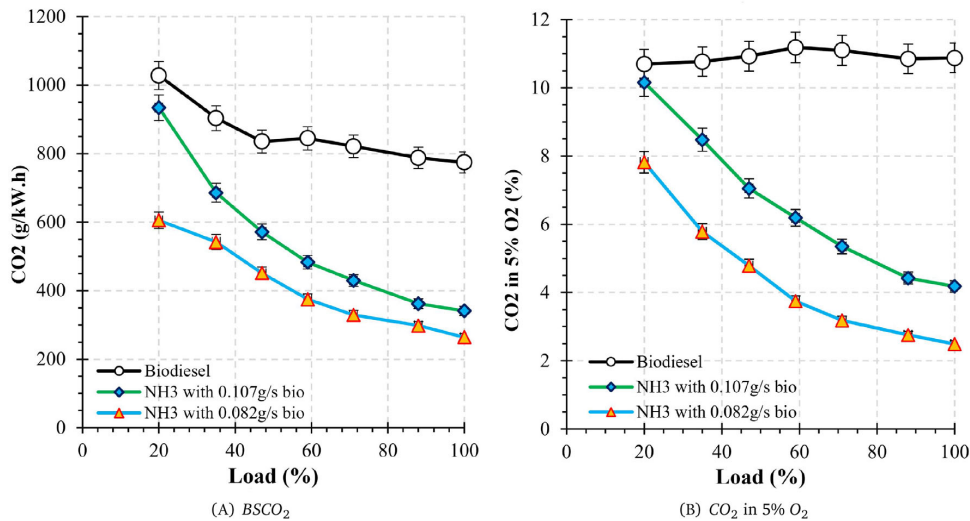


FIGURE 9 Comparison of CO₂ emissions between NH₃ with 0.107 g/s of bio and NH₃ with 0.082 g/s of bio with only biodiesel operation

PM (Figure 10B, 11B and 13). Observations of the NO emission in Figure 10 reveal that as more biodiesel is replaced by ammonia increases NO emission compared

with the only biodiesel test due to the presence of the N atom in NH₃. Furthermore, NO concentration curves for ammonia/biodiesel operation illustrate an interesting

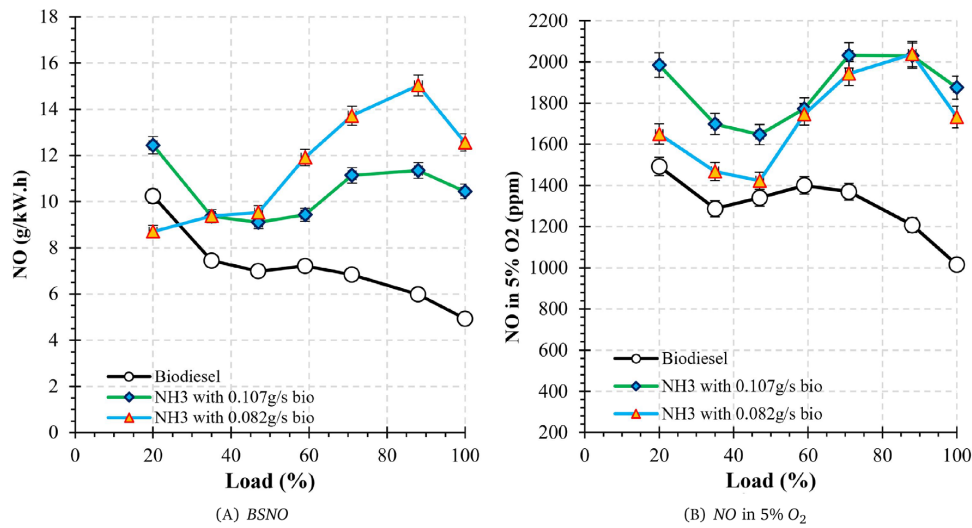


FIGURE 10 NO emissions of NH_3 with 0.107 g/s of bio and NH_3 with 0.082 g/s of bio compared with only biodiesel

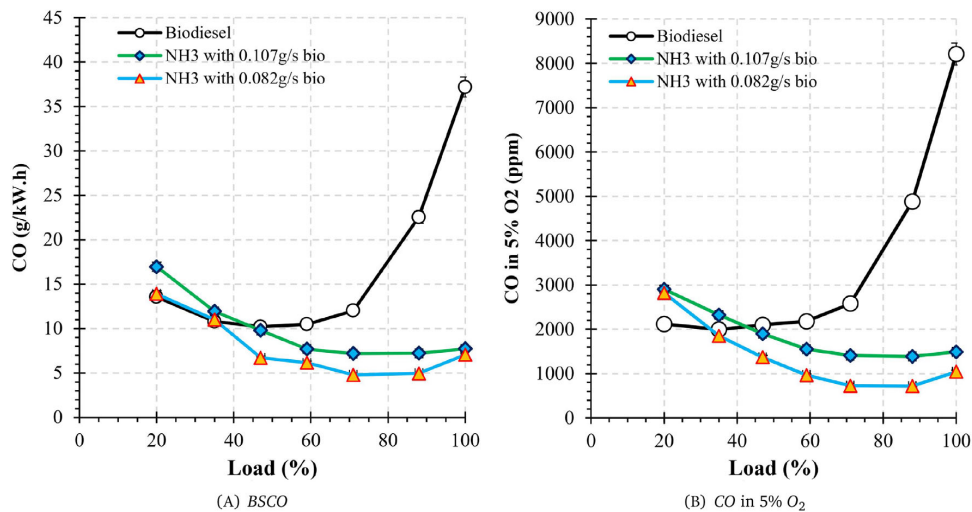


FIGURE 11 CO emissions of NH_3 with 0.107 g/s and with 0.082 g/s of biodiesel along with using only biodiesel

behavior, first decreasing until 50% of load, then increasing. This decrease of NO in 20% to 50% of the load is because of in-cylinder temperature, which results in destructing NO through reactions of 7 to 10. These reactions are started at temperature around 1100 K to 1400 K,^{41,42} where in-cylinder temperature is in the range of 20% to 50% of load for ammonia/biodiesel test.

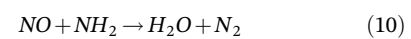
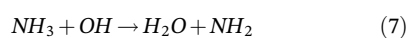


Figure 11 shows the CO emission for two sets of ammonia/biodiesel tests together with normal biodiesel

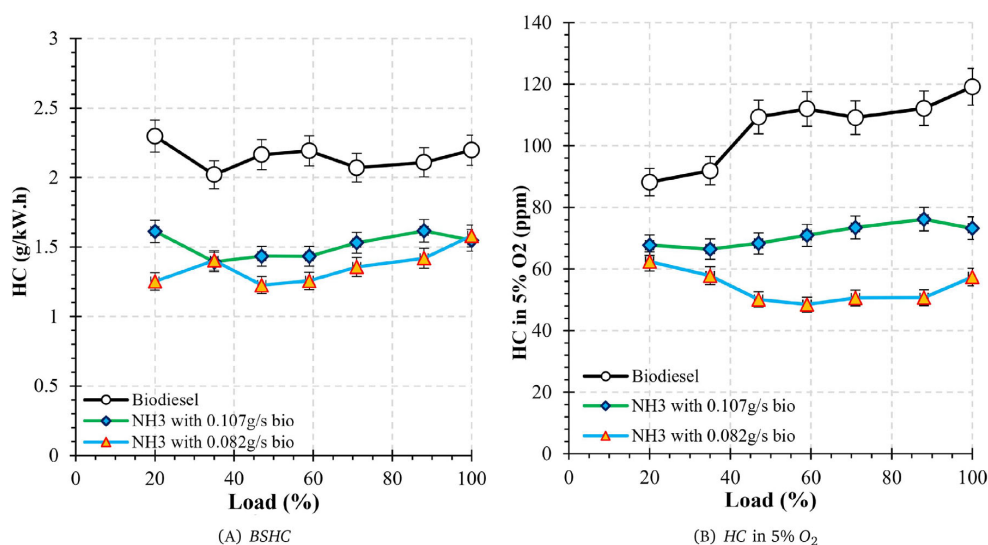


FIGURE 12 HC emissions of NH₃ with 0.107 g/s and 0.082 g/s of biodiesel compared with only biodiesel

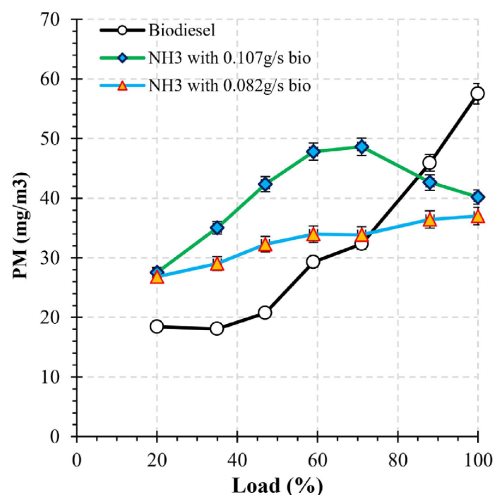


FIGURE 13 PM emission of test sets 1 and 2 compared with pure biodiesel

operation. Although the concentration of CO increases exponentially with increasing load due to the lack of O₂ at higher loads, it has decreased for the operation of ammonia/biodiesel. This decrease in CO is due to the low amount of carbon and premixed ammonia-air combustion. Therefore, the CO emission decreased significantly from 8210 ppm for biodiesel to 1042 ppm for set 2 at full load; in other words, the ammonia-/biodiesel-fueled engine produces 35.18 g/kW.h less CO compared with the normal biodiesel engine, as shown in Figure 11B.

Figure 12A,B show HC emissions for ammonia/biodiesel engine including pure biodiesel at different loads. HC concentration slightly increases from 88 ppm to 199 ppm by enhancing the load. However, biodiesel generally produces a lower amount of HC emission in contrast to diesel fuel due to the content of O, resulting in complete combustion.⁴³⁻⁴⁵ Nevertheless, as more ammonia is introduced into the intake manifold, the emission of HC decreases. For example, the equivalent concentration of HC is reduced from 119 ppm for pure biodiesel to 73 and 57 for ammonia with $\dot{m}_{bio} = 0.107\text{g/s}$ and ammonia with $\dot{m}_{bio} = 0.082\text{g/s}$ test, respectively, in full load operation (Figure 12B). This decline could be due to a couple of reasons. First, due to homogeneous premixed ammonia-air combustion with a low amount of carbon. Second, since the biodiesel dose only contributes 10% and 3.5% of the load in the set 1 and set 2 tests, it is attesting that spraying a small dose of biodiesel will not impinge on the cylinder wall, the small size of the droplets and complete combustion in the thin clearance between the cylinder and piston. All of this results in a decrease in the HC emission.^{46,47}

Furthermore, PM emission for ammonia-/biodiesel-fueled engine is presented in Figure 13. Typically, as the load increases, the formation of PM increases as a result of the high quantity of biodiesel fuel at high loads. Therefore, the higher the in-cylinder temperature, the longer the diffusion combustion phase, the constant SOI, and the decrease in the oxidation of the soot at high loads promote numerous PM formations. However, the ammonia-/biodiesel-fueled engine has higher PM emission compared with the reference biodiesel in low loads.

PM increases slightly as the AEC increases. This has also been addressed by other researchers.^{37,48} As discussed in the previous section, enhancing ALC decreases CD and the in-cylinder temperature, which support the formation of PM. However, PM was lower in dual-fuel mode at full load compared with pure biodiesel operation. This is mainly due to the perfect mixing of biodiesel with pre-mixed ammonia-air since ammonia was injected to obtain higher loads instead of biodiesel.

4 | CONCLUSION

This study demonstrates utilizing ammonia as a potential carbon-free fuel with biodiesel in the CI engine in dual-fuel mode. An experimental study along with a 1D model has been conducted to investigate the impacts of different ammonia and biodiesel load contributions on ammonia/biodiesel combustion, engine performance, and emissions. Therefore, the engine runs first with two different pilot doses of biodiesel at low loads, then ammonia is injected into the intake port to obtain higher loads. The main conclusions drawn from this study are summarized as follows:

- Ammonia-/biodiesel-fueled engine has a lower BTE compared with pure biodiesel at the same operating point. Additionally, as more biodiesel was replaced by ammonia, BTE decreased as a result of unsuccessful combustion of ammonia/biodiesel. Therefore, the BTE decreased from 31.8 for pure biodiesel to 29.4 for the highest ammonia input energy ratio at full load.
- Increasing ammonia input energy contribution (AEC) decreases the exhaust gas temperature. Therefore, the exhaust gas temperature was reduced by 100 K when the AEC was 69.4%.
- Increasing ALC increases the peak of in-cylinder pressure, for example, in-cylinder pressure of ammonia/biodiesel combustion increased by 11.15 bar compared with biodiesel at full load because the SOC and peak of HRR diagram occur close to the TDC (0CAD). Moreover, ammonia also increases the peak of the pressure rise rate diagram.
- The SOC is delayed with increasing AEC; additionally, the propagation of the ammonia/biodiesel flame is slower than the only biodiesel mode in low load due to the low flame speed of ammonia in the lean mixture. The SOC was delayed by 2.6 CAD and CD was reduced by 19.7 CAD at maximum load compared with the same operating point with pure biodiesel.
- Ammonia increases the peak of the HRR and decreases the diffusion combustion phase in the HRR diagram. Therefore, as more ammonia is introduced

into the intake manifold, the combustion mode changes from diffusion to premixed combustion.

- As more biodiesel was replaced by ammonia, CO_2 , CO , and HC emissions decreased significantly. The minimum CO_2 , CO , and HC emissions were achieved when the AEC was the highest ($AEC = 69.4\%$). Therefore, CO_2 decreases by 510 g/kW.h and CO reduces by 30.1 g/kW.h at the maximum AEC. However, NO emission increased with increasing ammonia flow since NH_3 consists of one nitrogen atom.

NOMENCLATURE

ABDC	after bottom dead center
AEC	ammonia energy contribution
ALC	ammonia load contribution
ATDC	after top dead center
BBDC	before bottom dead center
BDC	bottom dead center
BLC	biodiesel load contribution
BSFC	brake-specific fuel consumption
BTDC	before top dead center
BTE	brake thermal efficiency
CA10	CAD value for 10% MFB
CA50	CAD value for 50% MFB
CA90	CAD value for 90% MFB
CAD	crank angle degree
CD	combustion duration
CI	compression ignition
CR	compression ratio
EVC	inlet valve closing
EVO	exhaust valve opening
GDI	gasoline direct injection
GWP	global warming potential
HRR	heat release rate
ICE	internal combustion engine
IVC	inlet valve closing
IVO	inlet valve opening
LHV	lower heating value
MFB	mass fraction burned
P_b	brake power
rpm	rotation per minute
SCR	selective catalytic reduction
SI	spark ignition
SOC	start of combustion
SOI	start of injection
TDC	top dead center
w_{NH_3}	NH_3 ratio in fuel

AUTHOR CONTRIBUTION

Ebrahim Nadimi: Conceptualization, Methodology, Software, Validation, Formal analysis, Investigation, Experiment,

Data Curation, Figures, Original draft, Writing—Review and editing. **Grzegorz Przybyła**: Conceptualization, Methodology, Investigation, Experiment, Supervision, Writing—review and editing. **David Robert Emberson**: Writing—review and editing. **Terese Løvås**: Writing—review and editing. **Łukasz Ziolkowski**: Experiment. **Wojciech Adamczyk**: Writing—review and editing, project administration.

ACKNOWLEDGEMENT

The authors also thank AVL List GmbH for providing the license according to the university and AVL agreement.

FUNDING INFORMATION


This work was financed by Norway and Poland grants (Contract NO. NOR/POLNOR/ACTIVATE/0046/2019-00) to ACTIVATE project “Ammonia as carbon free fuel for internal combustion engine driven agricultural vehicle” (<https://ammoniaengine.org>.)

CONFLICT OF INTEREST

The authors have no conflict of interest to report.

ORCID

Ebrahim Nadimi  <https://orcid.org/0000-0003-3338-5288>

Grzegorz Przybyła  <https://orcid.org/0000-0001-8089-3475>

Wojciech Adamczyk  <https://orcid.org/0000-0002-9178-9566>

REFERENCES

- Liobikienė G, Butkus M. The European Union possibilities to achieve targets of Europe 2020 and Paris agreement climate policy. *Renew Energy*. 2017;106:298-309.
- Venugopal T, Sharma A, Satapathy S, Ramesh A, Gajendra Babu M. Experimental study of hydrous ethanol gasoline blend (e10) in a four stroke port fuel-injected spark ignition engine. *Int J Energy Res*. 2013;37(6):638-644.
- Sun C, Liu Y, Qiao X, et al. Experimental study of effects of exhaust gas recirculation and combustion mode on combustion, emission, and performance of DME-methanol-fueled turbocharged common-rail engine. *Int J Energy Res*. 2022;46(3):2385-2402.
- Venkanna B, Venkataramana Reddy C. Direct injection diesel engine performance, emission, and combustion characteristics using diesel fuel, nonedible honne oil methyl ester, and blends with diesel fuel. *Int J Energy Res*. 2012;36(13):1247-1261.
- Valera-Medina A, Xiao H, Owen-Jones M, David WI, Bowen P. Ammonia for power. *Progr Energy Combust Sci*. 2018;69:63-102.
- Valera-Medina A, Amer-Hatem F, Azad A, et al. Review on ammonia as a potential fuel: from synthesis to economics. *Energy Fuel*. 2021;35(9):6964-7029.
- Wijayanta AT, Oda T, Purnomo CW, Kashiwagi T, Aziz M. Liquid hydrogen, methylcyclohexane, and ammonia as potential hydrogen storage: comparison review. *Int J Hydrogen Energy*. 2019;44(29):15026-15044.
- Frigo S, Gentili R. Analysis of the behaviour of a 4-stroke si engine fuelled with ammonia and hydrogen. *Int J Hydrogen Energy*. 2013;38(3):1607-1615.
- MacKenzie J. J., Avery W. H., Ammonia fuel: the key to hydrogen-based transportation. Technical Report. Inst of Electrical and Electronics Engineers, Piscataway, NJ (United States). 1996.
- Lhuillier C, Brequigny P, Contino F, Mounaïm-Rousselle C. Experimental investigation on ammonia combustion behavior in a spark-ignition engine by means of laminar and turbulent expanding flames. *Proc Combust Inst*. 2021;38(4):5859-5868.
- Koch E. Ammonia—a fuel for motor buses. *J Inst Pet*. 1945;31:213.
- Starkman ES, Newhall H, Sutton R, Maguire T, Farbar L. Ammonia as a spark ignition engine fuel: theory and application. *SAE Trans*. 1967;75:765-784.
- Starkman ES, James G, Newhall H. Ammonia as a diesel engine fuel: theory and application. *SAE Trans*. 1968;76:3193-3212.
- Pearsall TJ, Garabedian CG. Combustion of anhydrous ammonia in diesel engines. *SAE Transactions*. 1968;76:3213-3221.
- Sawyer R. F., Starkman E. S., Muzio L., Schmidt W., Oxides of Nitrogen in the Combustion Products of an Ammonia Fueled Reciprocating Engine, Technical Report, SAE Technical Paper. 1968.
- Mounaïm-Rousselle C, Brequigny P. Ammonia as fuel for low-carbon spark-ignition engines of tomorrow's passenger cars. *Frontiers Mech Eng*. 2020;6:70.
- Schönborn A., Aqueous solution of ammonia as marine fuel, Proceedings of the Institution of Mechanical Engineers, Part M: Journal of Engineering for the Maritime Environment 2021; 235(1):142–151.
- Grannell SM, Assanis DN, Bohac SV, Gillespie DE. The fuel mix limits and efficiency of a stoichiometric, ammonia, and gasoline dual fueled spark ignition engine. *J Eng Gas Turb Power*. 2008;130(4).
- Salek F, Babaie M, Shakeri A, Hosseini SV, Bodisco T, Zare A. Numerical study of engine performance and emissions for port injection of ammonia into a gasoline-ethanol dual-fuel spark ignition engine. *Applied Sciences*. 2021;11(4):1441.
- Yapicioglu A, Dincer I. Experimental investigation and evaluation of using ammonia and gasoline fuel blends for power generators. *Appl Therm Eng*. 2019;154:1-8.
- Mounaïm-Rousselle C, Bréquigny P, Dumand C, Houillé S. Operating limits for ammonia fuel spark-ignition engine. *Energies*. 2021;14(14):4141.
- Lhuillier C, Brequigny P, Contino F, Mounaïm-Rousselle C. Experimental study on ammonia/hydrogen/air combustion in spark ignition engine conditions. *Fuel*. 2020;269:117448.
- Oh S, Park C, Kim S, Kim Y, Choi Y, Kim C. Natural gas-ammonia dual-fuel combustion in spark-ignited engine with various air–fuel ratios and split ratios of ammonia under part load condition. *Fuel*. 2021;290:120095.
- Dimitriou P, Javaid R. A review of ammonia as a compression ignition engine fuel. *Int J Hydrogen Energy*. 2020;45(11):7098-7118.
- Reiter AJ, Kong S-C. Combustion and emissions characteristics of compression-ignition engine using dual ammonia-diesel fuel. *Fuel*. 2011;90(1):87-97.

26. Reiter AJ, Kong S-C. Demonstration of compression-ignition engine combustion using ammonia in reducing greenhouse gas emissions. *Energy Fuel*. 2008;22(5):2963-2971.
27. Lee D, Song HH. Development of combustion strategy for the internal combustion engine fueled by ammonia and its operating characteristics. *Journal of Mechanical Science and Technology*. 2018;32(4):1905-1925.
28. Yousefi A, Guo H, Dev S, Liko B, Lafrance S. Effects of ammonia energy fraction and diesel injection timing on combustion and emissions of an ammonia/diesel dual-fuel engine. *Fuel*. 2021;134:122723.
29. Boost A., 2-theory, AVL List GmbH 769.
30. Kobayashi H, Hayakawa A, Somarathne KKA, Okafor EC. Science and technology of ammonia combustion. *Proc Combust Inst*. 2019;37(1):109-133.
31. Lewandowski DA. *Design of Thermal Oxidation Systems for Volatile Organic Compounds*. CRC Press; 2017.
32. Salek F, Babaie M, Redel-Macias MD, et al. The effects of port water injection on spark ignition engine performance and emissions fueled by pure gasoline, e5 and e10. *Processes*. 2020;8(10):1214.
33. Hasan AO, Al-Rawashdeh H, Ala'a H, Abu-Jrai A, Ahmad R, Zeaiter J. Impact of changing combustion chamber geometry on emissions, and combustion characteristics of a single cylinder si (spark ignition) engine fueled with ethanol/gasoline blends. *Fuel*. 2018;231:197-203.
34. Hasan AO, Osman AI, Ala'a H, et al. An experimental study of engine characteristics and tailpipe emissions from modern diesel engine fuelled with methanol/diesel blends. *Fuel Process Technol*. 2021;220:106901.
35. Gross CW, Kong S-C. Performance characteristics of a compression-ignition engine using direct-injection ammonia-dme mixtures. *Fuel*. 2013;103:1069-1079.
36. Kuta K., Nadimi E., Przybyła G., Żmudka Z., Adamczyk W., Ammonia CI Engine Aftertreatment Systems Design and Flow Simulation
37. Frost J, Tall A, Sheriff AM, Schönborn A, Hellier P. An experimental and modelling study of dual fuel aqueous ammonia and diesel combustion in a single cylinder compression ignition engine. *Int J Hydrogen Energy*. 2021;46(71):35495-35510.
38. Heywood J., *Internal combustion engine fundamentals* mcgraw-hill book co, New York
39. Ichimura R, Hadi K, Hashimoto N, Hayakawa A, Kobayashi H, Fujita O. Extinction limits of an ammonia/air flame propagating in a turbulent field. *Fuel*. 2019;246:178-186.
40. Pfahl U, Ross M, Shepherd J, Pasamehmetoglu K, Unal C. Flammability limits, ignition energy, and flame speeds in h₂-ch₄-nh₃-n₂-o₂-n₂ mixtures. *Combust Flame*. 2000;123(1-2):140-158.
41. Lyon RK. The nh₃-no-o₂ reaction. *Int J Chem Kinet*. 1976;8(2):315-318.
42. Lee G-W, Shon B-H, Yoo J-G, Jung J-H, Oh K-J. The influence of mixing between nh₃ and no for a de-nox reaction in the SNCR process. *J Ind Eng Chem*. 2008;14(4):457-467.
43. Shirneshan A. Hc, co, co₂ and nox emission evaluation of a diesel engine fueled with waste frying oil methyl ester. *Procedia Soc Behav Sci*. 2013;75:292-297.
44. Payri F, Bermúdez VR, Tormos B, Linares WG. Hydrocarbon emissions speciation in diesel and biodiesel exhausts. *Atmos Environ*. 2009;43(6):1273-1279.
45. Raja KSS, Srinivasan SK, Yoganandam K, Ravi M. Emissions and performance investigation on the effect of dual fuel injection in biodiesel driven diesel engine. *Energy Sourc A Recov Utilizat Env Effects*. 2021;1-11.
46. Matsui Y., Sugihara K., Sources of Hydrocarbon Emissions from a Small Direct Injection Diesel Engine, Technical Report, SAE Technical Paper. 1987.
47. Khair M. K., Jääskeläinen H., Emission Formation in Diesel Engines. 2008.
48. Kane SP, Northrop WF. Thermochemical recuperation to enable efficient ammonia-diesel dual-fuel combustion in a compression ignition engine. *Energies*. 2021;14(22):7540.

How to cite this article: Nadimi E, Przybyła G, Emberson D, Løvås T, Ziółkowski Ł, Adamczyk W. Effects of using ammonia as a primary fuel on engine performance and emissions in an ammonia/biodiesel dual-fuel CI engine. *Int J Energy Res*. 2022;46(11):15347-15361. doi:[10.1002/er.8235](https://doi.org/10.1002/er.8235)

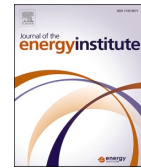
A.2 Paper II



Contents lists available at ScienceDirect

Journal of the Energy Institute

journal homepage: www.elsevier.com/locate/joei



Effects of ammonia on combustion, emissions, and performance of the ammonia/diesel dual-fuel compression ignition engine

Ebrahim Nadimi^{a,*}, Grzegorz Przybyła^a, Michał T. Lewandowski^b, Wojciech Adamczyk^a

^a Department of Thermal Engineering, Faculty of Energy and Environmental Engineering, Silesian University of Technology, Gliwice, Poland

^b Department of Energy and Process Engineering, NTNU, Norwegian University of Science and Technology, Trondheim, Norway

ARTICLE INFO

Handling Editor: Dr. Paul Williams

Keywords:

Ammonia
Dual fuel
Diesel engine
Emissions
GHG emissions

ABSTRACT

Ammonia is currently receiving more interest as a carbon-free alternative fuel for internal combustion engines (ICE). A promising energy carrier, easy to store and transport, being liquid, and non-carbon-based emissions which make ammonia a green fuel to decarbonize ICE and to reduce greenhouse gas (GHG) emissions. This paper aims to illustrate the impacts of replacing diesel fuel with ammonia in an ammonia/diesel dual fuel engine. Hence, the effects of various ammonia diesel ratios on emissions and engine performance were experimentally investigated. In addition, a developed 1D model is used to analyze the combustion characteristics of ammonia and diesel. Results show 84.2% of input energy can be provided by ammonia meanwhile indicated thermal efficiency (ITE) is increased by increasing the diesel substitution. Moreover, increasing the ammonia energy share (AES) changed the combustion mode from diffusion combustion in pure diesel operation to premixed combustion in dual fuel mode. Therefore, combustion duration and combustion phasing decreased by 6.8CAD and 32CAD, respectively. Although ammonia significantly reduced CO₂, CO, and particulate matter (PM) emissions, it also increased NO_x emissions and unburned ammonia (14800 ppm). Furthermore, diesel must be replaced with more than 35.9% ammonia to decrease GHG emissions, since ammonia combustion produces N₂O (90 ppm) that offsets the reduction of CO₂.

1. Introduction

Nowadays, internal combustion engines are used mainly for power generation and transportation. Compression ignition (CI) diesel engines, with high load operation and high efficiency, are commonly used in agriculture, heavy-duty, and marine vehicles [1]. However, conventional diesel engines lead to emissions of GHG such as CO₂. The ongoing developments in diesel engines or after-treatment systems are continuously reducing these emissions [2–4]. Yet, using fossil fuels implies inherent emissions of greenhouse gases, in particular, CO₂. The European Union (EU) has introduced strict limitations in the emissions of heavy vehicles [5]. The EU has also committed to reducing GHG emissions to at least 55% by 2030, according to the Paris climate agreement [6], but the long-term objective is to move towards a carbon-free society. Therefore, alternative green fuels, such as ammonia, could be one of the solutions to achieve this goal. Currently, ammonia is receiving more interest among other green fuels such as hydrogen, ethanol, etc. as a renewable carbon-free hydrogen carrier [7].

Ammonia can be easily stored in the liquid phase at ambient

temperature and under a pressure of 8 bar. It has 30% more volumetric energy compared to hydrogen [8,9]. However, hydrogen still is used in power generation in other applications [10,11]. As the second most produced chemical in the world, there are well-established infrastructures to produce and transport ammonia, making it a promising sustainable green fuel [12,13]. However, the challenges in using ammonia as fuel in ICE are the high ignition energy and temperature, low flame speed, and low adiabatic flame temperature compared to diesel fuel. Furthermore, the Lower Heat Value (LHV) of ammonia is around 60% lower than diesel fuel. Nevertheless, the stoichiometric mixture of ammonia/air has almost the same amount of energy compared to the stoichiometric mixture of diesel/air [14].

Ammonia is used mainly in spark ignition engines (SI) in dual fuel mode by blending with other promoter fuels such as hydrogen, gasoline, etc., or in pure ammonia mode, according to a recent review [15]. However, using pure ammonia in heavy-duty diesel engines requires a high compression ratio (CR) of around 27 and an auto-ignition temperature of 924 K [16]. Rousselle et al. [17] investigated the limitation of applying pure ammonia to the SI engine. Their results show that it is difficult to operate the engine in low load due to the low CR and high

* Corresponding author.

E-mail address: Enadimi@polsl.pl (E. Nadimi).

<https://doi.org/10.1016/j.joei.2022.101158>

Received 26 September 2022; Received in revised form 6 December 2022; Accepted 12 December 2022

Available online 24 December 2022

1743-9671/© 2022 The Authors. Published by Elsevier Ltd on behalf of Energy Institute. This is an open access article under the CC BY license (<http://creativecommons.org/licenses/by/4.0/>).

Nomenclature			
m	mass, kg	c	cylinder
V	Volume, m^3	BB	blow by
Q_w	Wall heat transfer, W	ex	exhaust
h	Enthalpy, J	u	Internal energy, J
γ	polytropic coefficient	Q_f	Fuel chemical energy, J
h_w	Heat transfer coefficient, $W/(m^2K)$	α	Crank angle degree, CAD
D	Bore, m	P	Pressure, Pa
Abbreviations		A_w	Surface area, m^2
ICE	Internal Combustion Engine	T	Temperature, K
SI	Spark Ignition	CI	Compression Ignition
TDC	Top Dead Center	CR	Compensation Ratio
BTDC	Before Top Dead Center	BDC	Bottom Dead Center
BBDC	Before Bottom Dead Center	ATDC	After Top Dead Center
ITE	Indicated Thermal Efficiency	ABDC	After Bottom Dead Center
IVO	Inlet Valve Opening	GHG	Greenhouse gas
EVO	Exhaust Valve Opening	IVC	Inlet Valve Closing
AES	Ammonia Energy Share	EVC	Inlet Valve Closing
ISFC	Indicated Specific Fuel Consumption	MFB	Mass Fraction of Burned
C	Constant	rpm	Revolutions Per Minute
COV	Coefficient of Variation	PM	Particulate Matter
SOI	Start of Injection	AFR	Air Fuel Ratio
Subscripts		SOC	Start of Combustion
b	burned	u	unburned
		w	wall
		f	fuel
		sto	Stoichiometry

speed around 2000 rpm due to the low flame speed of ammonia. However, they also mention that the engine can operate under all conditions by adding 10% hydrogen. In a similar work carried out by Lhuilliera et al. [18], they showed that blending ammonia with 20% hydrogen increases the efficiency and power of the SI engine. However, increasing the hydrogen fraction by more than 20% decreased the indicated efficiency due to the high wall heat loss. Ryu et al. [19] studied direct injection of ammonia with port injection of gasoline for the first time. They suggested a new ammonia injection strategy, and their results revealed that a good ammonia injection timing range is between 320 and 370 before TDC. Grannell et al. [20,21] proved that 70% of the gasoline energy can be replaced by ammonia, resulting in knock-free operation under high load. Although they observed a significant increase in N_2O and NO emissions either in lean or rich operations. Generally, N_2O and NO_x emissions increase due to the presence of N in ammonia (NH_3) [22]. Hence, Westlye et al. [23] measured nitrogen-based emissions in the ammonia/hydrogen-fueled SI engine. They also reported that the NO_x emission of the ammonia-fueled SI engine was 4% higher than the conventional SI engine at all the same operating points. Furthermore, the concentration of N_2O was below 60 ppm for different air-fuel ratios.

CI engines are a promising way to utilize ammonia, especially marine engines due to their high CR, which allows using pure ammonia [24,25]. Recently, Imhoff et al. [26] have analyzed the performance of ammonia powertrains on oceangoing vessels to assess the use of ammonia in the marine sector, concluding that ammonia-fueled CI engines are more efficient and easier to implement than others, such as gas turbines. However, ammonia can be used in dual fuel mode in light CI engines for the transportation sector. In dual-fuel diesel engines, ammonia is used with other fuels, e.g., diesel, to overcome the challenges of burning ammonia. In this approach, ammonia is introduced into the intake manifold, and then the pilot dose of diesel or biodiesel is sprayed to supply the minimum energy required to ignite the ammonia-air mixture [27]. The use of ammonia in dual fuel mode in CI engines is presented in Table 1. This table summarizes the main findings of using ammonia with different fuels and the key studied parameters.

According to the above literature review, there is revived interest in the research and development of using ammonia in ICE to reduce greenhouse gas emissions. For that purpose, it is also important to show that ammonia can be produced in a green and carbon-free way. The suitability of ammonia for SI engines has been successfully proven by using H_2 as a combustion promoter [18]. The utilization of ammonia in CI engines still presents notable research gaps. As can be seen from Table 1, researchers only investigated limited ratios of ammonia with other fuels. Ammonia is known for its carbon-free emissions, yet nitrogen oxides are an issue besides nitric oxides (NO) and nitrogen dioxide (NO_2), cumulatively known as NO_x , nitrous oxide N_2O is of particular concern as it can be emitted from ammonia-diesel combustion and has nearly 300 times larger greenhouse effects than CO_2 on the 100-year time scale. Considering the emissions by the greenhouse effect, it can offset the reduction of CO_2 . Furthermore, unburned ammonia on itself can be another challenge for dual fuel diesel ammonia engines. In this work, we investigate the impacts of replacing diesel fuel with ammonia to the maximum possible substitution in the CI engine under full loads conditions. Engine performance and emission characteristics are experimentally studied for various ammonia-diesel ratios. Moreover, 1D model is used to calculate the combustion characteristics indicators. Therefore, ignition delay, combustion phasing and duration are determined for different ammonia diesel ratios. Furthermore, unburned ammonia and N_2O emissions are discussed. Finally, CO_2 equivalent GHG emissions are presented to show the effectiveness of ammonia in reducing GHG emissions even with N_2O emission.

2. Experimental methodology

2.1. Experimental setup

All experiments were carried out on a single-cylinder diesel engine. The engine has been retrofitted for ammonia port injection. Table 2 lists the main specifications of the engine. Fig. 1 demonstrates the schematic of the test rig and experimental apparatus. Ammonia was stored at 10

Table 1
Summary of ammonia in dual-fuel CI engines and its effects on performance and emissions from the literature.

Researchers	Year	Fuel	Main studied parameters	Effects of ammonia
M.I. Lamas et al. [28]	2017	NH_3 , H_2 , diesel	- NH_3 direction injection	- Ammonia decrease more than 70% of NO_x
Lasocki et al. [29]	2019	NH_3 , diesel	- Port injection of ammonia to obtain higher loads	- The high amount of NO - Significant reduction of CO_2 and CO
Ryu et al. [30]	2014	Direct injection NH_3 , dimethyl ether	- 40% dimethyl ether and 60% NH_3 . - 60% dimethyl ether and 40% NH_3	-Suggested injection timing between 90 and 340 BTDC. - Soot and CO decreased. - NO_x and HRR increased
Grosset al. [31]	2013	Direct injection NH_3 , dimethyl ether	- 80% dimethyl ether and 20% NH_3 - 60% dimethyl ether and 40% NH_3	- Longer ignition delays. - Combustion temperature decreased. -Increasing injection pressure improved combustion and emissions
Sivasubramaniana et al. [32]	2019	NH_3 , mustard methyl ester	- Various loads - 10% and 20% of ammonia	- NO_x reduction of 3.9%. - Combustion temperature decreased. - 10.4% reduction of HC and 3.8% of CO
Wang et al. [33]	2013	H_2 , NH_3 , diesel	- 10% of H_2	- Increase in NH_3 slip, ignition delay, and NO_2 . - Efficiency was similar to only diesel operation
Yousefi et al. [34]	2022	NH_3 , diesel	- Ammonia energy fraction - Diesel injection timing	-40% of ammonia reduced the NO_x by around 58.8%. - Ammonia emission 4445 ppm
Frost et al. [35]	2021	Aqueous ammonia diesel	- Ammonia diesel load contribution - Different engine loads	- Ignition delay increased. - In-cylinder pressure peak increased. - Significant unburnt ammonia
Yousefi et al. [36]	2022	Ammonia, diesel	-Split diesel injection	- unburned NH_3 decreased 85.5%. - Greenhouse gas emissions decreased 23.7% - ITE increased 2% by split injection.

Table 1 (continued)

Researchers	Year	Fuel	Main studied parameters	Effects of ammonia
lee et al. [37]	2018	Ammonia, diesel	-Injection strategy	- NO is a function of SOI instead of engine load. -NO decreased from 8500 ppm to 3040 ppm by adjusting the SOI.
Nadimi et al. [38]	2022	Ammonia, biodiesel	-Different loads	- Longer ignition delay. - NO emission increased

Table 2
Specifications of diesel engine.

Engine info.	Valves	Units
Engine model	4 stroke, Lifan	
Bore and stroke	86 × 70	mm
Geometric CR	16.5:1	
Maximum power (3500 rpm)	6.4	kW
Conn. rod length	117.5	mm
IVO	14°	BTDC
IVC	45°	ABDC
EVO	50°	BBDC
EVC	16°	ATDC
SOI	-15.5	BTDC
Injection pressure	200	bar

bar in the cylinder and continuously injected into the intake port at 2 bar. The ammonia mass flow rate was measured with a Coriolis flow meter. A surge tank was installed before the intake manifold to prevent ammonia backflow and to decrease pressure oscillations. The air mass flow rate has been measured using a turbine-type flow meter. The temperatures of the inlet air, the exhaust gas (T_{ex}), diesel fuel, ammonia before injection, and the intake port (T_{port}) were measured. Cylinder pressure traces have been measured using a piezoelectric pressure transducer with a resolution of 1024 measuring points per shaft rotation and for 100 consecutive cycles. An electric motor dynamometer was coupled to the engine to control the engine load and rotational speed. All measured parameters have been monitored with LabVIEW software and National Instruments hardware.

A Fourier Transform Infrared Spectroscopy (FTIR) from Gasmeter company (Gasmeter DX4000) was used to analyze the exhaust gases. Calcmet software runs FTIR that can analyze 50 gas components in corrosive and wet gas streams at the same time. Various spectrum libraries are embedded in the software that can determine the concentration of each species with an accuracy of 2%. Besides FTIR, an additional gas analyzer is used to verify the measured emissions. Particulate Matter (PM) was measured using SMG200 M with a precision of 3% and particle sizes in the range of 0.04 μm –10 μm under normal conditions (1 atm and 0°C). The exhaust gas sample has been taken directly from the exhaust port through a heated pipe of FTIR at 180 °C.

2.2. Experimental methods

The test was carried out to determine the maximum diesel that can be replaced with ammonia. In addition, the impact of the Ammonia Energy Share (AES, calculated by Eq. (9)) on engine performance, combustion, and emissions characteristics was examined. Since ammonia has a low flame speed and a high minimum required ignition energy [39,40], low engine speed fixed at 1200 rpm and full load were chosen for all operating conditions. The first operating point regarded as the reference was taken at those conditions fueled with pure diesel. Subsequently, the

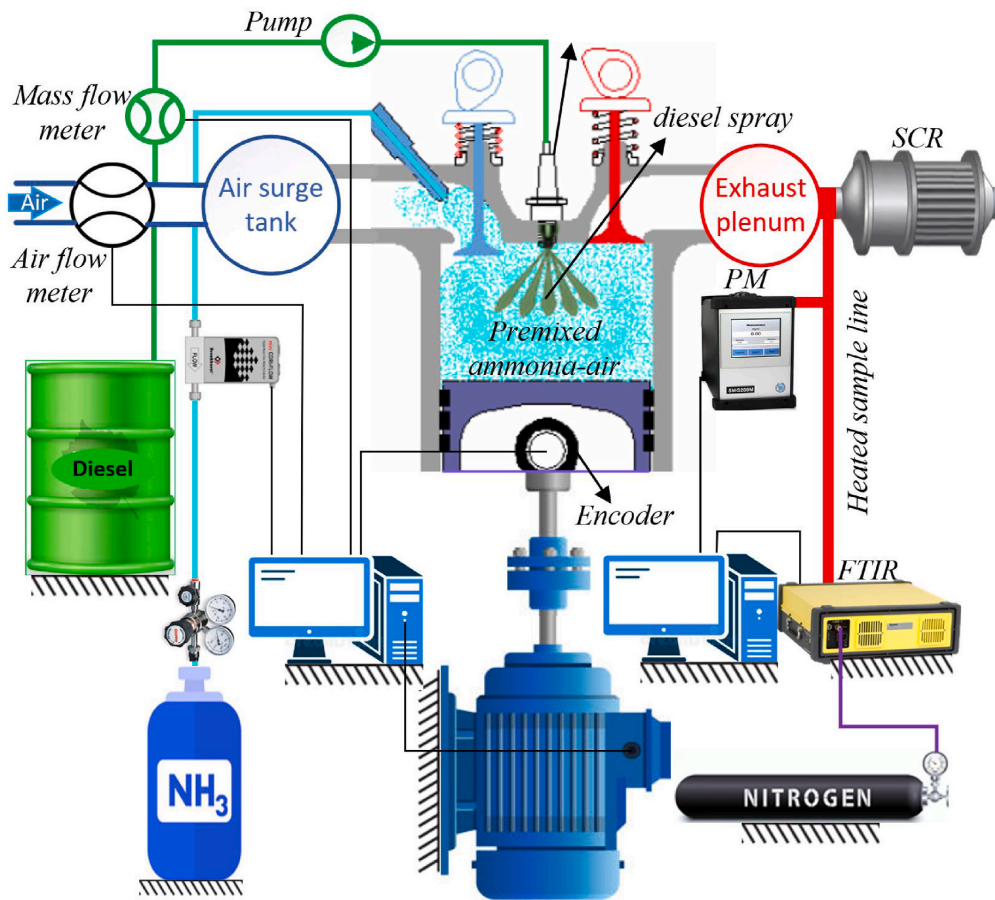


Fig. 1. The schematic of the test rig configuration.

mass flow of diesel is reduced and gaseous ammonia is aspirated to the intake port close to the inlet valve according to the AES values in Table 3, to achieve the same power as in the case of pure diesel.

Introducing more ammonia into the intake manifold to obtain a higher AES, decreases the air mass flow rate. Furthermore, the LHV of ammonia is lower compared to that of diesel, which requires a higher mass flow rate to achieve the same power as pure diesel. The stoichiometric air fuel ratio (AFR_{sto}) of the mixture decreases with increasing ammonia ratio, as ammonia has a stoichiometric AFR of 6.0 [41]. Thus, λ varies between 1.34 and 1.52 for all operating points, as reported in Table 3. The Coefficient Of Variation (COV) for maximum cylinder

pressure ($COV_{P_{max}}$), the location of the peak of the in-cylinder pressure and IMEP (COV_{IMEP}) have been calculated for each test and are presented in Fig. 2. COV is less than 2%, as can be seen in Fig. 2. However, it increases dramatically to 6.0% for maximum AES, which means unstable operation. Therefore, the maximum diesel fuel that could be replaced with ammonia was $AES = 84.2\%$ and for a higher value of AES, the engine could not run.

Table 3
Overview of the operating points conditions.

NO.	\dot{m}_{diesel}	\dot{m}_{NH_3}	\dot{m}_{air}	Y_{NH_3}	AES	T_{port}	T_{Ex}	P_i	AFR_{sto}	λ
	g/s	g/s	g/s	–	%	°C	°C	kW	kg/kg	–
OP1	0.220	0	4.27	0	0	33.6	460	3	14.59	1.35
OP2	0.186	0.074	4.25	0.286	14.90	31.3	450.6	3.05	12.15	1.36
OP3	0.152	0.135	4.25	0.470	27.94	28.1	399.2	3	10.58	1.41
OP4	0.127	0.162	4.25	0.561	35.85	26.6	387.7	2.95	9.80	1.51
OP5	0.103	0.212	4.21	0.674	47.44	26.0	373.5	3	8.84	1.52
OP6	0.09	0.249	4.15	0.735	54.81	24.9	370.6	3.06	8.32	1.48
OP7	0.076	0.279	4.03	0.786	61.62	24.8	357.7	3.06	7.89	1.45
OP8	0.040	0.338	3.97	0.894	78.73	23.6	335.4	2.98	6.96	1.51
OP9	0.030	0.364	3.88	0.924	84.16	22.5	328	3.03	6.71	1.47

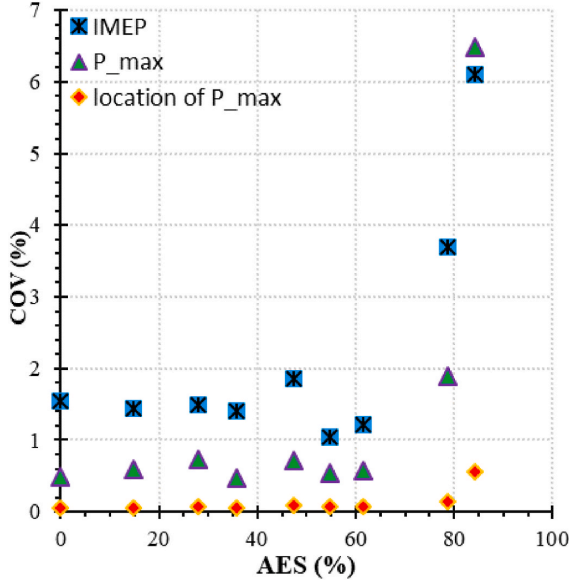


Fig. 2. COV of IMEP, the location of the maximum pressure, and peak of the in-cylinder pressure against AES.

3. Numerical methods

3.1. One dimensional model setup

A 1D model was used to analyze the ammonia-fueled engine by using AVL BOOST software and the BURN utility. A method called the “target pressure curve 2 zone” is used to model combustion in the cylinder. In this model, the measured in-cylinder pressure curves are used to calculate the Mass Fraction of Burned (MFB) fuel and the Heat Release Rate (HRR) profiles [42]. Hence, the combustion zone in the cylinder is divided between the unburned and burned gas regions [43]. The first law of thermodynamics is applied to the burned and unburned regions to calculate the gas temperature for each region [44,45]. First law for the burned zone:

$$\frac{dm_b u_b}{d\alpha} = -P_c \frac{dV_b}{d\alpha} + \frac{dQ_f}{d\alpha} - \sum \frac{dQ_{wb}}{d\alpha} + h_u \frac{dm_b}{d\alpha} - h_{BB,b} \frac{dm_{BB,b}}{d\alpha} \quad (1)$$

And for the unburned zone:

$$\frac{dm_u u_u}{d\alpha} = -P_c \frac{dV_u}{d\alpha} - \sum \frac{dQ_{wu}}{d\alpha} - h_u \frac{dm_u}{d\alpha} - h_{BB,u} \frac{dm_{BB,u}}{d\alpha} \quad (2)$$

The terms $\frac{dm_b u_b}{d\alpha}$, $P_c \frac{dV_b}{d\alpha}$, and $\frac{dQ_f}{d\alpha}$ denote the change in internal energy in the cylinder, the work of the piston, and the chemical energy input of the fuel, respectively. Also, $\sum \frac{dQ_{wb}}{d\alpha}$, $h_u \frac{dm_b}{d\alpha}$, and $h_{BB,b} \frac{dm_{BB,b}}{d\alpha}$ are heat losses from the combustion chamber, enthalpy transfer from the unburned zone to the burned zone, and enthalpy blow-by loss in the cylinder which is taken into account and calculated by the BOOST model [42]. In the above equations Eq. (1), and Eq. (2), the volume of the burned and unburned zone is equal to the cylinder volume:

$$V_b + V_u = V_c \quad (3)$$

and the changes of the volume of each zone are equal to the cylinder volume change:

$$\frac{dV_b}{d\alpha} + \frac{dV_u}{d\alpha} = \frac{dV_c}{d\alpha} \quad (4)$$

The volume work is calculated by Refs. [46,47]:

$$\frac{dW}{d\alpha} = P \frac{dV}{d\alpha} \quad (5)$$

The mass of the burned fuel in each CAD is calculated as follows [48, 49]:

$$MFB(\alpha) = \int \frac{dm_{bf}}{d\alpha} d\alpha \quad (6)$$

heat transfer Q_{wi} to the combustion chamber walls, namely, the cylinder head, piston, and liner, is determined by using the following equation:

$$Q_{wi} = A_{wi} \times h_w \times (T_c - T_{wi}) \quad (7)$$

where A_{wi} is the surface area, T_c is the cylinder temperature, and T_{wi} is the temperature of the respective chamber wall. The heat transfer coefficient (h_w) is calculated using the following Woschni model [50]:

$$h_w = 130 \times D^{-0.2} \cdot P_c^{0.8} \cdot T_c^{-0.53} \cdot \left[C_1 \cdot C_m + C_2 \cdot \frac{V_D \cdot T_{c,1}}{P_{c,1} \cdot V_{c,1}} (P_c - P_{c,o}) \right]^{0.8} \quad (8)$$

3.2. Performance parameters

Performance parameters monitored in the present study are now described and depend on the fuels' properties and their proportions. The LHV of diesel was measured and equals 42.4 MJ/kg, and the LHV value for ammonia was taken from the literature as 18.6 MJ/kg [51]. Other characteristic properties of the two fuels are shown in Table 4.

In this work, AES is defined as the ratio of the ammonia input energy to the total input energy in the dual fuel model in Eq. (9).

$$AES = \frac{\dot{m}_{NH_3} \times LHV_{NH_3}}{\dot{m}_f LHV_f + \dot{m}_{NH_3} LHV_{NH_3}} \quad (9)$$

The Indicated Thermal Efficiency (ITE) is defined as follows:

$$ITE = \frac{P_i}{\dot{m}_f \times LHV_f + \dot{m}_{NH_3} \times LHV_{NH_3}} \quad (10)$$

where P_i is the indicated power.

The mole fractions of each species were measured every 5 s in 10 min of a steady-state running engine using FTIR. Hence, the standard deviation of 120 measurements of exhaust gas samples was calculated and added to the figures [38]. Because the composition of the mixture varies for different operating points, the concentration of each species was recalculated according to Eq. (11) in 5% of O_2 [52].

$$(X_i)_{5\%O_2} = (X_i)_m \left[\frac{20.9\% - 5\%}{20.9\% - (O_2)_m} \right] \quad (11)$$

Where $(X_i)_m$ and $(O_2)_m$ are measured mole fraction of each species and the mole fraction of O_2 , respectively.

The indicated equivalent specific fuel consumption is defined in Eq. (12) in the dual fuel engine [53].

$$ISFC_{eq} = \frac{\dot{m}_f + \dot{m}_{NH_3} \frac{LHV_{NH_3}}{LHV_f}}{P_i} \quad (12)$$

4. Results

4.1. Engine performance

The engine was operated to obtain the same power at full load using

Table 4
Fuels elementary analysis and LHV.

Fuel	C(kg/kg)	H(kg/kg)	N(kg/kg)	LHV (MJ/kg)
Diesel	0.8078	0.1556	0.0003	42.4
Ammonia	0	0.176	0.824	18.6 [51]

different ammonia-diesel input energy ratios. However, the indicated thermal efficiency varies for various ammonia energy shares. Hence, Fig. 3 shows the increase in ITE with increasing AES. For example, ITE increases from 32.0% for pure diesel operation (OP1) to 37.6% for the maximum ammonia energy share (OP9). This 5.6% point rise in ITE is due to two main reasons. First, during ammonia/diesel combustion the in-cylinder temperature is lower than during pure diesel combustion [31], hence heat losses through the cylinder walls are lower (see eq. (8)). As can be seen in Fig. 4, a higher fraction of ammonia energy reduces the total heat loss through the piston, liner, cylinder, and head walls from 320 J/cycle for the pure diesel operation to 240 J/cycle for the highest AES, while volume work is the same. Secondly, as presented in Fig. 5 exhaust gas temperature decreases with higher AES, thus less energy is brought away. The lowest exhaust gas temperature was obtained at AES = 84.2% which is 132 °C lower than for pure diesel operation. This decrease in exhaust gas temperature is related to the lower in-cylinder temperature of ammonia/diesel combustion in the expansion stroke.

The effects of ammonia (AES) on the equivalent $ISFC_{eq}$ are presented in Fig. 6. $ISFC_{eq}$ decreases as more diesel fuel is replaced by ammonia; for example, $ISFC_{eq}$ decreased from 264g/kWh for the pure diesel mode to 224.9g/kWh for the highest AES. This 14.7% decrease in $ISFC_{eq}$ is related to the higher ITE of the ammonia/diesel operation. A similar trend was reported by Reiter et al. [54].

It is also interesting to assess the financial cost of indicated power P_i by comparing pure diesel operation (OP1) with the ammonia dual fuel mode (OP9). During the pure diesel operation (OP1) the fuel consumption is 264 g/kWh, whereas during the dual fuel operation, the engine consumes 35.6g/kWh diesel and 432.6g/kWh ammonia. Although ammonia consumption is higher, the P_i cost is significantly lower compared to the pure diesel mode. As can be seen in Table 5, the cost of P_i in the ammonia/diesel engine is approximately 0.24€/kWh, which is 44% less than the conventional diesel engine.

4.2. In-cylinder pressure

Fig. 7 shows the effects of ammonia on in-cylinder pressure traces. Increasing the ammonia energy share up to 61.6% increases the peak of

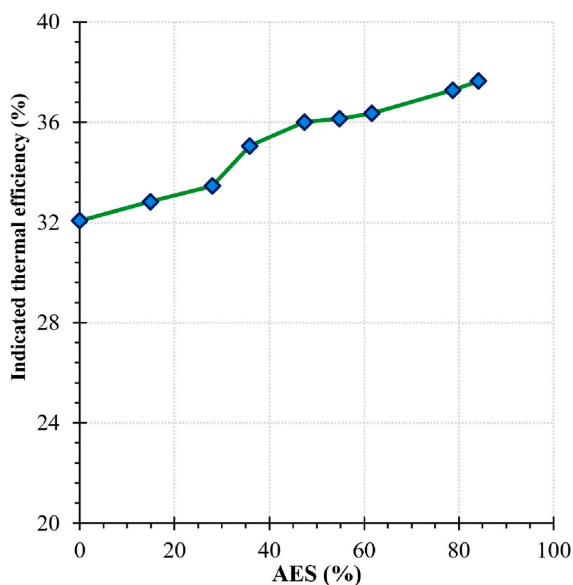


Fig. 3. Indicated efficiency of the ammonia/diesel fueled engine for different ammonia energy share.

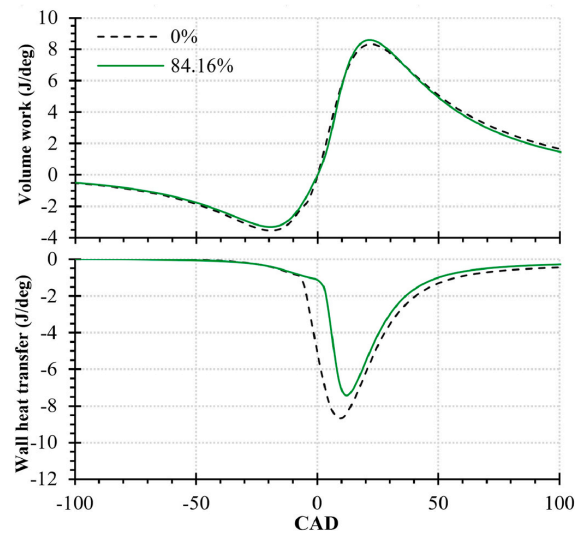


Fig. 4. Volume work and heat transfer of the ammonia/diesel-fueled engine against AES.

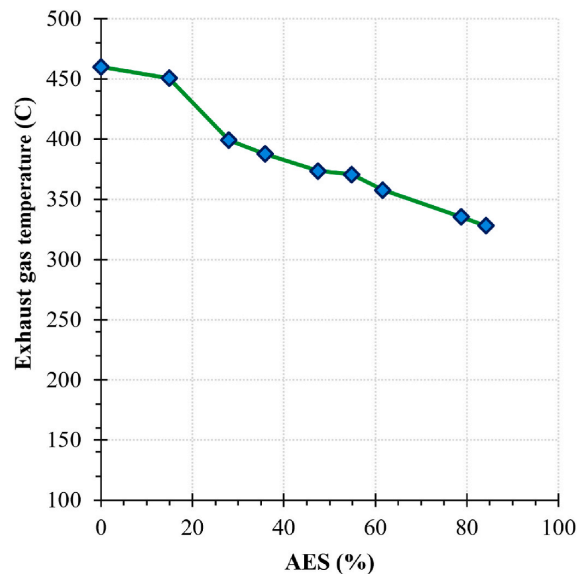


Fig. 5. Effects of ammonia energy share on exhaust gas temperature.

in-cylinder pressure. However for higher AES of 78.7% and 84.2% the peak pressure decreases. Hence, the peak of in-cylinder pressure increases from 76.3 bar for pure diesel to 86.2 bar when the AES is 61.6%. It is related to the fact that combustion occurs a few CAD before the TDC, as can be seen in the Fig. 8 where the maximum Pressure Rise Rate (PRR) is located close to 0 CAD. However, if diesel fuel is replaced with more than 61.6% ammonia, the in-cylinder pressure decreases dramatically since ammonia/diesel combustion occurs after TDC. For example, the pressure drops to 72.7 bar for the highest possible ammonia energy fraction. Furthermore, ammonia has a lower polytropic coefficient (γ) than air [55]. Hence, as more ammonia is introduced into the intake port, the γ of the mixture reduces, and therefore the motored pressure

E. Nadimi et al.

Journal of the Energy Institute 107 (2023) 101158

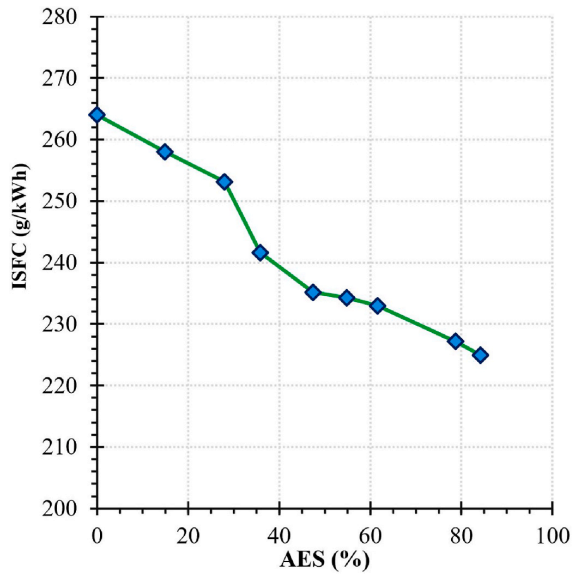


Fig. 6. Equivalent indicated specific fuel consumption of the ammonia/diesel fueled engine.

Table 5

Comparison of P_i cost in the ammonia diesel dual fuel mode with only diesel operation.

AES	0%	84.16% (dual fuel)	
Fuel	Diesel	Ammonia	Diesel
Fuel price (£/kg)	1.65	0.43	1.65
ISFC (g/kWh)	264	432.67	35.64
P_i cost (£/kWh)	0.43	0.24	

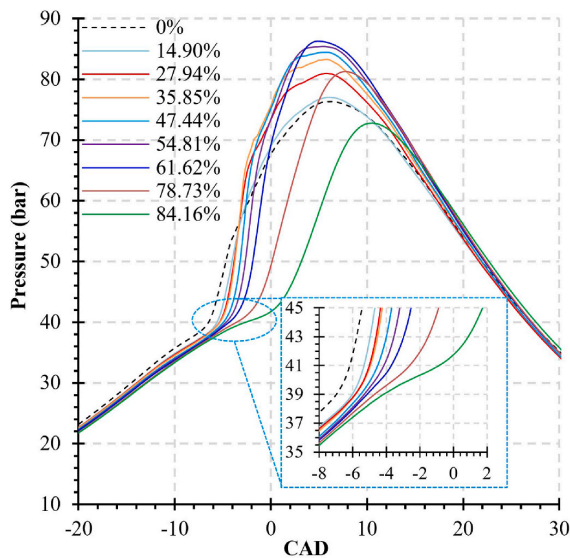


Fig. 7. In-cylinder pressure traces for different ammonia/diesel ratios.

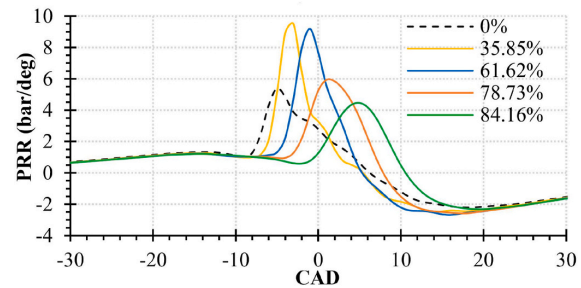


Fig. 8. Effects of different ammonia diesel energy shares on pressure rise rate traces.

decreases accordingly, as can be seen in Fig. 7. Although the pressure during compression and expansion is low for the highest ammonia energy share, the volume work for pure diesel operation and the AES of 84.2% are the same (Fig. 4).

The first derivative of the in-cylinder pressure known as the pressure rise rate is shown in Fig. 8. The results reveal the delay in the PRR profiles as more diesel is substituted by ammonia, which is caused by the high minimum ignition energy of ammonia compared to diesel. The maximum PRR rises to 9.5 bar/deg for the AES of 61.6%, which is 76.5% higher than for pure diesel. Moreover, PRR decreases parabolically for ammonia diesel combustion, whereas it is a linear decline for pure diesel mode. This is due to the combustion of the homogeneous mixture of ammonia air, the short combustion duration, and combustion phasing period. The peak of PRR diagram decreases for the highest AES because combustion starts after TDC (SOC = 0.38CAD).

4.3. Effects of ammonia on combustion characteristics

HRR curve of the regular diesel engine typically consists of four phases: ignition delay, premixed combustion, diffusion combustion, and late combustion [56]. However, the HRR diagram for the ammonia/diesel dual fuel mode differs because of the high premixed ammonia-air ratio. Therefore, increasing the ammonia ratio reduces diffusion and the late combustion stage but increases ignition delay and premixed combustion phases, as shown in Fig. 9(a). The HRR curves' peak reveals that high heat was released during the premixed combustion stage. MFB diagram describes the process of chemical energy release and energy conversion as a function of the crank angle. In addition, the characteristics of the combustion phases are determined by the MFB curves, such as the duration of combustion and the ignition delay (Fig. 13) [57,58]. The impacts of AES on the mass fraction of the burned ammonia/diesel mixture are presented in Fig. 9(b). The exponential growth of the MFB curves with increasing AES indicates premixed combustion as a result of the perfect mixing of ammonia and air. Hence, a shorter MFB can enhance output work during the combustion process [59].

Ammonia is known for its low flame speed and high ignition delay time. A pilot fuel is needed to provide the ignition energy to initiate combustion of the premixed ammonia-air mixture. The start of combustion and flame initiation are shown in Fig. 10(a). As more diesel is replaced with ammonia, SOC, CA05, and CA10 are delayed. However, for AES between 0 and 35.85%, the SOC and the ignition delay do not change. The ignition delay is almost 8 CAD when the AES is less than 35.9% due to the higher portion of diesel fuel. Fig. 10(b) shows that the effective in-cylinder ignition delay time increases from 8.7 CAD in case of pure diesel to 15.9 CAD for the highest AES. This is mainly due to the decrease in air mass flow as gaseous ammonia is introduced into the intake manifold, which decreases the oxygen concentration in the cylinder. In addition, ammonia reduces the compression pressure and consequently in-cylinder temperature; therefore, some of the preignition energy will be used to increase in-cylinder pressure and temperature.

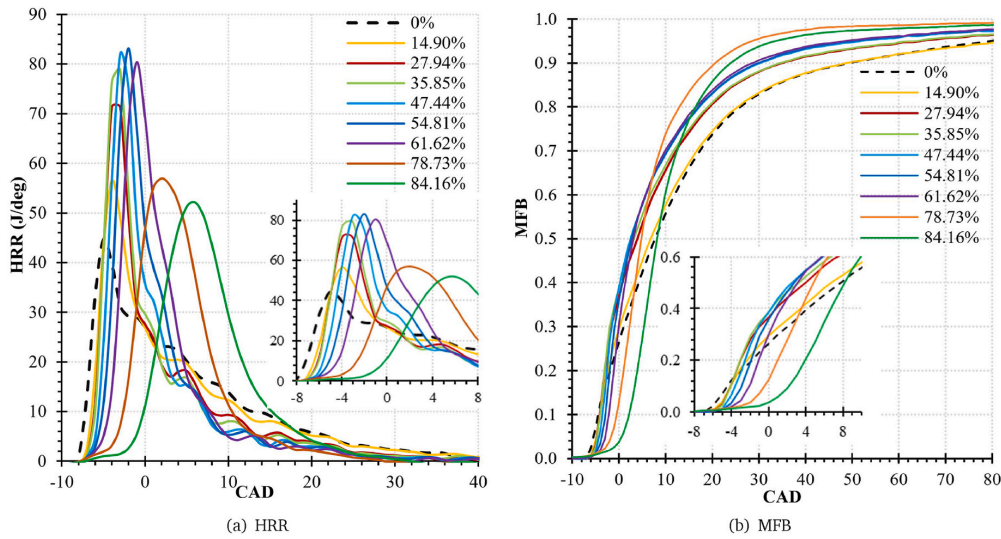


Fig. 9. MFB and HRR profiles for different ammonia diesel energy shares.

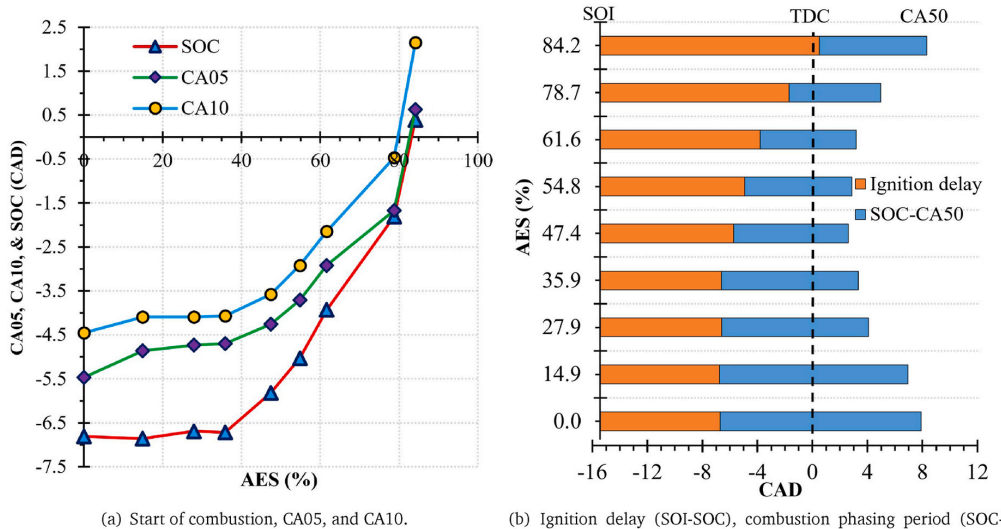


Fig. 10. Ammonia/diesel combustion characteristics indicators for different ammonia energy shares.

Also, ammonia's high required minimum ignition energy and temperature cause this longer ignition delay. For the highest AES, combustion starts in the TDC, where the pressure and temperature are higher as well as there are more desirable thermodynamic conditions for ignition. However, for AES greater than 84.2% combustion does not occur.

Furthermore, the effects of AES on combustion phasing period SOC-CA50 and combustion duration SOC-CA90 are shown in Figs. 10(b) and 11, respectively. As more diesel is replaced by ammonia, the CA50 and the combustion duration are reduced accordingly. Therefore, the CD was reduced from 56 CAD for only diesel operation to 24 CAD for the highest AES. This reduction in CA50 and CD is mainly due to the rapid combustion of premixed ammonia air and the greater heat released during the premixed combustion phase in the HRR diagram compared to pure diesel combustion, as discussed above. Moreover, a higher AES

decreases diffusion and the late combustion phases, resulting in a shorter SOC-CA50 and CD. Tay et al. [60,61] also reported similar results that ammonia decreases the CA50 and combustion duration.

4.4. Emissions analysis

Fig. 12 shows the effects of replacing diesel fuel with ammonia on CO₂ emission and H₂O in the same operation and the indicated power. This figure well demonstrates that ammonia significantly reduces CO₂ emission and instead produces only H₂O. Therefore, increasing the AES from 0 for only diesel mode to 84.2% for the highest diesel substitution, decreased CO₂ emission from 7.0% to 0.9% (7.3 time reduction). Similarly, H₂O increased significantly from 7.4% to 14.9%. Fig. 13(a) illustrates that CO emissions decreased markedly as more diesel fuel is

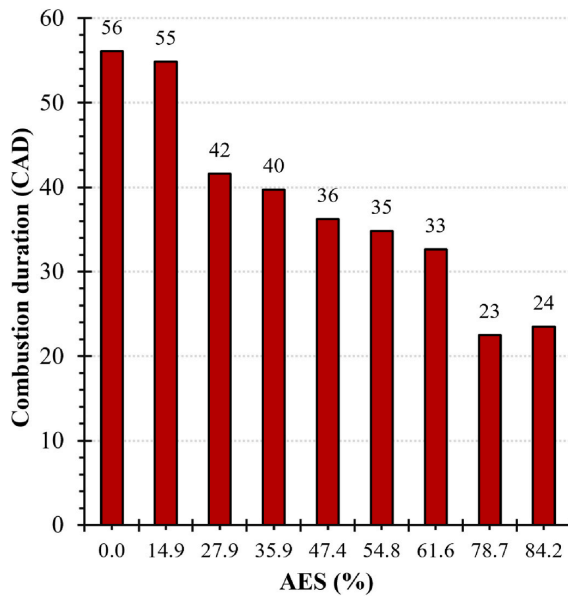


Fig. 11. Combustion duration (SOC-CA90) of ammonia/diesel fueled engine for various ammonia/diesel ratios.

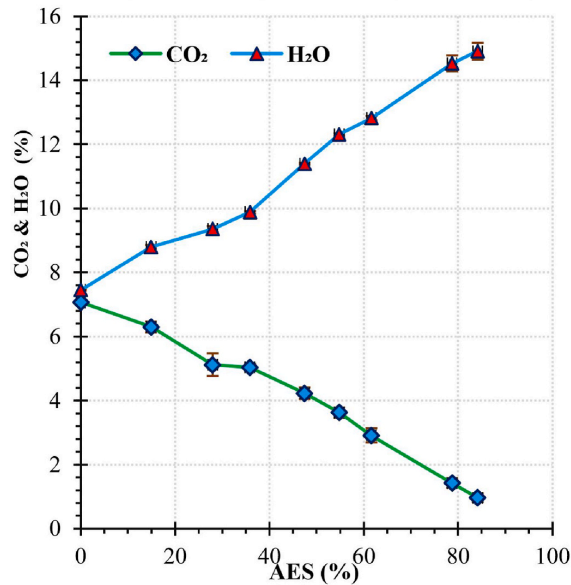
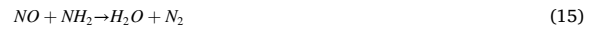


Fig. 12. CO₂ and H₂O emissions of ammonia fueled diesel engine for various ammonia energy shares.

replaced by ammonia. Hence, CO emission decreased drastically from 7592 ppm to 140 ppm. This is due to the fact that replacing diesel with ammonia diminished the carbon atom in the mixture, which results in a reduction in carbon-based emissions. However, the high amount of CO in the pure diesel mode is due to the low engine speed and the full load condition.

Fig. 13(b) illustrates an interesting trend in which NO emission first

decreases and then increases as more ammonia is introduced into the intake port. In other words, some amount of ammonia reduces NO emission, which can be seen in other articles [34,54,60]. Hence, NO emission decreased from 831 ppm for the only diesel case to 491 ppm when AES is 14.9%. Moreover, NO emission is lower than that in the case of pure diesel, while AES is below 35.85%. This is mainly due to firstly, ammonia changes combustion to low-temperature combustion as a result of the low flame temperature of ammonia [62]. Thermal NO formation is less when the combustion temperature is lower. Secondly, Mathieu and Petersen [63] by modeling the ammonia reactions mechanism have revealed that reactions 13, 14, and 15 are the three most dominant reactions with a high sensitivity coefficient in premixed ammonia-air combustion. Therefore, when the amount of NH₃ is low, NO reacts with NH₂ radicals, resulting in a reduction in NO levels.



However, as more ammonia was introduced into the intake manifold, NO increased considerably to 2359 ppm at the highest diesel replacement. Because NO formation depends both on the presence of N in NH₃ and on the cylinder temperature. Moreover, since the ignition of the premixed ammonia air starts near TDC for higher AES, this promotes the formation of NO.

Fig. 14 shows N₂O and NO₂ against the input energy share of ammonia/diesel. In general, conventional diesel engines fueled by fossil fuels generally produce a negligible amount of N₂O emission [64]. Thus, N₂O emission is about 3 ppm for the only diesel case. However, as soon as ammonia is injected into the intake manifold, the N₂O emission increased dramatically to 90 ppm and then decreased slightly to 42 ppm for high AES. Although the ammonia diesel dual fuel engine produces a low amount of N₂O emission, but it has 298 times GWP effects compared to CO₂ over 100 years. N₂O is formed during the ammonia ignition process and is nearly absent after complete combustion. It is suggested that N₂O emission can be formed during interruption of ignition and combustion e.g. by quenching on the wall. Therefore, proper design of injection strategy using direct injection of both fuels has a huge chance to improve the reduction of N₂O emission.

Fig. 15 shows the concentration of unburned ammonia in the wet exhaust gas for various ammonia energy shares. Ammonia emission increases significantly as more diesel fuel is replaced by ammonia. Unburned ammonia increased from 7 ppm for only the diesel case to the critical concentration of 14800 ppm for maximum AES. This is likely due to the high amount of excess ammonia in the cylinder, which causes significant amount of unburned ammonia since ammonia is injected continuously into the intake port. Also, owing to the low flame speed of ammonia, which causes unsuccessful flame propagation in the crevices volume, which often causes unburned fuel. More research is needed to reduce this level of unburned ammonia, such as direct injection of liquid ammonia, varying its injection timing and exhaust aftertreatment system. Since an ammonia concentration of more than 50 ppm is hazardous to health.

The effects of different ammonia diesel ratios on particulate matter emission are presented in Fig. 16. It can be observed that increasing the ammonia level significantly reduced the PM emission. In general, soot emissions are promoted by fuel-rich zones and are formed in crevices volume. When the premixed ignition fails in fuel-rich areas, the oxidation can not be complete because of insufficient oxygen. This causes a high PM emission for only diesel operation around 22 mg/m³. However, injecting gaseous ammonia by premixed combustion and reducing the amount of carbon in the mixture decreases PM formation. Therefore, the lowest PM of 4.7 mg/m³ was observed at the maximum AES.

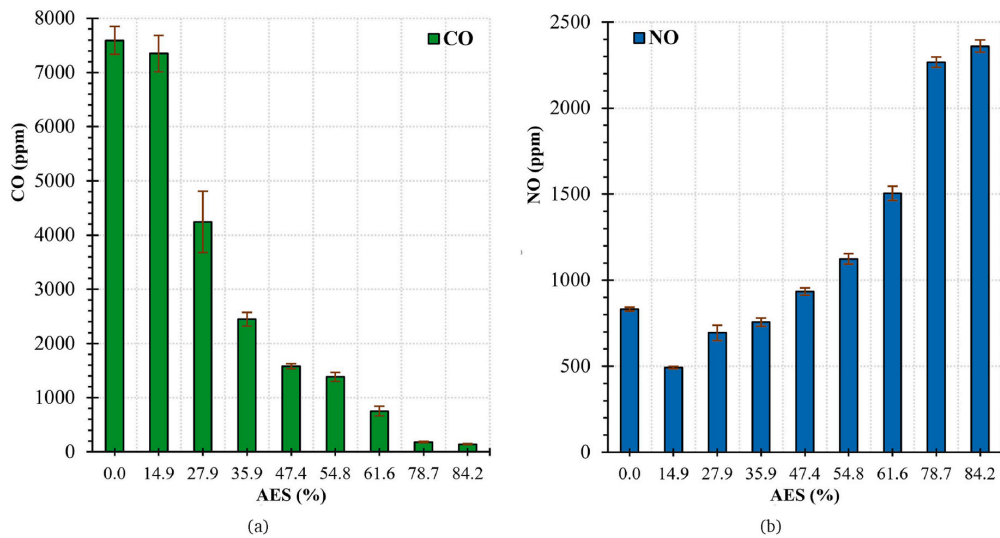


Fig. 13. Effects of ammonia on (a) CO and (b) NO emissions in the ammonia fueled diesel engine.

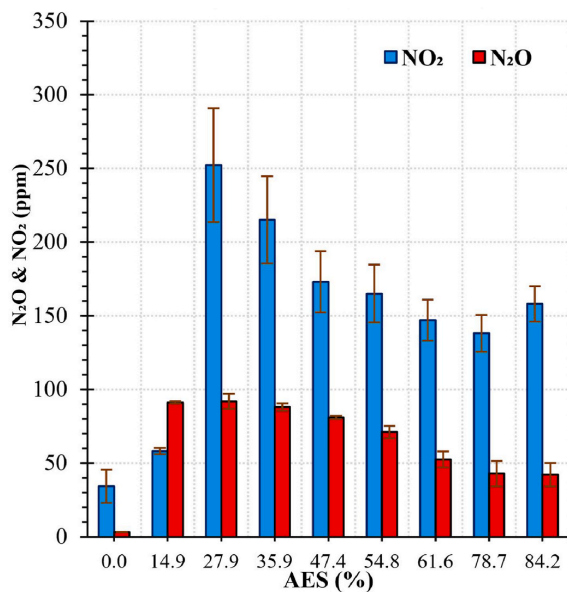


Fig. 14. NO₂ and N₂O emissions in the ammonia dual fuel diesel engine.

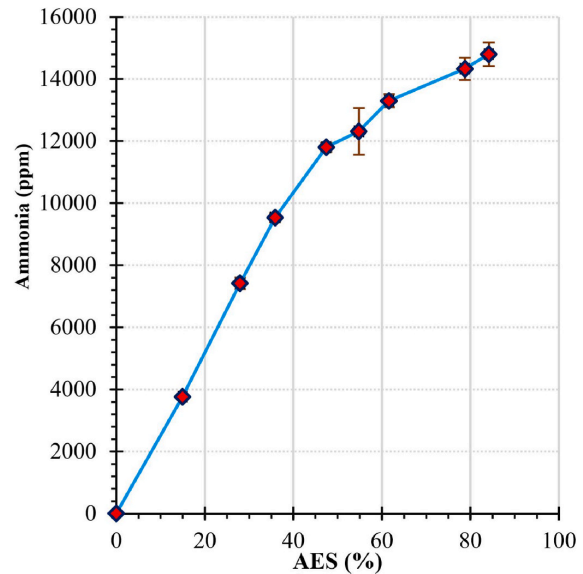


Fig. 15. Unburnt ammonia for various ammonia/diesel ratios in the ammonia fueled diesel engine.

4.5. Greenhouse gas emissions and CO₂ equivalents

Ammonia is considered a potential carbon-free fuel for ICE that can reduce CO₂ emissions. Hence, Ammonia diesel dual-fuel engine decreased CO₂ emission by 600g/kWh compared to the conventional diesel engine at the same power and at the highest diesel substitution. However, ammonia combustion in dual fuel mode also produces N₂O emission, which is one of the challenges of ammonia-fueled engines. N₂O is recognized to have a high global warming potential (GWP) of 298 on a 100-year scale relative to CO₂ itself. Therefore, even a small amount of N₂O emission can offset the benefits of reduced CO₂ in the ammonia dual fuel engine. Thus, Fig. 17 shows the GHG emissions for different

AES. Introducing a small amount of ammonia around 14.9% by input energy significantly increased N₂O emission by 0.84g/kWh (251.9g/kWh of equivalent CO₂) for OP2. This offset the 124.3g/kWh of reduction in CO₂ in OP2. In addition, CH₄ emission is also higher in low AES, which has 28 times GWP relative to CO₂. However, by replacing more diesel with ammonia, CO₂ and therefore total GHG emission decreased significantly. As a result, GHG emissions decreased notably from 727g/kWh for only diesel combustion mode to 243g/kWh for the highest AES. Furthermore, the lower amount of ammonia around 27.9% by AES has higher GHG emissions than the conventional diesel engine.

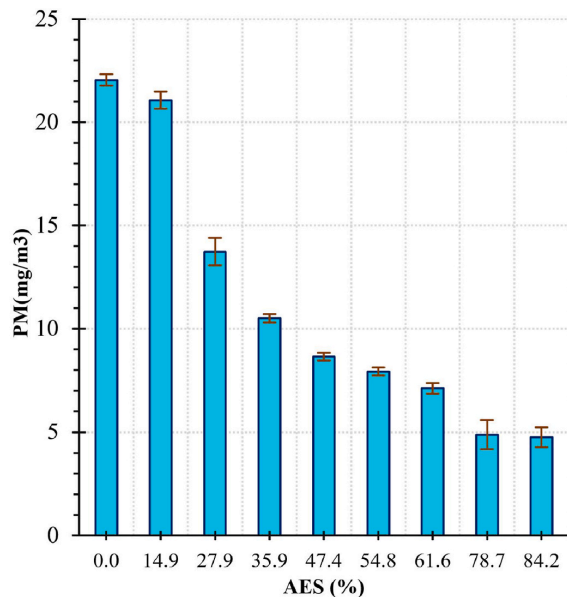


Fig. 16. Particulate matter emission for different ammonia energy shares.

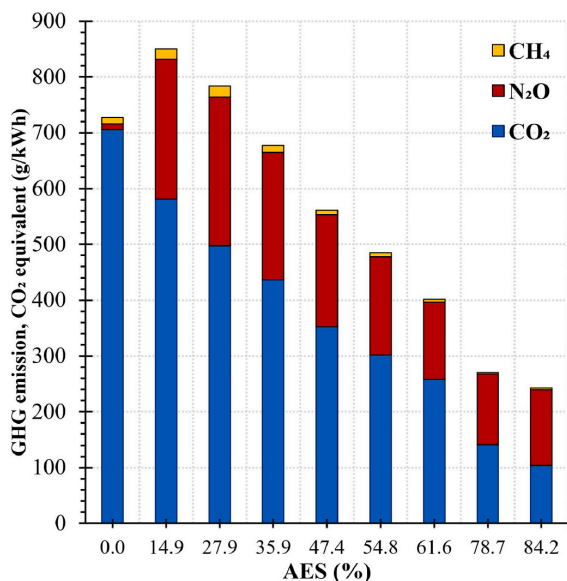


Fig. 17. Indicated specific GHG emissions equivalent to CO₂ over 100 years for different ammonia/diesel ratios.

5. Summary and conclusions

Ammonia is potential non-carbon fuel to replace current fossil fuels and decarbonize internal combustion engines. An extensive experiment was carried out to study various diesel substitutions with ammonia in the single-cylinder diesel engine. Thus, this work investigates the different ammonia energy shares on ignition, emission characteristics, and engine performance of the ammonia diesel dual fuel CI engine. Moreover, the ammonia/diesel combustion was studied by developed

1D model. The main results of this research are summarized as follows.

- The maximum 84.2% of input energy was provided by ammonia. As more ammonia was introduced into the intake port increased ITE by around 5.6% point at the highest AES. It also reduced the EGT by 132°C in this point. The P_i cost of the ammonia/diesel engine is approximately 0.247€/kWh, which 43.3% less than the conventional diesel engine.
- Since ammonia has a lower γ than air, the compression pressure decreases by increasing the ammonia mass flow. However, ammonia increases the peak of in-cylinder pressure. Furthermore, it also increases dramatically the peak of PRR to 9.5 bar/deg for AES of 61.6%, which is 76.5% higher than only the diesel case due to premixed combustion.
- Ammonia delayed the SOC by around 7.2CAD at the highest diesel substitution due to the low compression pressure and consequently in-cylinder temperature. Higher ammonia ratio also reduced diffusion combustion phase and increased premixed combustion mode at the highest AES. Thus, the combustion phase and the combustion duration decreased by 6.8CAD and 32CAD, respectively compared to the pure diesel.
- By substituting diesel fuel, carbon-based emissions were markedly reduced, but NO, NO₂ and N₂O emissions increased. However, a significant amount of unburned ammonia was measured that further investigation is need to reduced ammonia emission.
- Ammonia significantly reduced the CO₂ emission from 705g/kWh to 103g/kWh, but it also produced N₂O emission, which has 298 times GHG effects. The GHG emissions decreased when more than 35.9% of diesel was replaced. Hence, the equivalent CO₂ emission of the ammonia dual fuel engine is higher than the case of only diesel when diesel substitution is low. However, GHG emissions decreased significantly from 727g/kWh for only diesel operation to 243g/kWh for the highest AES.

CRedit authorship contribution

Ebrahim Nadimi: Conceptualization, Methodology, Software, Validation, Formal analysis, Investigation, Experiment, Data Curation, Figures, Original draft, Writing - review & editing. **Grzegorz Przybyła:** Conceptualization, Methodology, Investigation, Experiment, Writing - review & editing. **Michał T. Lewandowski:** Writing - review & editing. **Wojciech Adamczyk:** Writing - review & editing, project administration.

Declaration of competing interest

The authors declare that they have no known competing financial interests or personal relationships that could have appeared to influence the work reported in this paper.

Acknowledgment

This work was funded by Norway and Poland grant to ACTIVATE project (Contract NO. NOR/POLNOR/ACTIVATE/0046/2019-00) "Ammonia as carbon free fuel for internal combustion engine driven agricultural vehicle". The authors also thank AVL List GmbH for providing the license.

References

- [1] P. Senecal, F. Leach, Diversity in transportation: why a mix of propulsion technologies is the way forward for the future fleet, *Results in Engineering* 4 (2019), 100060.
- [2] S. Khandal, N. Banapurmath, V. Gaitonde, S. Hiremath, Paradigm shift from mechanical direct injection diesel engines to advanced injection strategies of diesel homogeneous charge compression ignition (hcci) engines-a comprehensive review, *Renew. Sustain. Energy Rev.* 70 (2017) 369–384.

- [3] K. Kuta, E. Nadimi, G. Przybyła, Z. Żmudka, W. Adamczyk, Ammonia ci engine aftertreatment systems design and flow simulation, *Combustion Engines* 61 (2022).
- [4] S. Jafarmadar, Multidimensional modeling of the effect of egr (exhaust gas recirculation) mass fraction on exergy terms in an indirect injection diesel engine, *Energy* 66 (2014) 305–313.
- [5] European Commission, Directive 2015/1513 of the European Parliament and of the Council amending Directive 98/70/EC relating to the quality of petrol and diesel fuels and amending Directive 2009/28/EC on the promotion of the use of energy from renewable sources, *Off. J. Eur. Union* (2015).
- [6] G. Liobikienė, M. Butkus, The European Union possibilities to achieve targets of Europe 2020 and Paris Agreement climate policy, *Renew. Energy* 106 (2017) 298–309.
- [7] A. Valera-Medina, F. Amer-Hatem, A. Azad, I. Dedoussi, M. De Joannon, R. Fernandes, P. Glarborg, H. Hashemi, X. He, S. Mashruk, et al., Review on ammonia as a potential fuel: from synthesis to economics, *Energy Fuels* 35 (9) (2021) 6964–7029.
- [8] H. Xiao, S. Lai, A. Valera-Medina, J. Li, J. Liu, H. Fu, Study on counterflow premixed flames using high concentration ammonia mixed with methane, *Fuel* 275 (2020), 117902.
- [9] S. Ni, D. Zhao, Y. You, Y. Huang, B. Wang, Y. Su, Nox emission and energy conversion efficiency studies on ammonia-powered micro-combustor with ring-shaped ribs in fuel-rich combustion, *J. Clean. Prod.* 320 (2021), 128901.
- [10] E. Nadimi, S. Jafarmadar, Thermal and exergy assessment of a micro combustor fueled by premixed hydrogen/air under different sizes: a numerical simulation, *J. Appl. Fluid Mech.* 13 (4) (2020) 1233–1243.
- [11] S. Mohseni, E. Nadimi, S. Jafarmadar, R.A. Rezaei, Enhance the energy and exergy performance of hydrogen combustion by improving the micro-combustor outlet in thermofluidic systems, *Int. J. Hydrogen Energy* 46 (9) (2021) 6915–6927.
- [12] J. Brightling, Ammonia and the fertiliser industry: the development of ammonia at Billingham, *Johnson Matthey Technology Review* 62 (1) (2018) 32–47.
- [13] A. Goldmann, F. Dinkelacker, Approximation of laminar flame characteristics on premixed ammonia/hydrogen/nitrogen/air mixtures at elevated temperatures and pressures, *Fuel* 224 (2018) 366–378.
- [14] A.J. Reiter, S.-C. Kong, Demonstration of compression-ignition engine combustion using ammonia in reducing greenhouse gas emissions, *Energy Fuels* 22 (5) (2008) 2963–2971.
- [15] C. Mounaim-Rousselle, P. Brequigny, Ammonia as fuel for low-carbon spark-ignition engines of tomorrow's passenger cars, *Front. Mech. Eng.* 6 (2020) 70.
- [16] A. Schönborn, Aqueous solution of ammonia as marine fuel, *Proc. IME M J. Eng. Marit. Environ.* 235 (1) (2021) 142–151.
- [17] C. Mounaim-Rousselle, P. Brequigny, C. Dumand, S. Houillé, Operating limits for ammonia fuel spark-ignition engine, *Energies* 14 (14) (2021) 4141.
- [18] C. Lhuillier, P. Brequigny, F. Contino, C. Mounaim-Rousselle, Experimental study on ammonia/hydrogen/air combustion in spark ignition engine conditions, *Fuel* 269 (2020), 117448.
- [19] K. Ryu, G.E. Zacharakis-Jutz, S.-C. Kong, Effects of gaseous ammonia direct injection on performance characteristics of a spark-ignition engine, *Appl. Energy* 116 (2014) 206–215.
- [20] S.M. Grannell, D.N. Assanis, S.V. Bohac, D.E. Gillespie, The fuel mix limits and efficiency of a stoichiometric, ammonia, and gasoline dual fueled spark ignition engine, *J. Eng. Gas Turbines Power* 130 (4) (2008).
- [21] S.M. Grannell, D.N. Assanis, D.E. Gillespie, S.V. Bohac, Exhaust emissions from a stoichiometric, ammonia and gasoline dual fueled spark ignition engine, *Internal Combustion Engine Division Spring Technical Conference* 43406 (2009) 135–141.
- [22] Y. Niki, Y. Nitta, H. Sekiguchi, K. Hirata, Diesel fuel multiple injection effects on emission characteristics of diesel engine mixed ammonia gas into intake air, *J. Eng. Gas Turbines Power* 141 (6) (2019).
- [23] F.R. Westlye, A. Ivarsson, J. Schramm, Experimental investigation of nitrogen based emissions from an ammonia fueled si-engine, *Fuel* 111 (2013) 239–247.
- [24] P. Dimitriou, R. Javadi, A review of ammonia as a compression ignition engine fuel, *Int. J. Hydrogen Energy* 45 (11) (2020) 7098–7118.
- [25] N. De Vries, Safe and Effective Application of Ammonia as a Marine Fuel, 2019.
- [26] T.B. Imhoff, S. Gkantonas, E. Mastorakos, Analysing the performance of ammonia powertrains in the marine environment, *Energies* 14 (21) (2021).
- [27] M. Yao, H. Wang, Z. Zheng, Y. Yue, Experimental study of n-butanol additive and multi-injection on hd diesel engine performance and emissions, *Fuel* 89 (9) (2010) 2191–2201.
- [28] M. Lamas, C. Rodriguez, Numerical model to analyze nox reduction by ammonia injection in diesel-hydrogen engines, *Int. J. Hydrogen Energy* 42 (41) (2017) 26132–26141.
- [29] J. Lasocki, M. Bednarski, M. Sikora, Simulation of ammonia combustion in dual-fuel compression-ignition engine, in: *IOP Conference Series: Earth and Environmental Science*, vol. 214, IOP Publishing, 2019, 012081.
- [30] K. Ryu, G.E. Zacharakis-Jutz, S.-C. Kong, Performance enhancement of ammonia-fueled engine by using dissociation catalyst for hydrogen generation, *Int. J. Hydrogen Energy* 39 (5) (2014) 2390–2398.
- [31] C.W. Gross, S.-C. Kong, Performance characteristics of a compression-ignition engine using direct-injection ammonia-dme mixtures, *Fuel* 103 (2013) 1069–1079.
- [32] R. Sivasubramanian, J. Sajin, G. Omanakuttan Pillai, Effect of ammonia to reduce emission from biodiesel fuelled diesel engine, *Int. J. Ambient Energy* (2019) 1–5.
- [33] W. Wang, J.M. Herreros, A. Tsolakis, A.P. York, Ammonia as hydrogen carrier for transportation; investigation of the ammonia exhaust gas fuel reforming, *Int. J. Hydrogen Energy* 38 (23) (2013) 9907–9917.
- [34] A. Yousefi, H. Guo, S. Dev, B. Liko, S. Lafrance, Effects of ammonia energy fraction and diesel injection timing on combustion and emissions of an ammonia/diesel dual-fuel engine, *Fuel* 314 (2022), 122723.
- [35] J. Frost, A. Tall, A.M. Sheriff, A. Schonborn, P. Hellier, An experimental and modelling study of dual fuel aqueous ammonia and diesel combustion in a single cylinder compression ignition engine, *Int. J. Hydrogen Energy* 46 (71) (2021) 35495–35510.
- [36] A. Yousefi, H. Guo, S. Dev, S. Lafrance, B. Liko, A study on split diesel injection on thermal efficiency and emissions of an ammonia/diesel dual-fuel engine, *Fuel* 316 (2022), 123412.
- [37] D. Lee, H.H. Song, Development of combustion strategy for the internal combustion engine fueled by ammonia and its operating characteristics, *J. Mech. Sci. Technol.* 32 (4) (2018) 1905–1925.
- [38] E. Nadimi, G. Przybyła, D. Emberson, T. Lovas, L. Ziolkowski, W. Adamczyk, Effects of using ammonia as a primary fuel on engine performance and emissions in an ammonia/biodiesel dual-fuel ci engine, *Int. J. Energy Res.* (2022).
- [39] S. Frigo, R. Gentili, Analysis of the behaviour of a 4-stroke si engine fuelled with ammonia and hydrogen, *Int. J. Hydrogen Energy* 38 (3) (2013) 1607–1615.
- [40] J.J. MacKenzie, W.H. Avery, Ammonia fuel: the key to hydrogen-based transportation, in: *Tech. Rep., Inst. of Electrical and Electronics Engineers, Piscataway, NJ (United States)*, 1996.
- [41] N.J. Vickers, Animal communication: when i'm calling you, will you answer too? *Curr. Biol.* 27 (14) (2017) R713–R715.
- [42] A. Boost, 2-theory, AVL List GmbH, 2013, p. 769.
- [43] Ş. Altun, H.F. Öztop, C. Oner, Y. Varol, Exhaust Emissions of Methanol and Ethanol-Unleaded Gasoline Blends in a Spark Ignition Engine, 2013.
- [44] G. Noske, A Quasi-Dimensional Model to Describe the Combustion Process in the Gasoline Engine, VDI-Verlag, 1988.
- [45] S. Iliiev, A comparison of ethanol and methanol blending with gasoline using a 1-d engine model, *Procedia Eng.* 100 (2015) 1013–1022.
- [46] A. Abassi, S. Khalilarya, S. Jafarmadar, The influence of the inlet charge temperature on the second law balance under the various operating engine speeds in di diesel engine, *Fuel* 89 (9) (2010) 2425–2432.
- [47] S. Jafarmadar, M. Mansoury, Exergy analysis of air injection at various loads in a natural aspirated direct injection diesel engine using multidimensional model, *Fuel* 154 (2015) 123–131.
- [48] I. Vibe, *Combustion and Cycle Process in Combustion Engines German Translation from Russian by Dr. Joachim Heinrich, 1970 published under the title: Brennverlauf und Kreisprozess von Verbrennungsmotorenby.*
- [49] S. Jafarmadar, N. Javani, Exergy analysis of natural gas/dme combustion in homogeneous charge compression ignition engines (hcci) using zero-dimensional model with detailed chemical kinetics mechanism, *Int. J. Exergy* 15 (3) (2014) 363–381.
- [50] G. Woschni, A universally applicable equation for the instantaneous heat transfer coefficient in the internal combustion engine, in: *Tech. Rep., SAE Technical paper*, 1967.
- [51] H. Kobayashi, A. Hayakawa, K.K.A. Somaratne, E.C. Okafor, Science and technology of ammonia combustion, *Proc. Combust. Inst.* 37 (1) (2019) 109–133.
- [52] D.A. Lewandowski, *Design of Thermal Oxidation Systems for Volatile Organic Compounds*, CRC Press, 2017.
- [53] F. Salek, M. Babaie, M.D. Redel-Macias, A. Ghodsi, S.V. Hosseini, A. Nourian, M. L. Burby, A. Zare, The effects of port water injection on spark ignition engine performance and emissions fueled by pure gasoline, e5 and e10, *Processes* 8 (10) (2020) 1214.
- [54] A.J. Reiter, S.-C. Kong, Combustion and emissions characteristics of compression-ignition engine using dual ammonia-diesel fuel, *Fuel* 90 (1) (2011) 87–97.
- [55] Y.A. Cengel, M.A. Boles, M. Kanoglu, *Thermodynamics: an Engineering Approach*, vol. 5, McGraw-hill, New York, 2011.
- [56] J. Heywood, *Internal Combustion Engine Fundamentals*, mcgraw-hill book co, New York, 1988.
- [57] A. Jamrozik, W. Tutak, M. Pyrc, M. Gruca, M. Kočiško, Study on co-combustion of diesel fuel with oxygenated alcohols in a compression ignition dual-fuel engine, *Fuel* 221 (2018) 329–345.
- [58] K.Z. Mendera, A. Spyra, M. Smereka, Mass fraction burned analysis, *J. KONES Internal Combustion Engines* 3 (4) (2002) 193–201.
- [59] V. Gnanamoorthi, V. Vimalananth, Effect of hydrogen fuel at higher flow rate under dual fuel mode in crdi diesel engine, *Int. J. Hydrogen Energy* 45 (33) (2020) 16874–16889.
- [60] K.L. Tay, W. Yang, J. Li, D. Zhou, W. Yu, F. Zhao, S.K. Chou, B. Mohan, Numerical investigation on the combustion and emissions of a kerosene-diesel fueled compression ignition engine assisted by ammonia fumigation, *Appl. Energy* 204 (2017) 1476–1488.
- [61] K.L. Tay, W. Yang, S.K. Chou, D. Zhou, J. Li, W. Yu, F. Zhao, B. Mohan, Effects of injection timing and pilot fuel on the combustion of a kerosene-diesel/ammonia dual fuel engine: a numerical study, *Energy Proc.* 105 (2017) 4621–4626.
- [62] C. Zamfirescu, I. Dincer, Ammonia as a green fuel and hydrogen source for vehicular applications, *Fuel Process. Technol.* 90 (5) (2009) 729–737.
- [63] O. Mathieu, E.L. Petersen, Experimental and modeling study on the high-temperature oxidation of ammonia and related nox chemistry, *Combust. Flame* 162 (3) (2015) 554–570.
- [64] T. Selli, A.D. Melas, A. Joshi, D. Manara, A. Perujo, R. Suarez-Bertoa, An overview of lean exhaust denox aftertreatment technologies and nox emission regulations in the European Union, *Catalysts* 11 (3) (2021) 404.

A.3 Paper III



Contents lists available at ScienceDirect

Energy

journal homepage: www.elsevier.com/locate/energy

Experimental and numerical study on direct injection of liquid ammonia and its injection timing in an ammonia-biodiesel dual injection engine

Ebrahim Nadimi^{a,*}, Grzegorz Przybyła^a, Terese Løvås^b, Grzegorz Peczkis^c, Wojciech Adamczyk^a

^a Department of Thermal Technology, Faculty of Energy and Environmental Engineering, Silesian University of Technology, Gliwice, Poland

^b Department of Energy and Process Engineering, Faculty of Engineering, Norwegian University of Science and Technology, Trondheim, Norway

^c Department of Power Engineering and Turbomachinery, Faculty of Energy and Environmental Engineering, Silesian University of Technology, Gliwice, Poland

ARTICLE INFO

Keywords:

Ammonia
Direct injection
Internal combustion engine
Emissions
Biodiesel

ABSTRACT

Ammonia is an alternative carbon-free fuel that can be easily stored in a liquid phase, unlike hydrogen, and then directly utilized in diesel engines. Hence, a single-cylinder diesel engine was retrofitted for direct injection of liquid ammonia with pilot ignition of biodiesel in dual fuel combustion mode. The effects of the liquid phase of ammonia and ammonia energy share (AES) on combustion, emissions, and engine performance were investigated and compared with pure biodiesel operation. Moreover, various ammonia injection timings were studied to improve ammonia/biodiesel combustion and reduce emissions. A CFD model was developed and validated with experimental data to study ammonia/biodiesel sprays, combustion characteristics, and emissions formation. The results showed higher AES significantly reduced the local cylinder temperature due to the strong cooling effects of ammonia, therefore, a maximum AES of 50% was achieved. Increasing AES to 50% decreased combustion duration and combustion phasing by 26.2 and 4.4 CAD, respectively. However, it deteriorated the indicated thermal efficiency (ITE) by 1.3 percent point compared to pure biodiesel. Furthermore, retarding ammonia injection from -25 to -10 CAD significantly reduced NO_x , CO, and ammonia emissions by 31.4%, 39.6%, and 31.3%, respectively. Ultimately, the optimal operating condition was suggested when ammonia was injected at -10 CAD and biodiesel at -16 CAD with AES of 50%.

1. Introduction

Greenhouse gas (GHG) emissions and their effects on climate change are the primary reasons to prevent internal combustion engines (ICE) from utilizing fossil fuels. ICEs also produce harmful emissions, such as nitrogen oxides (NO_x) and carbon monoxide (CO), and exceeding the threshold limit for these hazardous gases has harmful health effects. Nevertheless, ICEs are widely used in the transportation sector, such as heavy-duty vehicles, producing a significant amount of carbon dioxide CO_2 emission. European Union committed to reduce CO_2 emissions by 55% until 2030 according to the Paris agreement [1]. Therefore, ICEs must be decarbonized by replacing them either with electric motors or using alternative green fuels. Electrical vehicles are more feasible for light-duty vehicles, however, the majority heavy-duty engine manufacturers will still use diesel engines because of the challenges of batteries such as energy density and charging duration [2]. Moreover, the use of alternative carbon-free fuels such as hydrogen (H_2) and ammonia (NH_3) is a promising way to stop the production of GHG emissions from heavy-duty engines. The international energy agency predicts 125 million tons of ammonia will be used as an energy carrier by 2050 for

sustainable development and a net zero emissions scenario. In 2020, 185 million tons of ammonia were produced but demand for ammonia will grow to 355 million tons [3].

However, hydrogen has the potential to be a useful energy source for transportation, but there are currently obstacles to its widespread use, including challenges related to storage, distribution, and infrastructure deployment. Whereas, ammonia has several advantages as a potential energy carrier compared to hydrogen. One of the main advantages is that it can be easily stored in the liquid phase at ambient temperature and under relatively low pressure, making it more convenient to transport and handle than hydrogen [4,5]. Nevertheless, low flame speed, high ignition temperature and energy, and being toxic are some of the challenges of ammonia that need to be addressed in order to make it a viable carbon-free fuel for ICEs [6].

Using pure ammonia in CI engines requires a high auto-ignition temperature of 924 K and a compression ratio of around 27. Thus, ammonia can be assisted by secondary fuel in dual fuel mode, which is a practical method for burning ammonia in light-duty diesel engines [7]. In addition, in spark-ignited engines (SI), a combustion promoter such

* Corresponding author.

E-mail address: enadimi@polsl.pl (E. Nadimi).

<https://doi.org/10.1016/j.energy.2023.129301>

Received 25 March 2023; Received in revised form 25 August 2023; Accepted 5 October 2023

Available online 7 October 2023

0360-5442/© 2023 Elsevier Ltd. All rights reserved.

Nomenclature	
ICE	Internal combustion engine
SI	Spark ignition
AES	Ammonia energy share
ISFC	Indicated specific fuel consumption
SOI	Start of injection
AMR	Adaptive mesh refinement
DI	Direct injection
GDI	Gasoline direct injection
HRR	Heat release rate
IMEP	Indicated Mean Effective Pressure
LHV	Lower heating value
COV	Coefficient of variation
CI	Compression ignition
CR	Common rail
ITE	Indicated thermal efficiency
ID	Injection duration
CD	Combustion duration
GHG	Green house gases
Bio	Biodiesel
CAD	Crank angle degree
ABDI	Ammonia biodiesel direct injection
CFD	Computational fluid dynamics
FTIR	Fourier-transform infrared spectroscopy

as hydrogen or natural gas is used to overcome the low flame speed of ammonia and widen the flammability range [8]. Biodiesel can be used as a green pilot fuel instead of diesel oil, which can offset GHG emissions because biodiesel is produced from plants that are considered carbon neutral [9,10]. El-Seesy et al. [11–13] demonstrated that biodiesel can blend with diesel fuel, resulting in improved engine performance and reduced emissions. Nadimi et al. [14] experimentally used ammonia as the main fuel and biodiesel as a pilot fuel in the CI engine. Their results show a significant reduction in CO₂, CO, and HC emissions, while 69.4% of input energy was provided with ammonia and the rest with biodiesel.

Regarding SI engines, Oh et al. used natural gas with ammonia and experimentally investigated the effects of the ammonia energy fraction and the air–fuel ratio on combustion and emissions in dual fuel SI engine. Their results show that by adding ammonia and decreasing the air–fuel ratio NO_x emission increases. Additionally, advancing ignition timing prevents incomplete combustion [15]. Lhuillier et al. [16] mixed ammonia with different fractions of hydrogen and various equivalence ratios. They reported that the highest indicated efficiency was obtained in low hydrogen fractions around 20%. Furthermore, increasing the hydrogen fraction decreased ammonia emission, but it also increased NO_x emissions. Christine et al. [17] proved that the addition of 10% hydrogen decreased NO_x by 40% and ensured stable operation.

With respect to CI engines, all researchers focus on one strategy of utilizing ammonia with pilot fuel such as diesel so far. In this strategy, gaseous ammonia is injected into the port, mixed with air, and then diesel fuel is injected to start the combustion [18,19]. Reiter and Kong explained the strategy of introducing gaseous ammonia to the intake port and the modification of the engine [20,21]. Nadimi et al. [22] experimentally investigated the effects of substituting diesel fuel with gaseous ammonia. Their experimental results reveal that 84.2% of diesel can be replaced by ammonia with the indicated efficiency of 37.6%. Moreover, as more diesel is replaced by ammonia combustion duration and phasing are reduced noticeably. They also revealed that GHG emissions were reduced from 727 g/kWh for pure diesel to 243 g/kWh for ammonia/diesel operation considering the N₂O

emission. However, ammonia slip reached 14 800 ppm for 84.2% diesel substitution.

Currently, high NH₃ and nitrous oxide (N₂O) emissions are the main challenges of ammonia fuel engines, as NH₃ emissions even at a low level are dangerous and N₂O emission has a 298 times GHG effect over 100 years compared to CO₂ [23]. Yousefi et al. [24] by studying the diesel injection strategy and the gaseous ammonia energy fraction, it is shown that increasing the ammonia ratio reduced NO_x emissions by around 58.8% but increased ammonia emission by up to 4445 ppm. Generally, advancing the timing of diesel injection increased performance and emissions. They also mention that ammonia decreased CO₂ equivalent emissions by 12% compared to pure diesel operation. In their other similar work [25], they found that split injection of diesel reduced ammonia emissions by around 83.5% while increasing indicated efficiency by 2% relative to single injection. Furthermore, the preinjection of diesel in –57 CAD significantly reduced N₂O emission from 0.61 g/kWh to 0.18 g/kWh.

According above literature review, ammonia was applied in both SI and CI engines in the gaseous phase through introducing into the intake manifold. However, this can lead to high ammonia emissions in dual fuel CI engines due to unsuccessful flame propagation and uncontrolled combustion. Hence, combustion, emissions, and engine performance can be improved by injecting liquid ammonia directly into the cylinder. Therefore, in this work, the effects of liquid ammonia direct injection as well as ammonia energy share with using biodiesel are studied and compared with pure biodiesel operation. In addition, various ammonia injection timings are investigated in order to improve ammonia combustion and then reduce emissions. A CFD model is developed and validated with experimental data to study ammonia spray and combustion, as well as to predict local temperature and emissions.

2. Experimental methodology

All the test has been carried out on a retrofitted single-cylinder diesel engine. The test rig, engine specifications, and equipment are similar to those in our previous work on port injection of gaseous ammonia [14,22,26,27]. However, the ammonia fueling system and injectors were changed for the direct injection of liquid ammonia and biodiesel. Since biodiesel is used as a pilot fuel, three of the six holes in the CR injector were welded to inject a low amount of biodiesel under high pressure and with a long injection duration. The gasoline direct injection (GDI) injector was used without any modifications for the injection of ammonia. The location and angle of the injectors and the number of CR injector holes were adjusted in order to improve the ammonia/biodiesel combustion. Hence, the final configuration of the test rig is presented in Fig. 1. Two separate injection systems were used to adjust the injections of ammonia and biodiesel under different injection timings, pressures, or split injections. In-cylinder pressure was measured using a piezoelectric pressure transducer and an additional piezoresistive absolute pressure sensor was installed in the intake manifold. An optical encoder with a resolution of 0.35 CAD was used to measure crank angle displacement and indicate piston position at TDC. The indicated parameters are calculated for one hundred engine cycles. The total uncertainty of the in cylinder measurement system is 1% of the measured value. However, the coefficient of variation (COV) for the maximum cylinder pressure and location of maximum pressure were less than 1%. Furthermore, the COV of IMEP for pure biodiesel was 1.9%, but by increasing the ammonia ratio it reached a maximum of 3.7%. The concentration of each species was measured by Fourier Transform Infrared Spectroscopy (FTIR) every five seconds for three minutes on a steady-rung engine. The accuracy of FTIR is 2% of the measured value for each component.

In order to study ammonia biodiesel dual direct injections CI engine, two cases were designed. Since liquid ammonia has a higher heat of evaporation and high mass flow due to low LHV compared to

Table 1

The test procedures for the ammonia biodiesel dual direct injection engine (the injection pressure for biodiesel and ammonia is 300 bar and 100 bar, respectively)

	AES	\dot{m}_{bio}	\dot{m}_{NH_3}	SOI_{NH_3}	ID_{NH_3}	SOI_{bio}	ID_{bio}
	%	g/s	g/s	CAD	CAD	CAD	CAD
Case 1	0	0.206	0	*	*	-16	21
	20	0.137	0.073	-15	10.0	-16	13.5
	40	0.113	0.157	-15	15.6	-16	9.5
	50	0.087	0.18	-15	18.5	-16	8.5
Case 2	50	0.087	0.180	-25	18.5	-16	8.5
	50	0.087	0.180	-20	18.5	-16	8.5
	50	0.087	0.180	-15	18.5	-16	8.5
	50	0.087	0.180	-10	18.5	-16	8.5

fossil fuels, it can reduce the in-cylinder temperature resulting in the unsuccessful operation of the engine. Therefore, Case 1 investigates the effects of biodiesel substitution with liquid ammonia. The engine first runs with pure biodiesel at partial load that IMEP is 5.7 bar at a speed of 1500 rpm as a baseline for comparison. As ammonia emission increases with higher loads, therefore, the engine is operated under partial load condition. Thereupon, biodiesel is replaced by ammonia to achieve different AESs. For test case 1, the SOIs of ammonia and biodiesel are kept at -15 and -16 CAD, respectively, as shown in Table 1. However, a higher AES above 50% caused a striking amount of unburned ammonia and hydrocarbons and a drop in power. Therefore, a maximum AES of 50% was achieved during the test for direct injection of liquid ammonia. Furthermore, case 2 investigates the impacts of the ammonia injection timing, while the biodiesel injection timing, the biodiesel and the ammonia injection durations, and both fuel mass flow rates are kept constant. Therefore, the SOI of ammonia in -25, -20, -15, and -10 CAD are tested in case 2.

3. Numerical methods

3.1. Computational domain and grid generation

The simulations in this study were performed using the CONVERGE CFD software [28]. This software uses the finite-volume method with the Rhie-Choe interpolation scheme to solve the transport equations [29]. One of the main advantages is its ability to generate simple autonomous orthogonal grids and utilize the adaptive mesh refinement (AMR) algorithm, which allows it to simulate complex geometries. It can handle engine geometry motion by creating a new mesh at each time step instead of using the moving mesh approach [30]. Fig. 2 illustrates the geometry of the engine, including the intake and exhaust manifolds, valves, and piston with crevice which was designed in SpaceClaim software. The locations of CR and GDI injectors as well as the direction of the nozzles for ammonia and biodiesel spray are shown in this figure.

The maximum cell size of 2.8 mm was set for the entire domain at each time step. However, several fixed embeddings were defined to refine the mesh in certain regions such as exhaust and intake valves with scale 4, cylinder engine with scale 1, and biodiesel and ammonia sprays with fixed embedding scale 4. These fixed embeddings allow for the refinement of grids in defined regions around 0.175 mm (1 base cell was divided into 64 cells) to improve the accuracy of the model in flow through valves and biodiesel and ammonia sprays, as can be seen in Fig. 2. In addition, AMR was employed to divide cells for temperature greater than 2.5 K and velocity greater than 1 m/s during the simulation. The total number of cells varies for each crank angle degree but it reached 1.7 million cells at maximum during spray and combustion due to these fixed embeddings and AMR.

3.2. Spray, turbulence and combustion model

Ammonia and biodiesel sprays were stimulated by the Lagrangian solver to model discrete parcels and track individual droplets. The Kelvin–Helmholtz (KH) and Rayleigh–Taylor (RT) instability mechanisms are used to model the spray breakup process [31]. The KH mechanism is responsible for the primary breakup, while the RT mechanism is used mainly for the secondary breakup [32]. The O'Rourke model and the No Time Counter (NTC) method are selected to model turbulent dispersion and droplet collisions, respectively [33]. The thermal properties of Methyl Decanoate ($C_{11}H_{22}O_2$) from the CONVERGE library were used for the liquid properties of biodiesel. The droplets' evaporation and radius change rates are modeled by the Frossling model [34]. Finally, the Rebound/slide model was used to model the spray and wall interaction [35]. The Re-normalization Group (RNG) k-epsilon model was used to simulate turbulence flow in the cylinder. Further input data for ammonia spray simulation can be found in recent research conducted by Lewandowski et al. [36].

The combustion process was simulated using the SAGE solver, which calculates the concentrations of each species at each time step and the grid. The transport equations were then solved using the PISO method [29]. The ammonia/biodiesel chemical kinetics mechanism was generated by CONVERGE Chemistry Tools using the biodiesel reactions mechanism proposed by Brakora et al. [37,38] and ammonia reactions mechanism by Stagni et al. [39]. The reduced chemical kinetics mechanism for biodiesel contains 69 species and 192 reactions, while the ammonia reaction mechanism has 31 species and 203 reactions. The final ammonia/biodiesel chemical kinetics mechanism used in this study consisted of 89 species and 368 reactions.

3.3. Boundary conditions and validations

The experimental data were used to define the boundary conditions and validate the model. Average values were calculated for each operating point over three minutes of the steady-running engine. Also, intake temperature and pressure were measured and set for the inlet boundary conditions. In addition, the engine head temperature was measured to set the walls' temperature. Injection parameters such as SOI , ID , and mass flow rates for both biodiesel and ammonia, which are presented in Table 1, are used to set up the CR and GDI injectors and spray model in the simulation. For model validation, the numerical results are compared with the experimental data for all cases. Therefore, Fig. 3 compares the measured in-cylinder pressure and heat release rate (HRR) with the CFD results for pure biodiesel operation and the ammonia/biodiesel mode. It can be seen from Figs. 3(a) and 3(b) that the experimental and numerical in-cylinder pressures are very close and the maximum error is 4.3% at the peak of the in-cylinder pressure. Furthermore, the calculated mole fraction of each species e.g., CO_2 , CO , NO_x , NH_3 , and O_2 are also used as validation criteria and compared to the measured mole fraction of these species with FTIR and presented in Table 2. As can be seen in this table, the predicted species are close to the experimentally measured values. However, for some species, the error is less than 11% at the maximum difference. The sum of NO_2 , N_2O , and NO was defined as NO_x [40]. Overall, this comparison indicates that this CFD simulation is capable of accurately predicting the emissions and combustion characteristics of the pure biodiesel and ammonia/biodiesel direct injection engine.

4. Results and discussion

4.1. Ammonia spray

Ammonia has a lower LHV in comparison to biodiesel. Hence, more ammonia has to be injected to replace the same amount of biodiesel input energy with ammonia. Moreover, ammonia has a higher heat

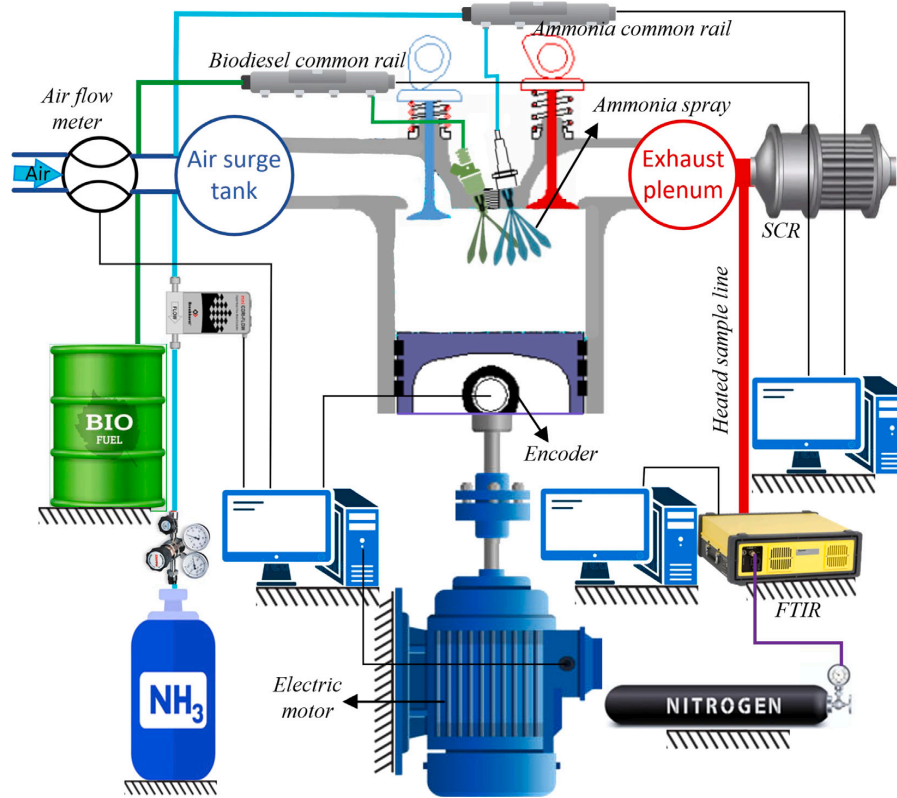


Fig. 1. Schematic of the test rig for ammonia direct injection dual fuel engine.

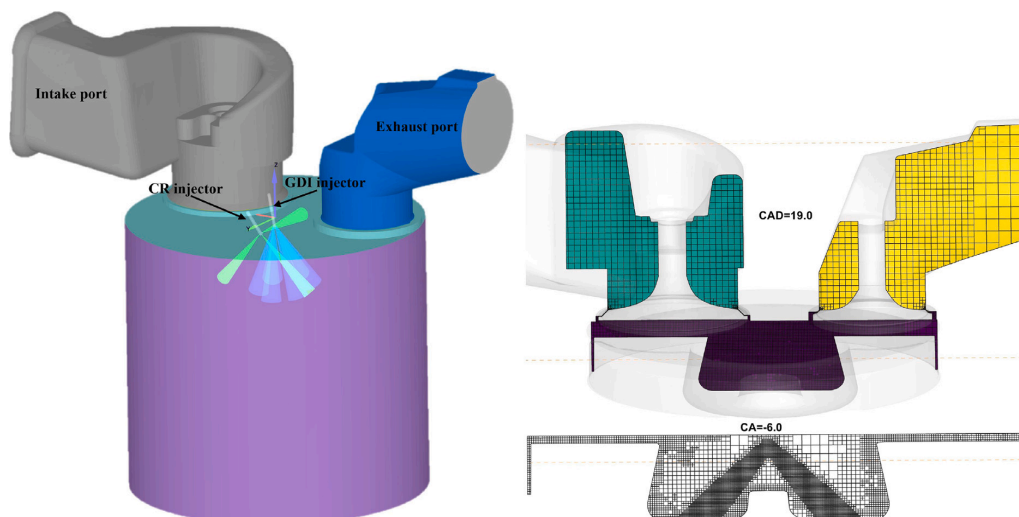


Fig. 2. Computational domain with the view of injector location and their sprays (left) and mesh including AMR and fixed embedding for nozzles (right).

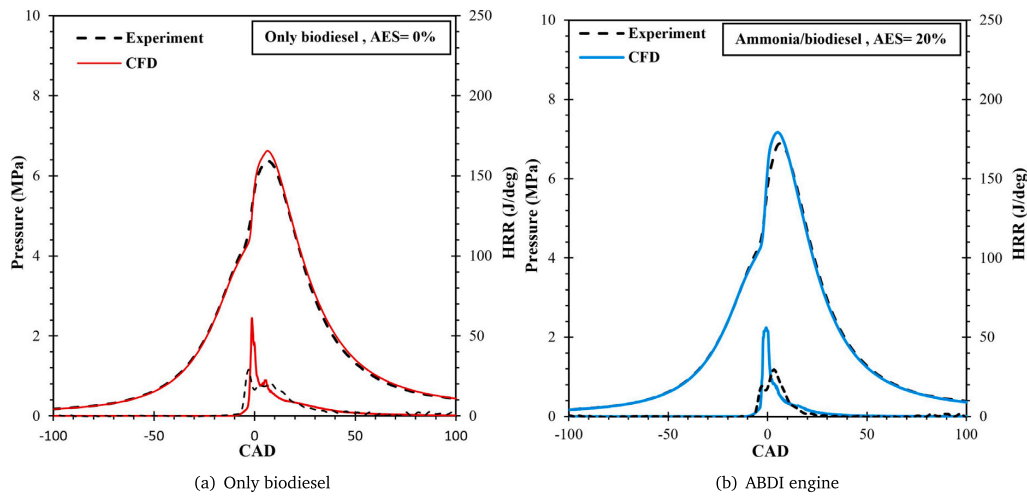


Fig. 3. Comparison of the experimentally measured pressure and HRR with the CFD results for (a) pure biodiesel and (b) ammonia/biodiesel mode when AES is 20%.

Table 2

Comparison of measured species with FTIR and corresponding values predicted by numerical simulation for AES = 0% and AES = 20%.

	AES = 0%		AES = 20%	
	Exp.	Num.	Exp.	Num.
CO_2	6.34	6.31	3.80	3.48
H_2O	6.91	7.31	7.40	8.12
O_2	10.43	10.0	12.35	11.72
CO	2714	2515	1534	1409
NO_x	408.8	453.6	736.4	790.3
NH_3	4.3	0	480.0	428.8

of evaporation around 1372 kJ/kg [41]. Direct injection of liquid ammonia during compression stroke significantly reduces the in-cylinder temperature.

Therefore, ammonia spray and the local cylinder temperatures are shown in Fig. 4 during the injection and just before the start of combustion. This figure illustrates that injecting ammonia at $SOI_{NH_3} = -25$ CAD reduces the local temperature in the bowl to 273 K in the ammonia spray regions due to droplets evaporation. Nevertheless, combustion occurs even with low local temperature because biodiesel is injected at -16 CAD, and combustion start before all droplets of ammonia were evaporated. However, advancing ammonia injection to -35 CAD, unsuccessful combustion with a significant amount of unburned ammonia was observed due to low in-cylinder temperature because of the cooling effects of ammonia. Hence, the mean cylinder temperatures for different SOI are presented in Fig. 5. This figure reveals that by advancing ammonia injection to -25 CAD cylinder temperature reduces from 831 K for pure biodiesel to 777 K, 54 °C drop in the mean temperature at -7 CAD. This reduction delayed the start of combustion. However, the earliest temperature raise point which corresponds to $SOI_{NH_3} = -10$ CAD has the lower maximum in-cylinder temperature because ammonia is injected between -10 and 8 CAD, causing a low in-cylinder temperature peak during the main combustion phase. Also, an enormous amount of unburned ammonia was observed when ammonia was injected after -5 CAD due to the reduction of maximum in-cylinder temperature.

When ammonia is injected at -25 CAD, due to the ammonia spray's strong cooling effect and dropping cylinder temperature, the vaporization rate of the droplets decreases considerably. This accelerates the flow of tiny droplets inside the cylinder, which increases the number of

droplets that are not participating in combustion resulting in high ammonia emissions [42]. Hence, Fig. 6 compares ammonia with biodiesel droplets morphologies and their temperatures for $SOI_{NH_3} = -25$ CAD and $SOI_{NH_3} = -10$ CAD. By comparing the number of droplets in 10 CA after TDC, the number of droplets at the earliest injection is higher than when it was injected at -10 CAD even though ammonia was injected 15 CAD later. Therefore, the ammonia droplets mass at 10 CAD is 1.9 mg and 0.5 mg for $SOI_{NH_3} = -25$ CAD and $SOI_{NH_3} = -10$ CAD, respectively. As a result, ammonia should be injected after or at the same time with biodiesel for better evaporation.

4.2. Effects of AES on engine performance

Fig. 7 shows the effects of ammonia energy share on ITE, ISFC, and exhaust gas temperature when liquid ammonia and biodiesel are injected at -16 and -15 CAD, respectively. ITE increases slightly from 37.8% for pure biodiesel to 38.5% when AES is 40%, a 0.7 percent point increase. Then, it decreases to 36.5% for 50% of AES, a 1.3 percent point reduction compared to pure biodiesel. Consequently, the equivalent fuel consumption was first reduced and then increased by replacing biodiesel with ammonia, as seen in Fig. 7(b). Thus, the ABDI engine at the highest biodiesel replacement of 50% consumes 8.7 g/kWh more fuels in comparison to the pure biodiesel mode. This increase in ITC and decrease in ISFC by increasing AES to 40% are mainly caused by the shift of combustion phasing towards TDC, resulting in higher in-cylinder pressure and temperature, which improves combustion efficiency. However, ITE was reduced when AES is 50% due to a considerable amount of unburned ammonia and lower in cylinder pressure.

Furthermore, direct injection of liquid ammonia significantly reduced EGT compared to pure biodiesel, as can be seen in Fig. 7(c). Therefore, by substituting biodiesel with liquid ammonia up to 50%, the EGT was reduced by 203 °C. This reduction firstly is due to the cooling effects of liquid ammonia and secondly due to the shorter combustion duration of ammonia/biodiesel combustion compared to pure biodiesel causing lower cylinder temperature during expansion stroke as can be noticed from cylinder temperature in Fig. 5. Nevertheless, the EGT is high enough to activate SCR.

4.3. Effects of AES and ammonia injection timing on combustion characteristics

The effects of direct injection of liquid ammonia and its energy share on in-cylinder pressure traces and HRR are shown in Fig. 8(a)

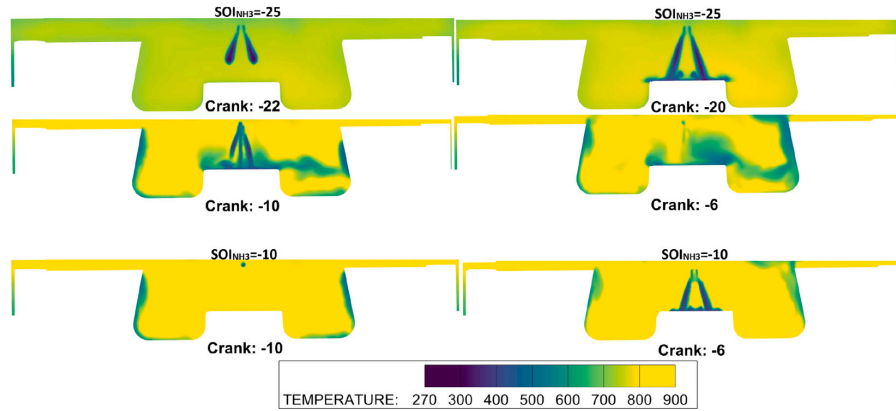


Fig. 4. Effects of liquid ammonia spray on the cylinder temperature field before the start of combustion for $SOI_{NH_3} = -25$ CAD (top) and $SOI_{NH_3} = -10$ CAD (bottom) when AES = 50%.

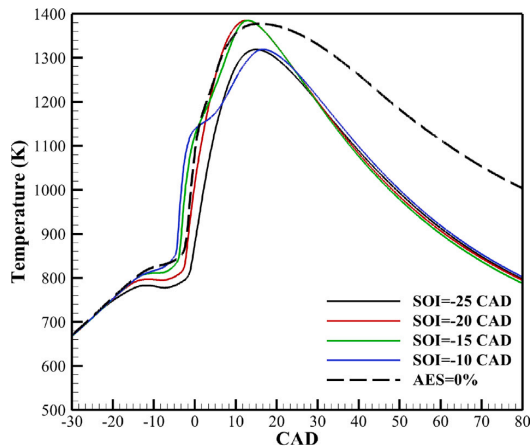


Fig. 5. Effects of various injection timing of liquid ammonia on mean in-cylinder temperature when AES is 50%.

and compared with pure biodiesel mode when the start of injections are same for this test. Substituting diesel with liquid ammonia shortens the ignition delay with main combustion phasing which results in an early start of combustion. Consequently, most of the heat is released a few degrees before TDC, causing an increase in the peak of in-cylinder pressure. Therefore, when AES = 40% the peak of in-cylinder pressure is 7.3 bar higher than pure biodiesel. However, the peak of in-cylinder pressure considerably decreased for AES = 50% due to, firstly, higher ammonia mass and its cooling effects, and secondly, due to longer injection duration of ammonia for AES = 50% which injection ends at 2.5 CA after TDC, but for the rest of the AES, the ammonia injection ends before TDC. In Fig. 8(b), advancing SOI of ammonia from -10 to -25 CAD delayed the ignition due to ammonia droplet evaporation which reduced in-cylinder temperature at the start of biodiesel injection, as can be seen from Fig. 8(b) and in-cylinder temperature in Fig. 5. As a result, the lowest in-cylinder pressure was observed when ammonia was injected at -25 due to a longer ignition delay which results in most of the heat released after TDC, as can be seen from the corresponding HRR profile. Additionally, the HRR profile has one peak for $SOI_{NH_3} = -25$ CAD which is similar to when gaseous ammonia is injected into the intake port owing to the formation of premixed ammonia-air [14]. However, when ammonia is injected after

the injection of biodiesel and since combustion is started by biodiesel, it increases the in-cylinder temperature to auto-ignition temperature of ammonia. Hence, delaying the injection of ammonia rises the first peak of the HRR, which corresponds to the premixed combustion phase in the HRR curve. Therefore, Table 3 illustrates the relation between the SOI of ammonia, the HRR peak, and the CAD in which the in-cylinder temperature reaches the autoignition temperature of ammonia. When the in-cylinder temperature reaches the auto-ignition of ammonia, the HRR peak occurs.

Fig. 9 depicts the effects of the liquid ammonia energy fraction and SOI_{NH_3} on the initial stage of the combustion (CA10), combustion phasing (CA50), and combustion duration (CA90-CA10). The CA10, CA50, and CA90 correspond to CAD where 10, 50, and 90 percent of cumulative heat is released. Ammonia significantly reduced CD and combustion phasing compared to pure biodiesel mode. Hence, by increasing the ammonia ratio, the CD was reduced from 45.6 CAD for pure biodiesel to 19.4 CAD for the highest AES. Furthermore, liquid ammonia also reduced combustion phasing (CA50) compared to biodiesel mode; similar trends for CA50 and CD were reported when gaseous ammonia was injected into the intake manifold [43,44]. The longer CD of biodiesel is related to the high viscosity of biodiesel compared to ammonia, which requires more time for evaporation and mixing subsequently combustion. However, the slight increase in CA50 with increasing AES is owing to a longer ammonia injection duration, resulting in a longer mixing control combustion phase. Furthermore, Fig. 9(a) shows that with increasing AES, CA10 decreases slightly from -1.4 CAD for pure biodiesel to -3.2 CAD for AES = 50%, meaning a shorter ignition delay for higher liquid ammonia ratios. Also, advanced ammonia injection due to the strong cooling effects of ammonia, which results in a low cylinder temperature (Fig. 5) during biodiesel spray, causes a longer ignition delay. The other reason can be the formation of premixed ammonia air when ammonia is injected earlier delayed ignition because premixed ammonia air suppresses pilot biodiesel ignition, resulting in a longer ignition delay [22,45,46]. Therefore, once ammonia is injected at -25 CAD, combustion starts near TDC (CA10 = -0.3 CAD) when the in-cylinder temperature increases to the auto-ignition temperature of ammonia.

4.4. Effects of ammonia injection timing and AES on emissions

Fig. 10 shows the effects of AES on CO_2 , H_2O , CO, NO_x , and ammonia emissions. By substituting biodiesel with ammonia, carbon-based emissions were significantly reduced. Thus, CO_2 and CO emissions decreased from 647.6 and 18.3 g/kWh for pure biodiesel operation to 340.2 and 12.3 g/kWh for ammonia/biodiesel mode when AES is 50%,

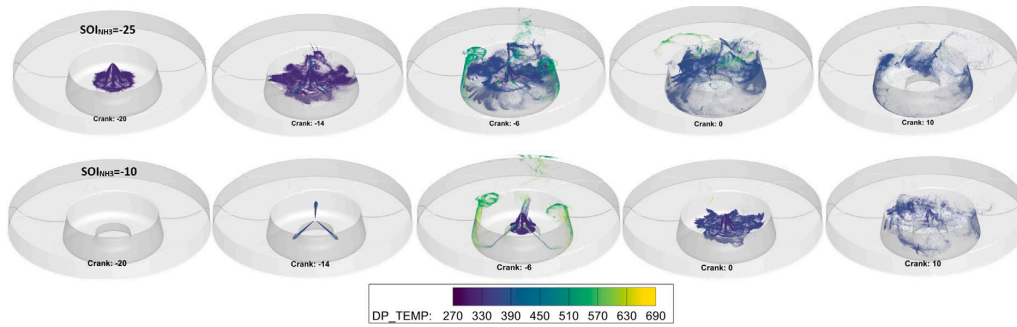


Fig. 6. Liquid ammonia and diesel spray morphologies, droplets distribution and their temperature for $SOI_{NH_3} = -25$ CAD (top) and $SOI_{NH_3} = -10$ CAD (bottom) at $AES = 50\%$.

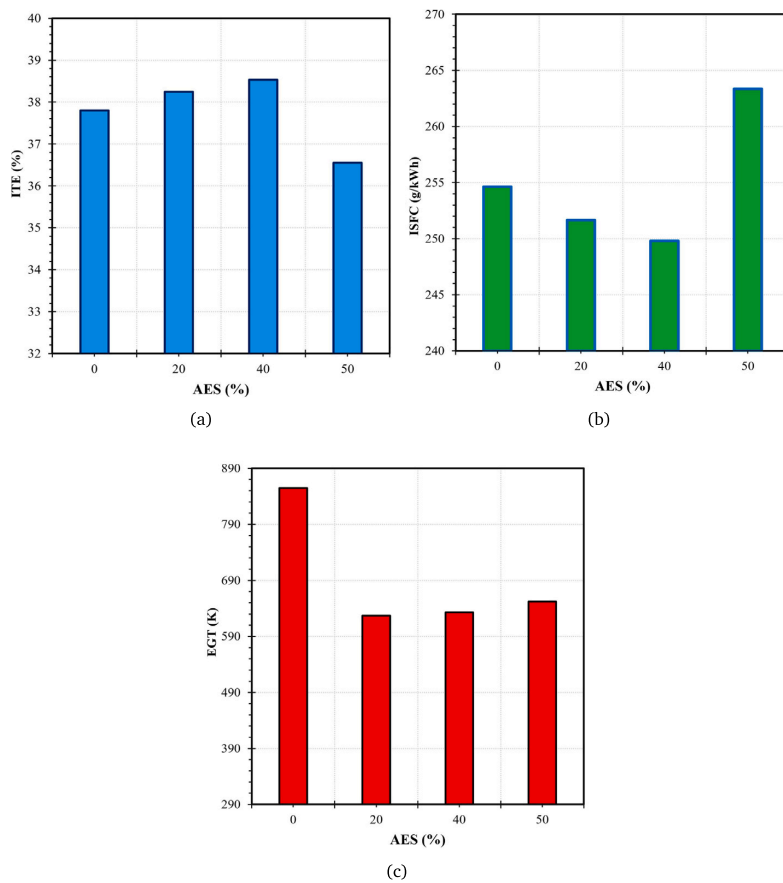


Fig. 7. Effects of AES on (a) indicated thermal efficiency, (b) indicated specific fuel consumption and (c) exhaust gas temperature.

respectively. However, CO emission is constant when AES is around 40% and 50%, although more diesel was replaced with liquid ammonia. This is mainly due to the locally low in-cylinder temperature and a high amount of liquid ammonia when the AES is 50%, resulting in incomplete combustion of biodiesel/ammonia. Furthermore, this can also be seen in a notable amount of unburned ammonia at $AES = 50\%$ in Fig. 10(d). Nevertheless, 5216 ppm of ammonia emission is significantly lower than when gaseous ammonia was injected into the intake manifold, which was measured at 16165 ppm. Thus, direct

injection of ammonia strikingly reduced ammonia emission by almost 3 times. The reason is that when ammonia is injected into the intake manifold, and then the pilot fuel initiates the combustion. Unsuccessful flame propagation around the cylinder walls and crevices causes a significant amount of ammonia emissions, as shown in Fig. 11. This figure illustrates unburned ammonia concentrations near cylinder walls and crevices cause a significant amount of ammonia emission compared to direct injection, this is also highlighted in other studies [21,44].

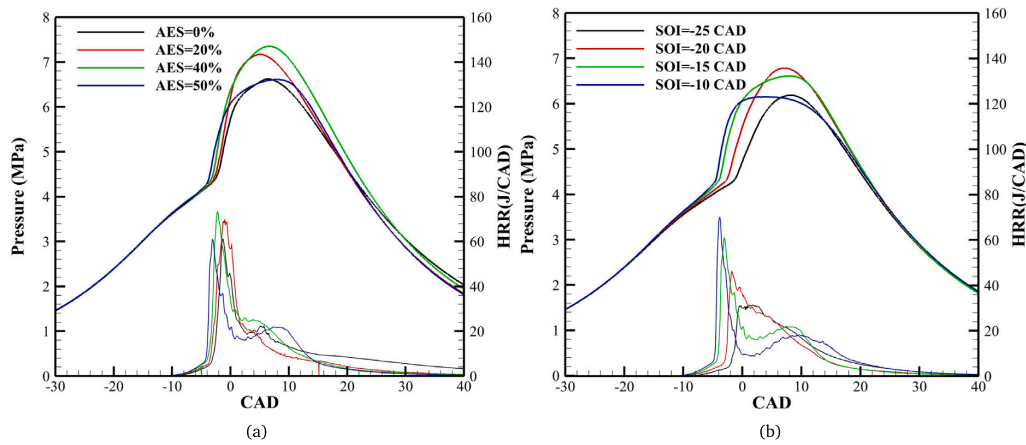


Fig. 8. In-cylinder pressure along with HRR for (a) different AES when $SOI_{NH_3} = -15$ CAD and $SOI_{biod} = -16$ CAD. (b) injection timing of liquid ammonia when AES = 50%.

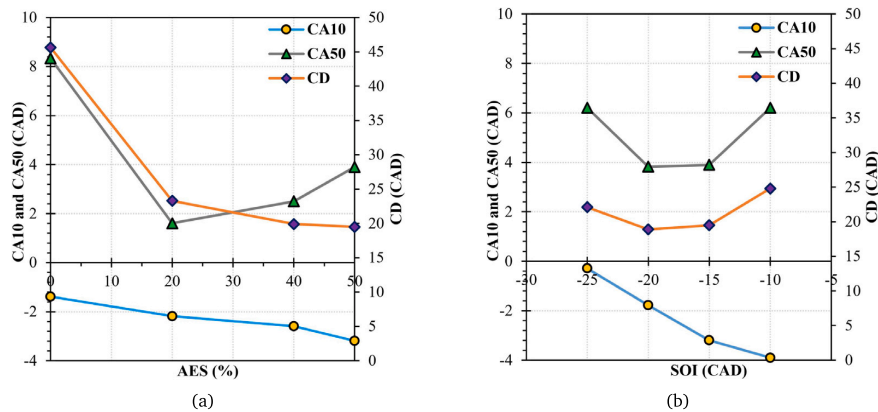


Fig. 9. Combustion indicators such as CA10, CA50, CD (combustion duration CA90-CA10) for pure biodiesel and ABDI engine: effects of AES, (b) effects of ammonia injection strategies.

Table 3

Impacts of ammonia injection timing on the peak of HRR and its location along with the location of in-cylinder temperature which reaches the auto-ignition temperature of ammonia ($T = 924$ K [23]).

SOI_{NH_3} CAD	HRR peak J/CAD	HRR peak CAD	$T = 924$ K CAD
-25	31.4	1.3	0.8
-20	46.3	-1.8	-1.2
-15	61.0	-3.0	-3.0
-10	70.1	-3.8	-3.9

However, injecting ammonia into the bowl during biodiesel combustion avoids moving ammonia near the cylinder wall, where the local temperature is low (Fig. 12). Therefore, direct injection of ammonia considerably reduced unburned ammonia emission.

Fig. 10(c) shows that NO_x emission first increased and then slightly decline when AES is higher than 20%. This higher NO_x emission in ammonia biodiesel combustion can be explained by Fig. 12. This figure compares NO_x formation of pure biodiesel and ammonia/biodiesel direct injection mode in different CAD and alongside local in-cylinder temperature. Three high-temperature flame fronts, which are the result of biodiesel spray combustion, lead to thermal NO_x for both pure biodiesel and ammonia/biodiesel combustion modes. However, it can

be observed that ammonia combustion directly contributes to the formation of NO_x in addition to thermal NO_x due to the reaction kinetics and fuel type NO_x [47,48]. Hence, the fuel type NO_x dominates the NO_x formation in the ABDI engine. However, ammonia itself can reduce NO_x emission due to the $HN_2 + NO = N_2 + H_2O$ reaction [24,49]. Therefore, increasing the ammonia ratio up to 50% slightly reduced NO_x emissions relative to AES of 20%.

The emissions of the ABDI engine can be further reduced by optimizing the ammonia injection timing. Therefore, the effects of ammonia injection timing on CO, NO_x , and ammonia emissions are presented in Fig. 13. Retarding ammonia injection slightly increases H_2O due to improved ammonia combustion. However, the level CO_2 is constant. Fig. 13 (b) shows that early ammonia injection significantly increased CO emissions from 946 ppm to 1567 ppm. Several studies showed that delayed injection timing results in incomplete and late combustion and increased CO emission [50,51]. Similarly, early injection of ammonia at -25 CAD by reducing the in-cylinder temperature and longer ignition delay lead to late combustion of biodiesel which worsens CO emissions. As can be seen from the numerical results in Fig. 14, the mole fraction of CO reaches the maximum level at 4 CAD after TDC, which means late combustion of biodiesel. However, when ammonia is injected at -10 CAD, CO formation reaches its peak before TDC and then reacts with oxygen due to ongoing combustion of ammonia around 10 CAD (the second peak of the HRR curve).

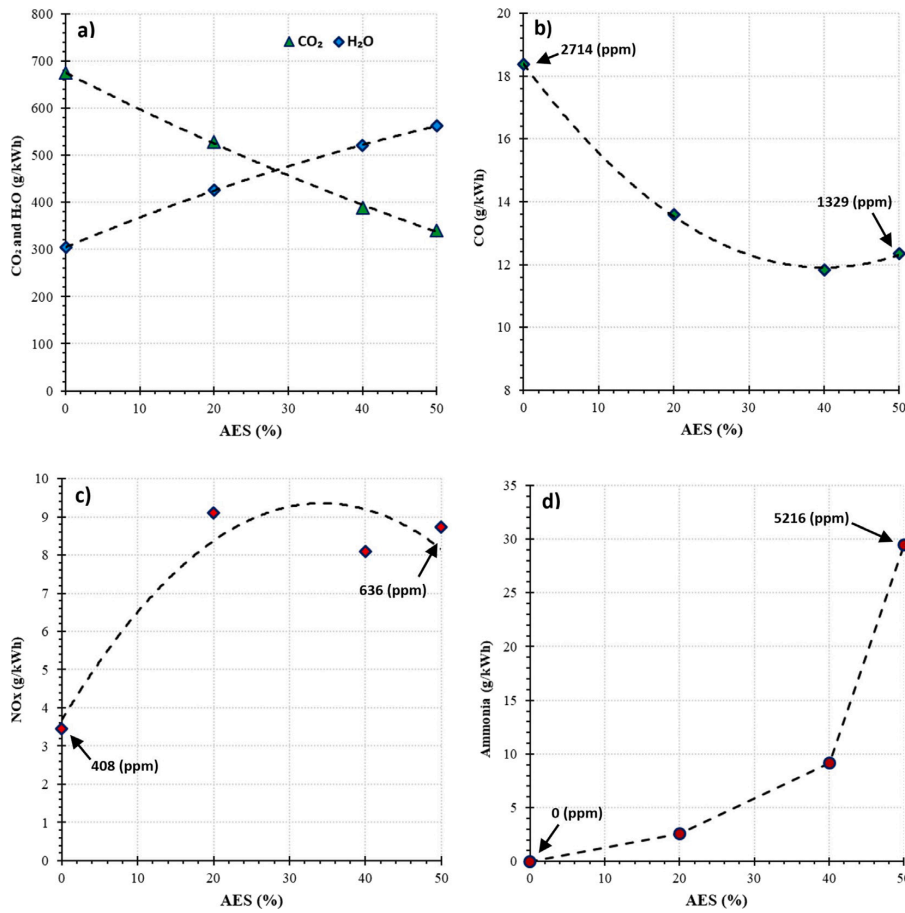


Fig. 10. Effects of different AES on (a) CO₂ and H₂O, (b) CO, (c) NO_x, and (d) ammonia slip.

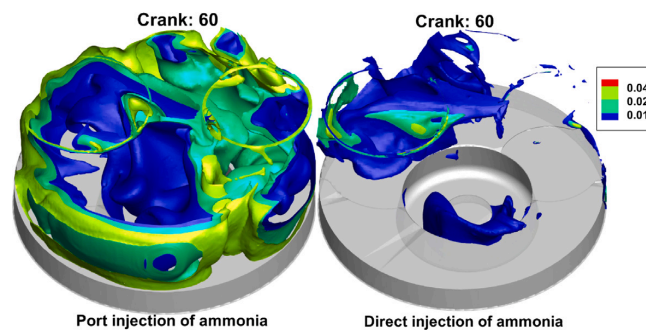


Fig. 11. Ammonia mole fraction isosurface at 0.01, 0.02, and 0.04 for direct injection of liquid ammonia (case 2) versus port injection of gaseous ammonia when AES = 50%.

Generally, NO_x and ammonia emission are the main challenges of ammonia-fueled engines. Thus, direct injection of ammonia remarkably reduced these emissions. In addition to this, retarded ammonia injection decreased NO_x and ammonia emissions by 31.4% at the same time, as can be seen in Fig. 13. The retarding of ammonia injection increases NO_x emission due to the formation of premixed ammonia air and therefore premixed combustion near to TDC [52]. Similarly, late injection of ammonia at -10 CAD significantly reduced ammonia

emission from 7797 ppm to 5352 ppm compared to when it was injected at 25 CAD (16165 ppm for port injection). This exceptional reduction in ammonia emission can be explained from CFD results in Fig. 15. This figure depicts the ammonia mole fraction in the cross-section of the cylinder with the corresponding temperature contours in different CADs for SOI_{NH₃} of -25 and -10 when AES is 50%. When ammonia is injected at -25 CAD, the in-cylinder temperature decreases and combustion starts at TDC due to the favorable thermodynamic

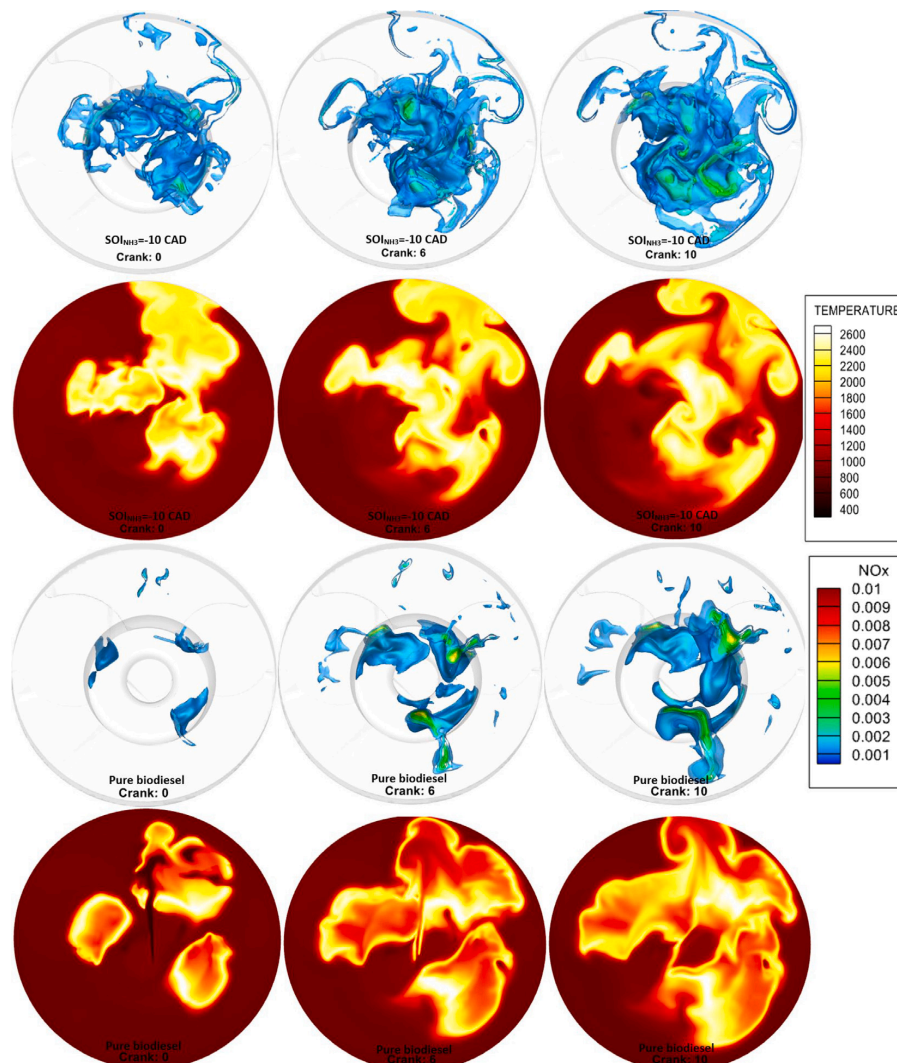


Fig. 12. Comparison of NO_x mole fraction for ABDI engine when $\text{AES} = 50\%$ and $\text{SOI}_{\text{NH}_3} = -10$ CAD with pure biodiesel in different CADs along with respective temperature distribution.

condition. During this 25 CAD period, premixed ammonia air is formed and ignited with biodiesel in three sprays in three zones. Therefore, ammonia is combusted only in hot temperature flames and ammonia will not be burned in low temperature zones causing high ammonia emission. However, as ammonia is injected after the start of combustion or at the same time with biodiesel, it results in a sharp reduction in unburned ammonia, as can be observed in the ammonia mole fraction contour for $\text{SOI}_{\text{NH}_3} = -10$ in Fig. 15.

5. Summary and conclusions

In this study, a single-cylinder CI engine was retrofitted for direct injection of the liquid phase of ammonia with biodiesel as pilot fuel in dual fuel mode. The effects of ammonia/biodiesel ratios on combustion, engine performance, and emissions were studied. Furthermore, the impacts of ammonia injection timing were also investigated. The CFD model was used to explain the ammonia spray and its combustion

with biodiesel, flame propagation, and emissions formation, as well as to address unburned ammonia. The main conclusions are summarized below:

- The injection of liquid ammonia significantly reduced the local and average in-cylinder temperature during injection due to the strong cooling effects of ammonia compared to pure biodiesel operation. When AES is 50%, combustion only occurs when ammonia is injected between -25 to -10 CAD and out of this range significant amount of unburned ammonia and CO emission was observed due to the cooling effects of ammonia.
- Increasing liquid ammonia energy share slightly increased the ITE by 0.7 percent point and reached 38.5% for AES of 40% compared to only biodiesel operation. However, it then decreased to 36.5% when AES is 50% due to incomplete combustion. Moreover, ammonia notably decreased EGT by 203 K.
- Increasing ammonia energy share up to 40% raised the peak of cylinder pressure by 7.3 bar then it significantly decreased for

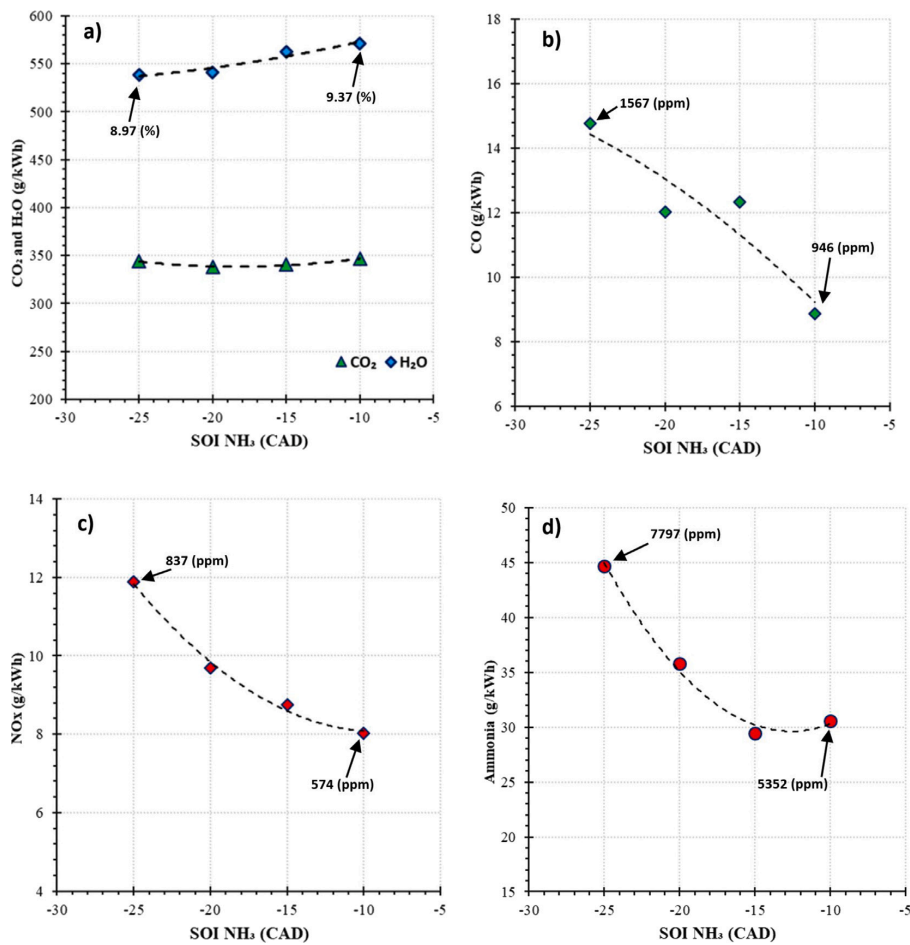


Fig. 13. Effects of SOI of ammonia on (a) CO₂ and H₂O, (b) CO, (c) NO_x, and (d) ammonia slip.

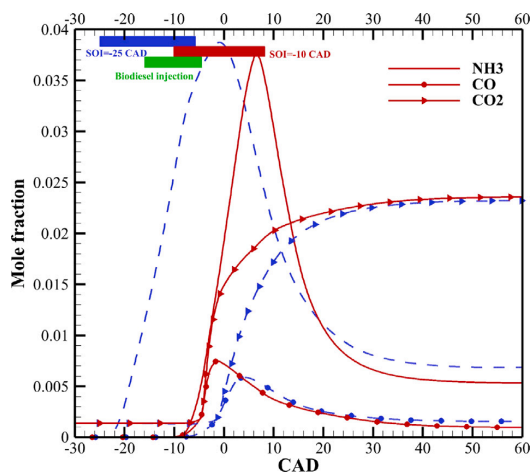


Fig. 14. CO, CO₂, and NH₃ mole fraction in cylinder for $SOI_{NH_3} = -25$ CAD (blue) and $SOI_{NH_3} = -10$ CAD (red) when $AES = 50\%$. (For interpretation of the references to color in this figure legend, the reader is referred to the web version of this article.)

AES of 50% due to a shorter ignition delay and combustion phase compared to pure biodiesel. Moreover, late injection of ammonia not only increased the peak of the HRR curve but also caused the second peak.

- Ammonia notably reduced combustion duration by 26.2 CAD compared to pure biodiesel at the highest AES. Furthermore, the early injection of ammonia at -25 CAD delayed the start of combustion by 3.6 CAD relative to when it was injected at -10 CAD. Because, as ammonia is injected before biodiesel, it reduces in-cylinder temperature during biodiesel injection, resulting in a longer ignition delay and combustion starts near the TDC.
- Liquid ammonia energy share diminished CO₂ and CO emissions by 47.4% and 51.2% when AES is 50% and SOI_{NH_3} is -15 CAD compared to pure biodiesel. Additionally, direct injection of ammonia significantly reduced ammonia emissions by approximately three times compared to the port injection strategy. Nevertheless, unburned ammonia still is considerable for direct injection.
- Retarding the ammonia injection from -25 to -10 CAD markedly reduced all emissions when AES is 50%. Hence, NO_x, CO, and ammonia emissions decreased by 31.4%, 39.6%, and 31.3%, respectively, due to the improvement in ammonia combustion.

In future research, to further improve the performance of the ammonia-biodiesel engine and reduce emissions, particularly ammonia

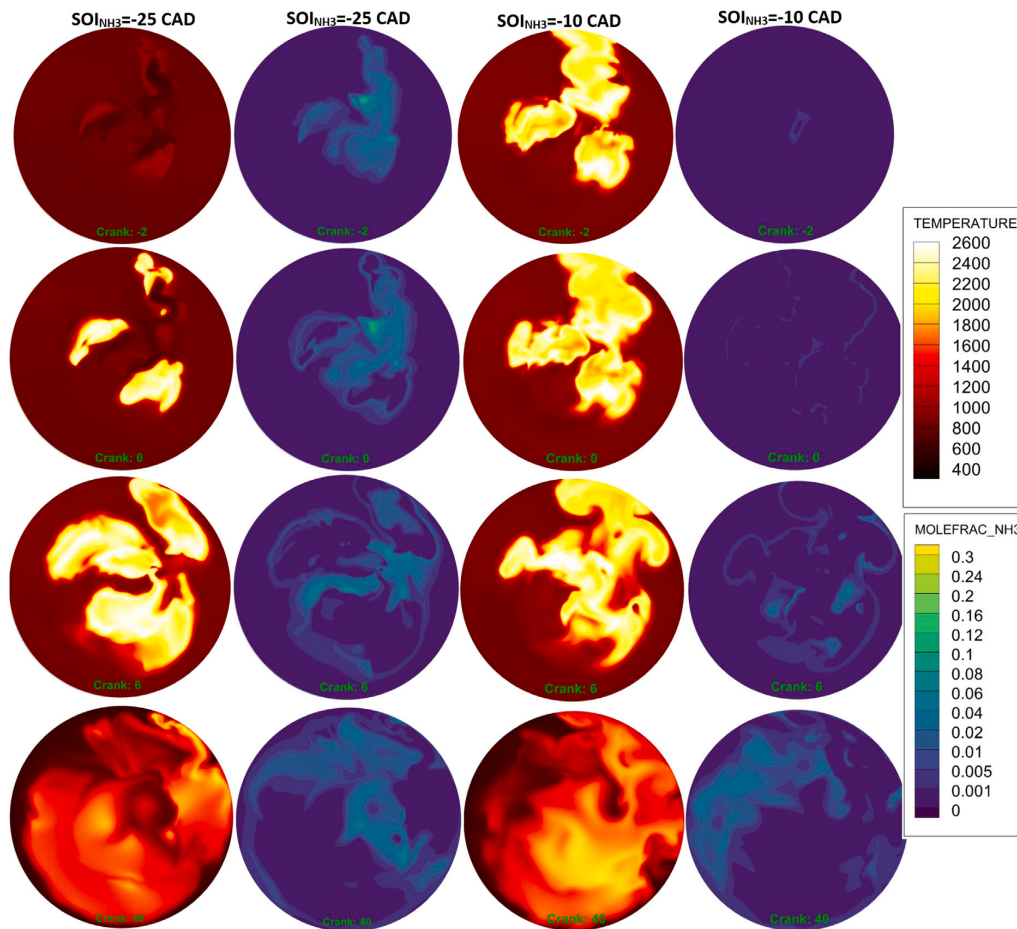


Fig. 15. Effects of SOI_{NH_3} (earliest and latest injection timing) on ammonia emissions and cylinder temperature in different CADs.

slip, it is suggested to study various configurations of CR and GDI injectors. Hence, the impacts of spray interactions, the number of CR injector nozzles, and combustion will be evaluated. Additionally, it is recommended to investigate the effects of the split injection of ammonia or biodiesel and the different injection pressures of ammonia on combustion, emissions, and engine performance.

CRediT authorship contribution statement

Ebrahim Nadimi: Conceptualization, Methodology, Software, Validation, Formal analysis, Investigation, Experiment, Data curation, Visualization, Figures, Writing – original draft, Writing – review & editing. **Grzegorz Przybyła:** Supervision, Conceptualization, Methodology, Investigation, Experiment, Writing – review & editing. **Terese Lövås:** Writing – review & editing. **Grzegorz Peczkis:** Writing – review & editing. **Wojciech Adamczyk:** Funding acquisition, Writing – review & editing, Project administration.

Declaration of competing interest

The authors declare that they have no known competing financial interests or personal relationships that could have appeared to influence the work reported in this paper.

Data availability

Data will be made available on request

Acknowledgment

This research was funded by Norway and Poland grants in ACTIVATE project (Contract NO. NOR/POLNOR/ACTIVATE/0046/2019-00).

The authors thank CONVERGENT Science Inc. for their support and for providing a super-base license.

References

- [1] Rogelj J, Shindell D, Jiang K, Fifita S, Forster P, Ginzburg V, et al. Mitigation pathways compatible with 1.5 C in the context of sustainable development. In: Global warming of 1.5 C. Intergovernmental Panel on Climate Change; 2018, p. 93–174.
- [2] Senecal P, Leach F. Diversity in transportation: Why a mix of propulsion technologies is the way forward for the future fleet. *Results Eng* 2019;4:100060.
- [3] International Energy Agency. Ammonia technology roadmap: towards more sustainable nitrogen fertiliser production. OECD Publishing; 2021.
- [4] Xiao H, Lai S, Valera-Medina A, Li J, Liu J, Fu H. Study on counterflow premixed flames using high concentration ammonia mixed with methane. *Fuel* 2020;275:117902.

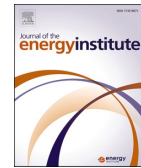
- [5] Ni S, Zhao D, You Y, Huang Y, Wang B, Su Y. NO_x emission and energy conversion efficiency studies on ammonia-powered micro-combustor with ring-shaped ribs in fuel-rich combustion. *J Clean Prod* 2021;320:128901.
- [6] Lhuillier C, Brequigny P, Contino F, Rousselle C. Performance and emissions of an ammonia-fueled SI engine with hydrogen enrichment. Tech. rep., SAE Technical Paper; 2019.
- [7] Schönborn A. Aqueous solution of ammonia as marine fuel. *Proc Inst Mech Eng Part M: J Eng Marit Environ* 2021;235(1):142–51.
- [8] Starkman ES, Newhall H, Sutton R, Maguire T, Farbar L. Ammonia as a spark ignition engine fuel: Theory and application. *Sae Trans* 1967;765–84.
- [9] Aljaafari A, Fattah I, Jahirul M, Gu Y, Mahlia T, Islam MA, et al. Biodiesel emissions: A state-of-the-art review on health and environmental impacts. *Energies* 2022;15(18):6854.
- [10] EL-Seesy AI, Waly MS, He Z, El-Batsh HM, Nasser A, El-Zoheiry RM. Influence of quaternary combinations of biodiesel/methanol/n-octanol/diethyl ether from waste cooking oil on combustion, emission, and stability aspects of a diesel engine. *Energy Convers Manage* 2021;240:114268.
- [11] EL-Seesy AI, Waly MS, El-Batsh HM, El-Zoheiry RM. Enhancement of the waste cooking oil biodiesel usability in the diesel engine by using n-decanol, nitrogen-doped, and amino-functionalized multi-walled carbon nanotube. *Energy Convers Manage* 2023;277:116646.
- [12] EL-Seesy AI, Xuan T, He Z, Hassan H. Enhancement the combustion aspects of a CI engine working with Jatropha biodiesel/decanol/propanol ternary combinations. *Energy Convers Manage* 2020;226:113524.
- [13] El-Seesy AI, Hassan H, Ookawara S. Effects of graphene nanoplatelet addition to Jatropha biodiesel–diesel mixture on the performance and emission characteristics of a diesel engine. *Energy* 2018;147:1129–52.
- [14] Nadimi E, Przybyla G, Emberson D, Lovas T, Ziolkowski L, Adamczyk W. Effects of using ammonia as a primary fuel on engine performance and emissions in an ammonia/biodiesel dual-fuel CI engine. *Int J Energy Res* 2022.
- [15] Oh S, Park C, Oh J, Kim S, Kim Y, Choi Y, et al. Combustion, emissions, and performance of natural gas–ammonia dual-fuel spark-ignited engine at full-load condition. *Energy* 2022;258:124837.
- [16] Lhuillier C, Brequigny P, Contino F, Mounaïm-Rousselle C. Experimental study on ammonia/hydrogen/air combustion in spark ignition engine conditions. *Fuel* 2020;269:117448.
- [17] Mounaïm-Rousselle C, Brequigny P, Dumand C, Houillé S. Operating limits for ammonia fuel spark-ignition engine. *Energies* 2021;14(14):4141.
- [18] Yapicioglu A, Dincer I. A review on clean ammonia as a potential fuel for power generators. *Renew Sustain Energy Rev* 2019;103:96–108.
- [19] Pham Q, Park S, Agarwal AK, Park S. Review of dual-fuel combustion in the compression-ignition engine: Spray, combustion, and emission. *Energy* 2022;123778.
- [20] Reiter AJ, Kong S-C. Demonstration of compression-ignition engine combustion using ammonia in reducing greenhouse gas emissions. *Energy Fuels* 2008;22(5):2963–71.
- [21] Reiter AJ, Kong S-C. Combustion and emissions characteristics of compression-ignition engine using dual ammonia–diesel fuel. *Fuel* 2011;90(1):87–97.
- [22] Nadimi E, Przybyla G, Lewandowski M, Adamczyk W. Effects of ammonia on combustion, emissions, and performance of the ammonia/diesel dual-fuel compression ignition engine. *J Energy Inst* 2022.
- [23] Dimitriou P, Javaid R. A review of ammonia as a compression ignition engine fuel. *Int J Hydrogen Energy* 2020;45(11):7098–118.
- [24] Yousefi A, Guo H, Dev S, Liko B, Lafrance S. Effects of ammonia energy fraction and diesel injection timing on combustion and emissions of an ammonia/diesel dual-fuel engine. *Fuel* 2022;314:122723.
- [25] Yousefi A, Guo H, Dev S, Lafrance S, Liko B. A study on split diesel injection on thermal efficiency and emissions of an ammonia/diesel dual-fuel engine. *Fuel* 2022;316:123412.
- [26] Kuta K, Nadimi E, Przybyla G, Żmudka Z, Adamczyk W. Ammonia CI engine aftertreatment systems design and flow simulation. *Combust Engines* 2022;61.
- [27] Proniewicz M, Petela K, Szlęk A, Przybyla G, Nadimi E, Ziolkowski L, et al. Energy and exergy assessments of a diesel-, biodiesel-, and ammonia-fueled compression ignition engine. *Int J Energy Res* 2023;2023.
- [28] Richards K, Senecal P, Pomraning E. *Converge 3.0*. Madison, WI, USA: Convergent Science; 2023.
- [29] Richards K, Senecal P, Pomraning E. *Converge Manual 3.0*. Madison, WI, USA: Convergent Science; 2022.
- [30] Liu X, Wang H, Yao M. Investigation of the chemical kinetics process of diesel combustion in a compression ignition engine using the large eddy simulation approach. *Fuel* 2020;270:117544.
- [31] Beale JC, Reitz RD. Modeling spray atomization with the Kelvin-Helmholtz/Rayleigh-taylor hybrid model. *Atom Sprays* 1999;9(6).
- [32] Lewandowski MT, Netzer C, Emberson DR, Lovás T. Numerical investigation of optimal flow conditions in an optically accessed compression ignition engine. *Transp Eng* 2020;2:100036.
- [33] Schmidt DP, Rutland C. A new droplet collision algorithm. *J Comput Phys* 2000;164(1):62–80.
- [34] Faeth G. Current status of droplet and liquid combustion. In: *Energy and combustion science*. Elsevier; 1979, p. 149–82.
- [35] Gonzalez D MA, Lian ZW, Reitz RD. Modeling diesel engine spray vaporization and combustion. *SAE Trans* 1992;1064–76.
- [36] Lewandowski MT, Pasternak M, Haugsvar M, Lovás T. Simulations of ammonia spray evaporation, cooling, mixture formation and combustion in a direct injection compression ignition engine. *Int J Hydrogen Energy* 2023.
- [37] Brakora JL. A comprehensive combustion model for biodiesel-fueled engine simulations. [Ph. D. thesis], 2012.
- [38] Brakora JL, Ra Y, Reitz RD, McFarlane J, Daw CS. Development and validation of a reduced reaction mechanism for biodiesel-fueled engine simulations. *SAE Int J Fuels Lubr* 2009;1(1):675–702.
- [39] Stagni A, Cavallotti C, Arunthanayothin S, Song Y, Herbinet O, Battin-Leclerc F, et al. An experimental, theoretical and kinetic-modeling study of the gas-phase oxidation of ammonia. *Reaction Chem Eng* 2020;5(4):696–711.
- [40] Zhou X, Li T, Wang N, Wang X, Chen R, Li S. Pilot diesel-ignited ammonia dual fuel low-speed marine engines: A comparative analysis of ammonia premixed and high-pressure spray combustion modes with CFD simulation. *Renew Sustain Energy Rev* 2023;173:113108.
- [41] Angellilli L, Pérez FEH, Im HG, Ciottoli PP, Valorani M. Evaporation and clustering of ammonia droplets in a hot environment. *Phys Rev Fluids* 2022;7(11):114301.
- [42] Zhang Y, Xu L, Zhu Y, Xu S, Bai X-S. Numerical study on liquid ammonia direct injection spray characteristics under engine-relevant conditions. *Appl Energy* 2023;334:120680.
- [43] Tay KL, Yang W, Chou SK, Zhou D, Li J, Yu W, et al. Effects of injection timing and pilot fuel on the combustion of a kerosene–diesel/ammonia dual fuel engine: A numerical study. *Energy Procedia* 2017;105:4621–6.
- [44] Tay KL, Yang W, Li J, Zhou D, Yu W, Zhao F, et al. Numerical investigation on the combustion and emissions of a kerosene–diesel fueled compression ignition engine assisted by ammonia fumigation. *Appl Energy* 2017;204:1476–88.
- [45] Li T, Zhou X, Wang N, Wang X, Chen R, Li S, et al. A comparison between low-and high-pressure injection dual-fuel modes of diesel–pilot-ignition ammonia combustion engines. *J Energy Inst* 2022;102:362–73.
- [46] Niki Y, Yoo D-H, Hirata K, Sekiguchi H. Effects of ammonia gas mixed into intake air on combustion and emissions characteristics in diesel engine. In: *Internal combustion engine division fall technical conference*, Vol. 50503. American Society of Mechanical Engineers; 2016, V001T03A004.
- [47] Mathieu O, Petersen EL. Experimental and modeling study on the high-temperature oxidation of ammonia and related NO_x chemistry. *Combust flame* 2015;162(3):554–70.
- [48] Kobayashi H, Hayakawa A, Somarathne KKA, Okafor EC. Science and technology of ammonia combustion. *Proc Combust Inst* 2019;37(1):109–33.
- [49] Zhang Z, Long W, Dong P, Tian H, Tian J, Li B, et al. Performance characteristics of a two-stroke low speed engine applying ammonia/diesel dual direct injection strategy. *Fuel* 2023;332:126086.
- [50] Agarwal AK, Srivastava DK, Dhar A, Murya RK, Shukla PC, Singh AP. Effect of fuel injection timing and pressure on combustion, emissions and performance characteristics of a single cylinder diesel engine. *Fuel* 2013;111:374–83.
- [51] Ganapathy T, Gakkhar R, Murugesan K. Influence of injection timing on performance, combustion and emission characteristics of Jatropha biodiesel engine. *Appl Energy* 2011;88(12):4376–86.
- [52] Sayin C, Ilhan M, Canakci M, Gumus M. Effect of injection timing on the exhaust emissions of a diesel engine using diesel–methanol blends. *Renew Energy* 2009;34(5):1261–9.

A.4 Paper IV



Contents lists available at ScienceDirect

Journal of the Energy Institute

journal homepage: www.elsevier.com/locate/joei

Effects of biodiesel injector configuration and its injection timing on performance, combustion and emissions characteristics of liquid ammonia dual direct injection engine

Ebrahim Nadimi^{a,*}, Grzegorz Przybyła^a, Terese Løvås^b, Wojciech Adamczyk^a^a Department of Thermal Technology, Faculty of Energy and Environmental Engineering, Silesian University of Technology, Gliwice, Poland^b Department of Energy and Process Engineering, Faculty of Engineering, Norwegian University of Science and Technology, Trondheim, Norway

ARTICLE INFO

Handling Editor: Dr. Paul Williams

Keywords:

Liquid ammonia
Dual direct injection
Injector
Emissions
Internal combustion engine

ABSTRACT

Ammonia is a promising carbon-neutral fuel that can be stored and transported in liquid form, offering a viable alternative to diesel fuel. In addition, it can be used directly in diesel engine in its liquid form in dual fuel mode. Hence, a single-cylinder diesel engine was modified to implement two common rail (CR) injection systems, allowing the direct injection of liquid ammonia with biodiesel. As biodiesel was used for a pilot fuel with lower injected mass, this study aims to investigate the influence of the number of nozzles in the biodiesel injector on the performance, combustion, and emissions characteristics of the liquid ammonia-biodiesel dual direct injection engine. Therefore, the number of holes in the CR injector was closed in various configurations to improve injection parameters. Furthermore, various biodiesel start of injection (SOI) timings were tested, ranging from -24 to -14 CAD, while the SOI of ammonia was kept at -10 CAD with an ammonia mass ratio of 67.2%. The results showed that welding three nozzles from the original six-nozzle injector resulted in a remarkable 29.2% reduction in NH_3 and CO emissions. Furthermore, the highest indicated thermal efficiency of 39.7% was obtained for the injector with 3b nozzles. Additionally, late injection of both fuels led to an increase in particulate matter emissions, from 10.5 to 15.2 mg/m^3 , due to the formation of fuel-rich zones at high temperatures. However, it reduced NO_x and CO emissions by 1.4 and 4.4 g/kWh , respectively, compared to the early SOI of biodiesel. Moreover, the lowest N_2O emission was measured at 115.0 ppm in the earliest SOI of biodiesel at -24 CAD.

1. Introduction

The evolution of internal combustion engine (ICE) technology has been greatly influenced by the effect of greenhouse gas (GHG) emissions on global warming. Concerns about global warming have been raised due to carbon dioxide (CO_2) emissions and the growing demand for fossil fuels [1]. Global CO_2 emission regulations are becoming increasingly stringent in order to meet the goals of the Paris Agreement to reduce CO_2 emissions [2,3]. The decarbonization of ICE must be achieved to prevent GHG emissions and stop climate change. Also, the widespread use of electric vehicles is hindered by limitations such as Lithium ion batteries [4–6]. Therefore, exploring alternative and sustainable carbon-free fuels emerges as a promising way to mitigate CO_2 emissions [7,8]. Ammonia has currently received interest as a potential green fuel mainly due to its carbon-free nature and its combustion only produces water similar to hydrogen [9]. Being liquid in ambient

temperature and relatively low pressure of 8 bar, ammonia can be used as energy storage and easily transported to Europe [10]. The transportation cost of ammonia is lower compared to liquid hydrogen. Thus, direct utilization of liquid ammonia presents an attractive option in terms of cost-effectiveness [11]. While ammonia exhibits various advantages as a green fuel such as easy storage in the liquid phase, high energy density, and existing infrastructure for production and transportation, its use in ICE faces challenges due to its high autoignition temperature and low flame speed [12].

The use of pure ammonia in diesel engines remains a challenge due to the high autoignition temperature of 924 K [13]. However, pure ammonia can be utilized in spark ignition (SI) engines, although it produces a high amount of NO_x emission and unburned ammonia [14–16]. Additionally, the limitation of using pure ammonia is reported by Rousselle et al. [17]. They suggested mixing ammonia with 10% hydrogen for reasonable engine operation. The effective use of ammonia

* Corresponding author.

E-mail address: Enadimi@polsl.pl (E. Nadimi).<https://doi.org/10.1016/j.joei.2024.101605>

Received 1 December 2023; Received in revised form 11 March 2024; Accepted 12 March 2024

Available online 19 March 2024

1743-9671/© 2024 Energy Institute. Published by Elsevier Ltd. All rights reserved.

in SI engines is by adding promoter fuels such as hydrogen [18], methane [19,20], or other fuels [21].

In the case of diesel engine, the main strategy for applying ammonia in the diesel engine which most researchers focus on, is to introduce gaseous ammonia into the intake port and then ignite the premixed ammonia air with pilot diesel in dual-fuel mode. Hence, Nadimi et al. [22] experimentally studied various ammonia diesel ratios from 0 to 84.2% of ammonia. They showed that increasing the ammonia ratio prolonged the ignition delay and shortened the combustion duration, while the indicated thermal efficiency (ITE) increased. Their results revealed that although carbon-based emissions were markedly reduced, the NO_x emission increased from 831 ppm for pure diesel to 2359 ppm in the highest ammonia ratio. They also point out that since ammonia combustion produces N_2O emission which has a 298 greenhouse effect than CO_2 , diesel must be substituted by more than 35.9% of ammonia to benefit from the reduction of CO_2 . This means that when the ammonia ratio is below 35.9%, the ammonia-diesel engine produces more CO_2 equivalent than only diesel engine operation. Similarly, Bjørgen et al. [23] also found that N_2O emission can increase CO_2 equivalent GHG emissions compared to diesel engine. Yousefi et al. [24] achieved a maximum ammonia energy fraction up to 40%. They observed that with the increase in the ammonia energy ratio from 0 to 40%, the ITE was reduced from 38.1 to 27.2%. However, their subsequent work [25] shows that the split injection of diesel fuel improved ITE to 39.7%, which is higher than pure diesel operation. Shin and Park [26] conducted numerical optimization on the combustion strategy of the dual-fuel ammonia engine, achieving an ammonia energy ratio of up to 90%. This resulted in 11% increase in ITE and 80.6% reduction of GHG emissions relative to the pure diesel mode.

Therefore, diesel was employed as a pilot fuel in ammonia diesel dual fuel mode. However, an alternative option is to use biodiesel as a pilot igniter, which can reduce more CO_2 emissions and achieve a net zero CO_2 emission target. Since biodiesel derived from vegetable oil, offers a promising and sustainable alternative to diesel. Its appeal lies in the fact that plants absorb CO_2 during their growth, making biodiesel a viable candidate as a green fuel [27–29]. Hence, Nadimi et al. [30] demonstrated the utilization of ammonia as the main fuel along with biodiesel as a secondary fuel. They found that the engine can run in 3.5% of load with pure biodiesel and then ammonia can be added to obtain higher load and power. Sivasubramanian et al. [31] compared emissions of pure biodiesel with adding 10 and 20% of ammonia in dual fuel engine. Their findings revealed that NO_x and smoke decreased by nearly 3.5% by adding 20% ammonia compared to pure biodiesel; however, CO was reduced by 10.4%. Reiter and Kong et al. [32] noted that the engine could run on 95% ammonia and 5% biodiesel. However, they observed that when the ammonia energy share remained below 60%, NO_x emission was lower than that of pure biodiesel. As a result, biodiesel can be employed as a pilot fuel and also to enhance combustion by providing an additional oxygen source [33].

The process of biodiesel injection and its related parameters significantly influence biodiesel atomization, air/fuel mixing, and consequently its combustion with ammonia. Since biodiesel is employed as pilot fuel with low injected mass, conducting a study on the number of nozzles and their orientation contributes to gaining a deeper insight into the combustion process. In this context, the number of holes in the common rail biodiesel injector is blocked by welding in various configurations to ensure effective injection and combustion of biodiesel with liquid ammonia in the engine. The present study aims to explore the influence of the number of nozzles on the performance, combustion, and emissions characteristics of liquid ammonia biodiesel dual direct injection engine. Additionally, the interactions of ammonia spray with biodiesel spray, along with the cooling effect of ammonia spray, can significantly impact engine performance and emissions. In our previous study, we suggested the optimal injection timing for liquid ammonia, which was found at SOI -10 CAD [34]. Therefore, in this study, we also conducted tests to determine the optimal injection timing for biodiesel

while keeping SOI ammonia at -10 CAD.

2. Experimental setup and CFD simulation

2.1. Engine setup and injection systems

A single-cylinder Lifan engine was used for this work and the specifications of the diesel engine are presented in Table 1. The description of the test rig and equipment are already described in our previous works [22,30,34–36]. In the present work, the engine head was modified to install two common rail injection systems for injecting ammonia and biodiesel into the cylinder. Therefore, the gasoline direct injection (GDI) injector is used for liquid ammonia injection and the CR injector for pilot injection of biodiesel, as can be seen in Fig. 1. The GDI injector is located near the center of the piston bowl at an angle of 15° while the CR injector enters the cylinder at an angle of 33° . The distance between the two injectors in the engine head is 11 mm.

The ammonia fuel system was specifically designed and constructed for high-pressure injection. Therefore, nitrogen gas is used to pressurize the ammonia tank up to 100 bar. The liquid ammonia is then transferred to the GDI injector at a pressure of 100 bar. Two distinct injection systems with their own Electronic Control Unit (ECU) are employed for injection of ammonia and biodiesel. This allows control of the injecting timing parameters such as SOI, main dose, injection pressure, and split injection for both fuels. As biodiesel is used as a pilot fuel along with ammonia, the injected dose of biodiesel is lower compared to using biodiesel alone for the same operating point. Consequently, various configurations of CR injector nozzles are closed by welding using laser welding techniques to achieve longer injection duration. Therefore, Fig. 2 shows the welded nozzles of the CR injector. The original CR injector has six nozzles with a nozzle diameter of $140\ \mu\text{m}$. The biodiesel spray angle with respect to the injector axes (injector drill angle) was measured at 70° . Additionally, the spray plume cone angle for biodiesel was 9° .

The approach used for closing the hole of the injector is in this way that firstly three of them are blocked by welding in two different configurations and spray orientations. Then, 4 and 5 nozzles are welded. Therefore, five different injectors with 6, 3a, 3b, 2, and 1 nozzle are studied, as can be seen in Fig. 3. The blocked and open nozzles in the CR biodiesel injector are shown in this figure along with biodiesel and ammonia sprays. However, the GDI injector nozzles and the locations of both GDI and CR injectors on the engine head are fixed for all five configurations.

2.2. Biodiesel characteristics

Biodiesel, also known as bioester B100, is a type of fatty acid methyl ester (FAME) derived from the transesterification process of plant oils with methanol. In this study, the specific type of FAME which is produced from rapeseed oil, known as rapeseed methyl ester (RME), is used with ammonia in dual fuel combustion [37]. Table 2 presents the main properties of biodiesel. The lower heating value of biodiesel was determined at 37.4 MJ/kg.

Table 1
Specifications of Lifan single cylinder engine.

Parameter	Valves	Units
Bore \times stroke	86 \times 70	mm
Compression ratio	16.45	
Rated power at 3500 rpm	6.4	kW
Connecting rod length	117.5	mm
Exhaust valve opening	50	$^\circ\text{CAD}$ bBDC
Exhaust valve closing	16	$^\circ\text{CAD}$ aTDC
Inlet valve opening	14	$^\circ\text{CAD}$ bTDC
Inlet valve closing	45	$^\circ\text{CAD}$ aBDC

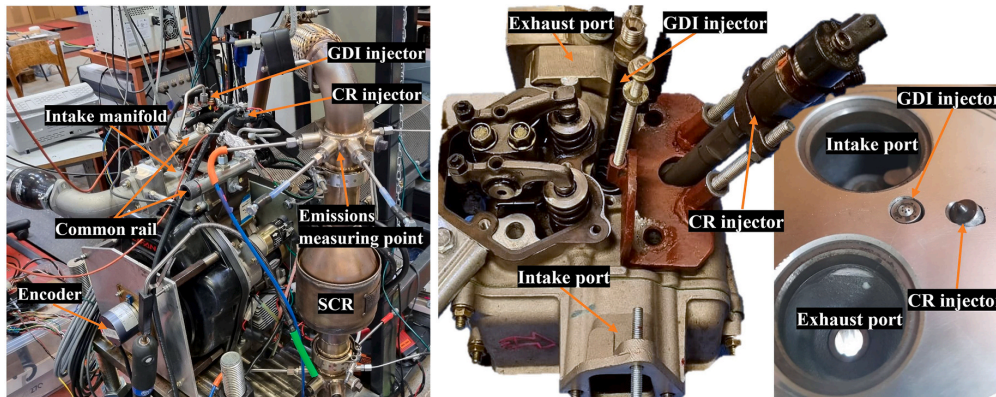


Fig. 1. Photo of the test rig, engine head, and location of GDI and CR injectors on engine head.

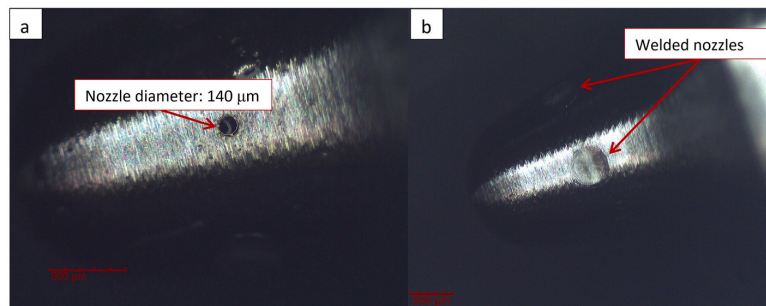


Fig. 2. A microscopic photo of injectors: a) open nozzles and b) welded nozzles using laser technology.

2.3. Operating conditions

In order to investigate the impact of the CR injector on the ammonia biodiesel engine, two specific cases have been designed and are shown in Table 3. This table shows the main parameters of engine operation as well as studied variables for the number of nozzles and SOI of biodiesel. Thus, the first case examines the various CR injector configurations and nozzle numbers while keeping other operating parameters constant. Once the optimal CR injector configuration with its nozzle number was identified, the second case investigates the effects of the SOI of biodiesel for the corresponding injector. Hence, the second case aims to determine the best injection timing of biodiesel in terms of ammonia biodiesel combustion and emissions, particularly unburned ammonia. Furthermore, for all operating points, the engine runs at a speed of 1500 rpm and a partial load with ammonia energy share (AES) of 50%, which corresponds to 67.2% of ammonia and 32.8% biodiesel by mass.

A piezoelectric pressure transducer was used to measure the in-cylinder pressure trace, while a piezoresistive pressure sensor was located in the intake port to measure the absolute pressure. The position of the piston in the TDC was indicated using an optical encoder to measure crank angle displacement with a resolution of 0.35 CAD. The indicated parameters are obtained in 100 consecutive cycles. The entire in-cylinder measurement system has an overall uncertainty of 1% with respect to the measured values. The coefficient of variation (COV) of IMEP was less than 3.4% but it raised to a maximum of 4.5% for SOI biodiesel at -14 CAD.

The LabVIEW software and National Instruments hardware were used to monitor all the measured parameters such as mass flow rates (air, ammonia, and biodiesel), and temperatures (intake, exhaust,

engine head, and both fuels) over 5 min of engine operation. Furthermore, Fourier transform infrared spectroscopy (FTIR) was employed to measure the concentration of each species every 5 s in wet exhaust for 5 min at the corresponding operating point. The precision of FTIR for each component is within 2% of the measured value. Regarding particulate matter (PM) measurements, the SMG200 M instrument can measure particle sizes in the range of 0.04–10 μm , with a maximum PM measurement of up to 250 mg/m^3 .

2.4. CFD simulation

Numerical simulation was performed using a commercial CONVERGE CFD software [38]. As illustrated in Fig. 4, the computational domain consisted of the entire engine geometry, including the intake port, cylinder, piston, both valves, and exhaust port. The mesh was generated during each time step with a maximum cell size of 2.8 mm. Adaptive mesh refinement (AMR) was performed in the cylinder and intake port with a scale of 1 based on cell velocity differences that exceeded 1.0 m/s and temperature differences reaching 2.5 K. Furthermore, several fixed embeddings were used for valves, cylinder, and ammonia and biodiesel sprays during injections with scales of 4, 1, and 4, respectively. Therefore, with a scale of 4, one cell can divide into 64 cells, refining the cell size to 0.175 mm. Fig. 4 presents the total number of cells in each CAD. The number of cells varied depending on the conditions in each CAD due to defined fixed embeddings and AMR. Hence, the minimum cells of 124K were generated near the TDC before injection and then raised to 2.02 million during ammonia-biodiesel sprays and their combustion. Ammonia-biodiesel combustion was modeled using a transient chemical kinetics solver known as SAGE [38].

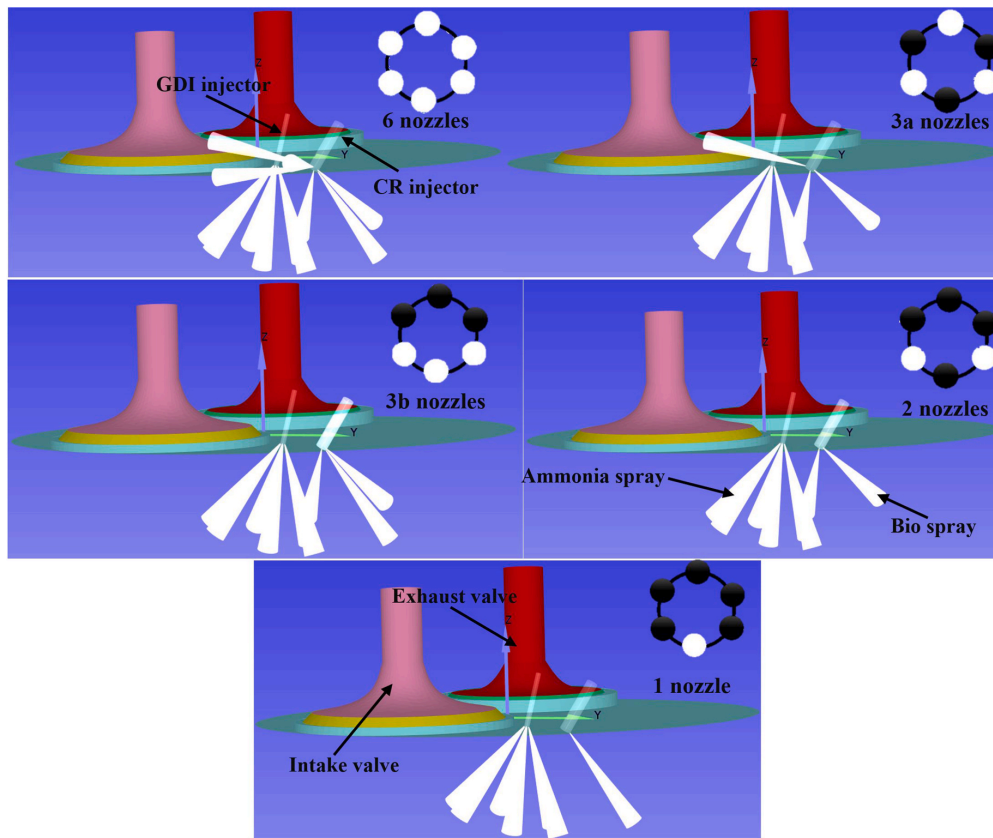


Fig. 3. Various configurations of biodiesel spray and welded nozzles along with GDI injector and ammonia spray on engine head.

Table 2
RME biodiesel physiochemical properties.

Property, unit	Value
RME, % by mass	96.5
Carbon, kg/kg	75.33
Hydrogen, kg/kg	13.97
Oxygen, kg/kg	10.7
Polyene acid methyl ester, %	1
Cetane number	51.0
Density, kg/m ³	860–900
Water content, mg/kg	500
Flash point, °C	101
LHV, MJ/kg	37.4
Stoichiometric AFR	12.96

Brakora et al. [39,40] proposed a reduced reaction mechanism for a biodiesel-fueled engine. This reaction mechanism consists of 69 species and 192 reactions. The reaction mechanism used in this study for ammonia was selected from recent work by Stagni et al. [41], which consists of 31 distinct species with a total of 203 reactions. These two reactions were then merged by the CONVERGE Chemistry Tool. Therefore, the final ammonia-biodiesel reaction mechanism was created with 89 species and 368 reactions.

The Lagrangian particle model was employed for the injection, distribution, and tracking of individual droplets of both liquid ammonia and biodiesel [42]. Droplet breakup was simulated by the Kelvin Helmholtz and Rayleigh Taylor (KH-RT) model [43] with a KH model

Table 3
Engine operation conditions in two cases to study effects of nozzle numbers and SOI of biodiesel.

Parameters	Case 1 (Nozzle number)	Case 2 (SOI biodiesel)	Units
Engine speed	1500	1500	rpm
IMEP	2.65–5.09	4.82–5.09	bar
Ammonia mass ratio	67.2	67.2	%
AES	50	50	%
Ammonia injection pressure	100	100	bar
Biodiesel injection pressure	300	300	bar
SOI liquid NH ₃	–10	–10	°CAD
Injection duration NH ₃	18.5	18.5	°CAD
CR injector nozzles	6, 3a, 3b, 2, 1	3b	°CAD
SOI biodiesel	–16	–24, –22, –20, –18, –16, –14	°CAD
Injection duration of biodiesel	4.5, 8.5, 8.5, 13, 25	8.5	°CAD

breakup time constant of 7.0 and a KH model size constant of 0.6. The drag of the droplet was calculated using the dynamic drop drag model, and droplet collisions were handled with the No Time Counter (NTC) model [44]. The O'Rourke and Frossling models [45] were used for turbulent dispersion and droplet evaporation, respectively. Additional parameters required for ammonia spray simulation can be referenced to study carried out by Lewandowski et al. [46]. Moreover, the

E. Nadimi et al.

Journal of the Energy Institute 114 (2024) 101605

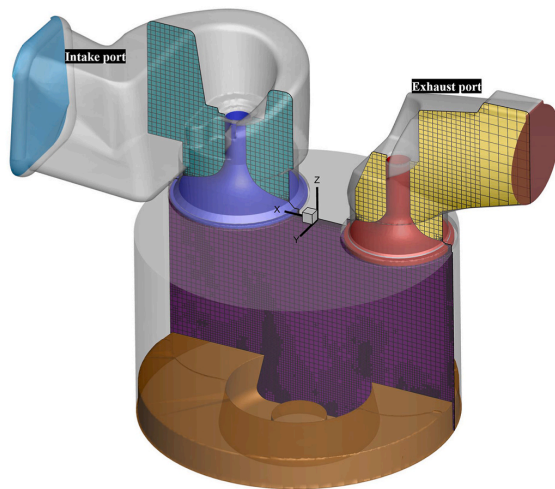
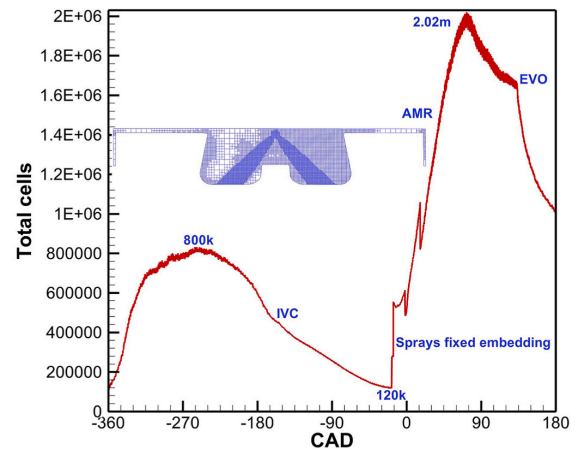


Fig. 4. Full geometry of engine and number of cells at each CAD, including fixed embeddings and adaptive mesh refinements.



Re-Normalization Group (RNG) k-epsilon model was employed to predict turbulent flow characteristics.

2.5. Validation

The predicted CFD pressure and the heat release rate (HRR) are compared with the experimentally measured values in Fig. 5 for the injector with 3b nozzles. It can be seen from Fig. 5 that the simulation results are closely aligned with the experimental data. The peak of in-cylinder pressure was measured at 65 bar, but the CFD model predicted 3.1 bar higher, which has a maximum error of 4.7%. Subsequently, ITE and ISFC are calculated for both the CFD simulations and the experimental data for various SOI of biodiesel, as illustrated in Fig. 9. Furthermore, the comparison of the emissions of CO_2 , H_2O , CO , $NO + NO_2$ (NO_x), and NH_3 for different SOI biodiesel is shown in Fig. 14. The

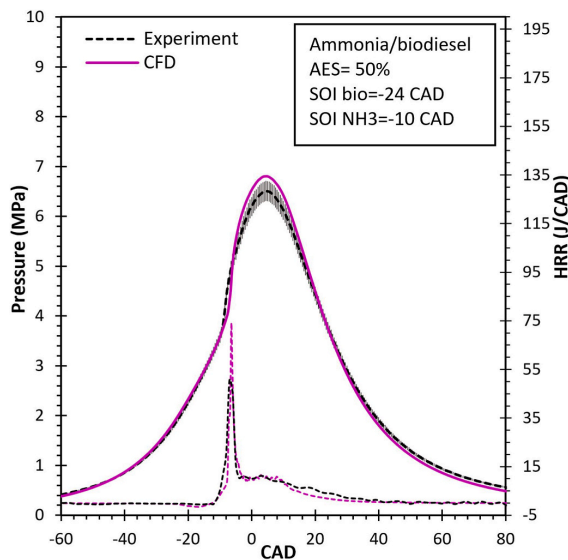


Fig. 5. Validating CFD model by comparing predicted in-cylinder pressure and HRR with experimental data for CR injector with 3b nozzles.

CFD model can capture the overall trends of the emissions and most of them are closely aligned with the experimental values. Nevertheless, some disparities are noticeable at specific operating points. The CFD model utilized a reduced reaction mechanism; therefore, soot formation was not considered in the simulation. Instead, the experimentally measured PM will be discussed in Fig. 13.

3. Results and discussion

3.1. Engine performance

In this section, the effects of the biodiesel injector configuration and its SOI on engine performance are discussed. Fig. 6 displays in-cylinder pressure traces and HRR diagrams for different number of nozzles and various SOI of biodiesel. Unsuccessful combustion and operation were observed for the biodiesel injector with one nozzle. Low ITE and significant amounts of CO and NH_3 emissions were observed for one nozzle injector, as can be seen in Table 4. This can also be noticed from HRR and pressure traces where the peak of pressure reached 48.6 bar at 3.6 CAD, which is only 5 bar higher than the motoring pressure. This is probably due to poor combustion as a result of the longer injection duration. When considering the different configurations of the nozzles, the injector with 3b has the highest pressure peak at 66.4 bar and HRR which indicates effective mixture formation and combustion of biodiesel with liquid ammonia. In contrast, injector 6 and 3a nozzles both have a spray that injects fuel out of the bowl, resulting in air-fuel mixture formation out of the bowl in the squish area and crevice, causing high CO and NH_3 emissions.

Furthermore, the pressure traces for the biodiesel injector with 3b nozzles at different injection timings are illustrated in Fig. 6 as this particular injector has shown better engine performance. Early SOIs result in earlier combustion and a slight increase in cylinder peak pressure, as depicted in Fig. 6. Note that the SOI of ammonia is kept at -10 CAD for all cases.

Fig. 7 depicts the influence of SOI biodiesel on CA10, CA50, ignition delay (ID), and combustion duration (CD). Retarding biodiesel injection leads to a slight increase in both CA10 and CA50 while shortening the ignition delay and combustion duration. Consequently, increasing SOI_{bio} from -24 to -14 CAD increased CA10 and CA50 by 6 and 3.2 CAD, respectively. Simultaneously, it reduced the ignition delay by 4 CAD and shortened the combustion duration by 10.3 CAD. This trend can also be seen in Fig. 8. This figure illustrates the local temperature and flame

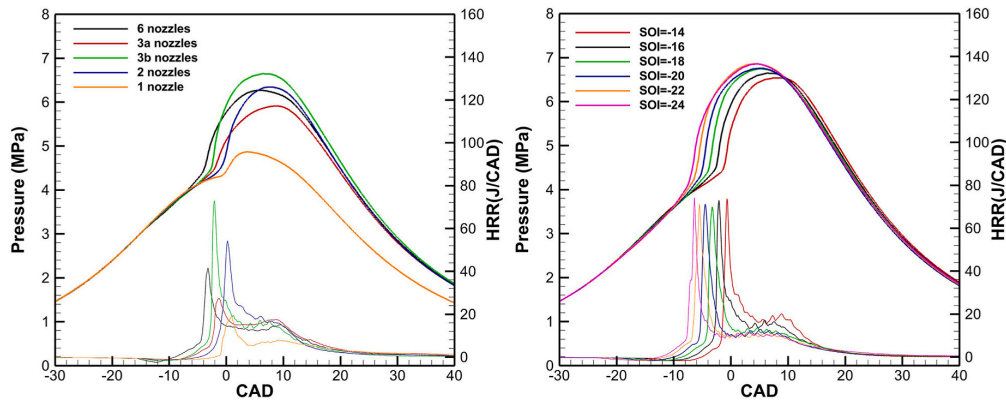


Fig. 6. Effects of nozzle number with injector configuration and various SOI of biodiesel on in-cylinder pressure and HRR when AES is 50%.

Table 4

Engine performance and emission of the ammonia biodiesel engine using a single nozzle CR injector.

Parameters	IMEP	ITE	ISFC	H ₂ O	CO ₂	CO	NO _x	NH ₃
Unit	bar	%	g/kWh	g/kWh	g/kWh	g/kWh	g/kWh	g/kWh
1 nozzle	2.65	20.0	478.9	564.9	580.9	46.5	1.6	329

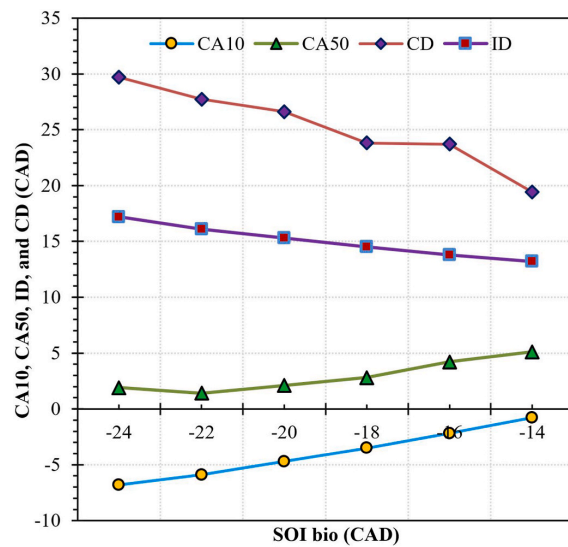


Fig. 7. Effects of SOI of biodiesel on CA10, CA50 and ignition delay (SOI-CA10) combustion duration (CA90-CA10) for injector 3b nozzles at AES = 50%.

propagation for the latest and earliest injection of biodiesel. As ignition is initiated by biodiesel, it provides the energy for ammonia combustion. Therefore, when biodiesel is injected at -24 , ignition starts earlier on the side of three spray zones and then ammonia burns. Conversely, with late biodiesel injection, combustion nearly starts at the TDC under favorable thermodynamic conditions, ultimately reaching the auto-ignition temperature of ammonia. Therefore, the majority of heat is released near the TDC when biodiesel is injected at -14 CAD. Thus, a low cylinder volume and high temperature lead to shorter combustion and ignition delay times in the case of late biodiesel injection [26,47]. Moreover, it can also be noticed from Fig. 8 that the local temperature

distribution demonstrates an opposite relation to the ammonia spray, leading to the accumulation of ammonia in areas with lower temperatures.

The common rail injector configuration and the number of nozzles can have a substantial effect on engine performance, especially in the dual-injection mode of ammonia with biodiesel. These alter injection duration, spray characteristics, droplet evaporation, mixture uniformity, and ultimately influence combustion and engine performance. Fig. 9 illustrates the ITE and ISFC for Case 1, where various nozzle numbers are considered, as well as for Case 2, which shows different biodiesel SOIs. As depicted in Fig. 9, the highest ITE of 38.5% (experimental value 39.7%) was achieved with injector 3b nozzles. This is primarily due to the effective combustion and mixture formation of biodiesel. On the contrary, lower ITEs were observed for the 6 and 3a nozzles, which inject biodiesel out of the piston bowl and into the quench region, resulting in incomplete combustion. Hence, through the blocking of the three nozzles from the original injector, the ISFC was markedly reduced by 5.9%.

Therefore, since the CR injector with 3b nozzles achieved the highest ITE, it was selected to investigate the influence of SOI_{bio} when the AES is 50% and the SOI ammonia is -10 CAD. Therefore, the impact of SOI of biodiesel on ITE and ISFC is depicted in Fig. 9. It is evident that retarding the SOI timing for biodiesel from -24 to -20 CAD initially reduces ITE and then subsequently increases to a peak of 39.7% at SOI of -16 CAD. This is probably due to improved combustion, indicated by lower CO and NH₃ emissions, along with a favorable combustion phasing (CA50). However, further retarding SOI to -14 CAD leads to a decrease in ITE to 38.5% because of late combustion phasing [47]. As a result, when biodiesel and ammonia are injected at -16 and -10 CAD, respectively, at AES of 50%, the equivalent ISFC reaches its lowest point at 241.4 g/kWh, indicating minimal consumption of ammonia-biodiesel fuels.

3.2. Emissions analysis

Since biodiesel serves as a pilot fuel to ignite ammonia in dual fuel mode, its flow rate is relatively lower compared to pure biodiesel combustion. Thus, reducing the number of CR injector nozzles extends the injection duration, promoting the formation of a lean mixture during combustion. Given that combustion of the lean mixture and the low

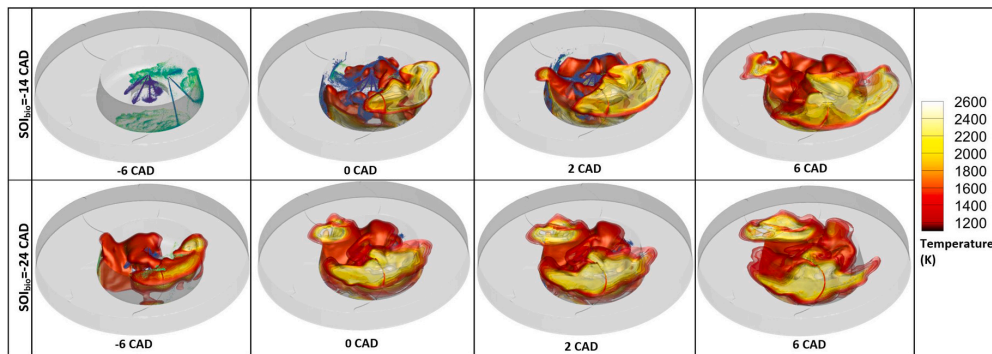


Fig. 8. The comparison of local temperature (iso-surface by contour levels) for earliest and latest injection of biodiesel.

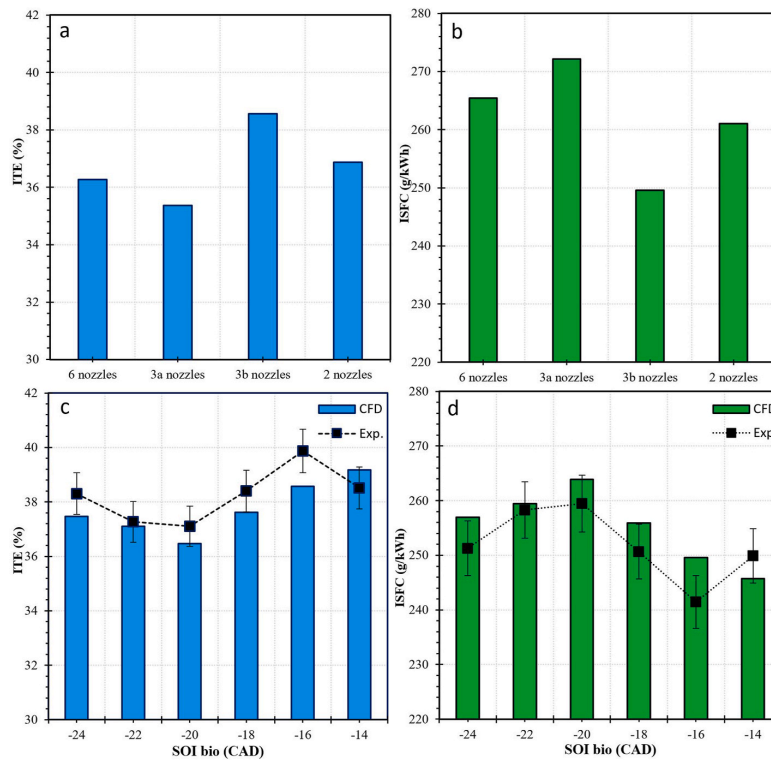


Fig. 9. Effects of CR injector nozzle number and SOI_{bio} on ITE and ISFC of ammonia-biodiesel engine.

equivalence ratio reduce CO emission. Fig. 10 presents the effects of decreasing the number of nozzles on CO , NO_x , and NH_3 emissions when biodiesel is injected at -16 CAD with AES of 50%. CO emission decreased markedly from 26.9 to 8.9 g/kWh by welding three nozzles of the original six nozzles CR injector. This substantial decrease in CO emissions can be further explained in Fig. 11. This figure shows the biodiesel droplet morphology, iso-contour of the mole fraction of CO , and local temperature for the original and 3b injectors. The original injector has three sprays that inject biodiesel out of the piston bowl and into the quench and crevice areas. This worsens the air-fuel mixture and combustion accordingly, resulting in high CO emissions. Furthermore, the CR injector with 3b nozzles demonstrated the lowest NH_3 emission at

11.1 g/kWh, representing a notable reduction of 29.2% in NH_3 emission compared to the original injector with 6 nozzles, which has an ammonia emission of 15.7 g/kWh.

Additionally, Fig. 10c also shows that the decrease in the number of nozzles reduced NO_x emissions. The NO_x emissions decreased significantly from 4.1 g/kWh (305.3 ppm) for the original injector to 2.0 g/kWh (175.0 ppm) for the injector with two nozzles. With increasing number of nozzles, more local stoichiometric mixtures and high local temperature regions are generated (as depicted in Fig. 11), resulting in increased NO_x formation.

Furthermore, Akihama et al. [48] by plotting the equivalence ratio against temperature showed zones leading to NO_x and soot formation.

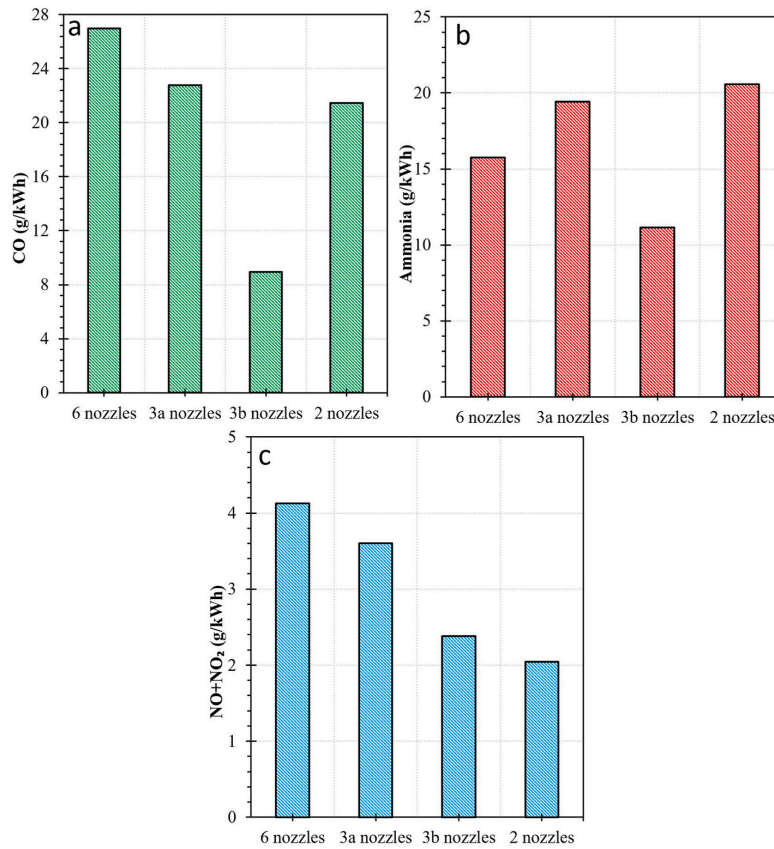
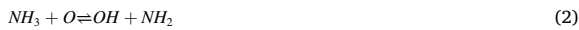


Fig. 10. Effects of different nozzle numbers on specific emissions: a) CO, b) NH₃, and c) NOx.

Therefore, the equivalence ratio and the temperature of each cell are plotted in Fig. 12a for different CADs and compared with the zone of NOx and soot formation. The high temperature and low equivalence ratio are prone to NOx formation, the injection of liquid ammonia from -10 to 8.5 CAD reduces the maximum temperature and also avoids lean conditions in the hot region of the bowl in TDC, which all cause a significant decrease in NOx formation, as can be notice form Fig. 12. The peak of the $\Phi - T$ diagram reaches NOx formation reigns during -4 to 20 CAD. A slight reduction in the maximum local temperature can result in a significant decrease in NOx formation. Hence, the formation of NO reaches its maximum of 370 ppm at 14 CAD and then decreases significantly by reacting with NH₂ due to the presence of NH₃ through the following reactions [49,50]:



These reactions take place when the local temperature is around 1100–1400 K [52,53], reducing the formation of NO. Yousefi et al. [24] also demonstrated that NO level in the cylinder decreased after reaching its peak in the presence of NH₃, while for pure diesel combustion, NO emission did not decrease after reaching the maximum level.

Moreover, Fig. 12a also shows that fuel-rich zones at relatively high

temperatures are prone to soot formation. Replacing biodiesel with ammonia can significantly reduce the formation of PM emission [22]. Additionally, avoiding biodiesel combustion under the mentioned $\Phi - T$ condition, by optimizing the injection timing of biodiesel, can reduce PM formation. Therefore, Fig. 13 depicts PM emission for different SOIs of biodiesel. Retarding biodiesel SOI from -24 CAD to -16 CAD increases PM by 44.8% from 10.5 to 15.2 mg/m³. Late injection of biodiesel causes fuel-rich zones at high temperature, since the main combustion occurs near the TDC. The same trend was observed in similar studies [54,55] that their findings indicated a noticeable increase in PM emissions when SOI was near the TDC. Moreover, this increase in PM may also be due to the wall impingement of the biodiesel spray.

The impacts of biodiesel SOIs on H₂O, CO₂, CO, NOx, and NH₃ emissions are illustrated in Fig. 14 by considering the CR injector with 3b nozzles in AES of 50% and ammonia SOI at -10 CAD. Additionally, Fig. 14 provides a comparison between CFD-predicted emissions and experimental emissions. Shifting SOI of biodiesel from -24 to -14 CAD initially led to a slight increase in H₂O, CO₂, and CO emissions, reaching their peak at -20 CAD and then declining toward -14 CAD. Therefore, the highest CO₂, CO, and NH₃ emissions of 372, 13.8, and 24.1 g/kWh were measured at biodiesel SOI of -20 CAD. This can be attributed to the deterioration in efficiency, as observed in Fig. 9, which resulted in a slight increase in emissions at -20 CAD. Furthermore, the lowest CO emission was recorded at 9.4 when biodiesel was injected late at -14 CAD. Late injection of both fuels was found to reduce NH₃ and CO emissions. Combustion of ammonia aids in CO oxidation [34]. Hence, direct injection of liquid ammonia at -10 CAD enhances swirl and

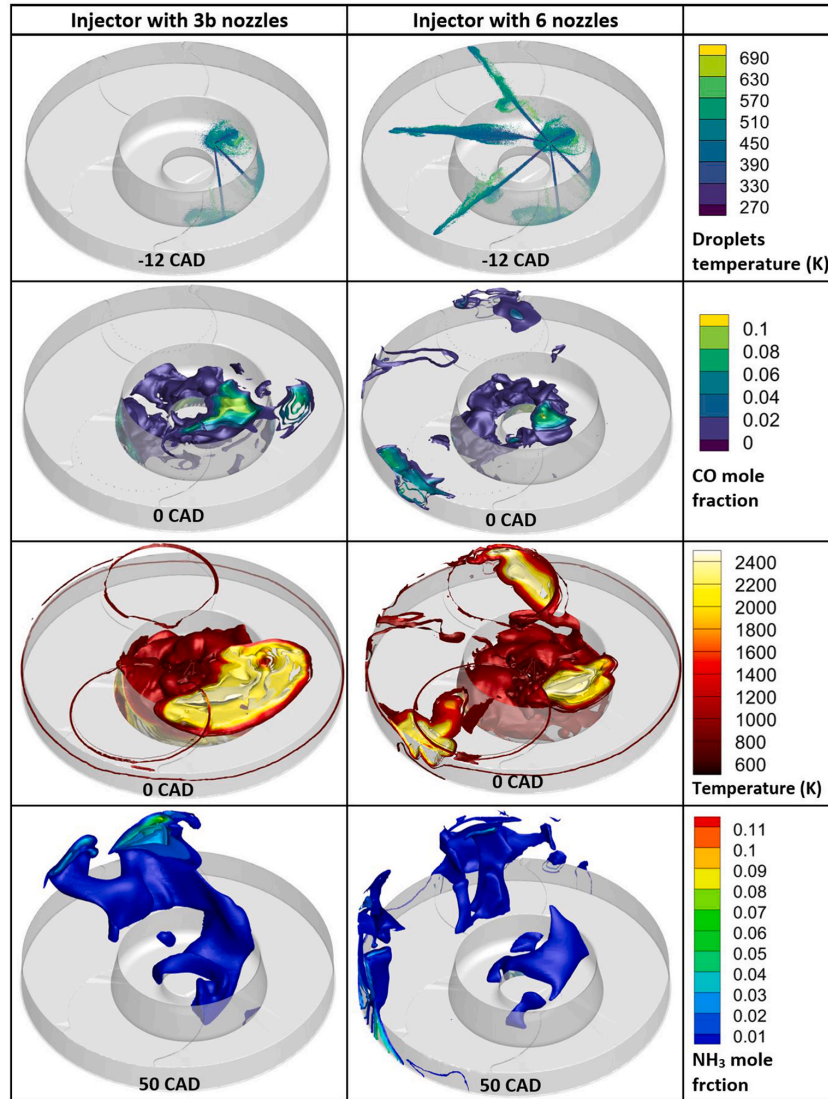


Fig. 11. Biodiesel droplet morphology, iso-contours for CO mole fraction, temperature, and ammonia mole fraction for CR injector with 6 and 3b nozzles when $SOI_{bio} = -16$ CAD.

turbulence, further promoting the formation of the fuel-air mixture within the biodiesel spray. The interaction of the biodiesel mixture with the ammonia spray contributes to cleaner combustion, as also mentioned by Zhang et al. [56].

Furthermore, retarding SOI_{bio} slightly reduced NO_x emissions, decreasing from 3.1 to 1.7 g/kWh for SOI of biodiesel at -14 CAD. This reduction can be primarily attributed to the decrease in peak of combustion temperature resulting from ammonia injection at -10 CAD. It is also associated with the De NO_x process that occurs during the expansion stroke in the ammonia-biodiesel dual combustion operation, as previously discussed in Fig. 12. Besides, when biodiesel is injected at -24 CAD, the main combustion occurs in TDC under high temperature conditions, which promotes the formation of NO_x [57,58].

One of the challenges that appears in ammonia combustion is the formation of N_2O , a compound that significantly contributes to global

warming potentials (GWP). In fact, it has 298 times CO_2 equivalent emissions over a 100-year scale. The N_2O is produced by the following reactions (5) and (6) together with when the temperature is below 1400 K [49,59].



The reaction of NH_3 with the radical OH according to the reaction (1) produces NH_2 . Subsequently, NH_2 reacts with NO and NO_2 and results in the formation of N_2O . This can also be seen in Fig. 12 that NO and NO_2 decreased during combustion in the expansion stroke. Therefore, increasing the combustion temperature with advanced SOI biodiesel can reduce the formation of N_2O . Fig. 15 presents that early injection of biodiesel can reduce N_2O emissions. The lowest level of N_2O emission

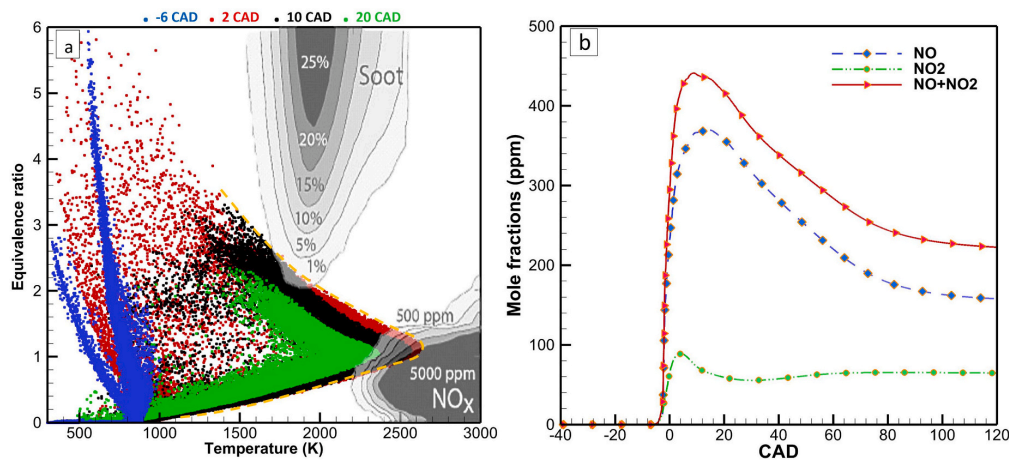


Fig. 12. a) Equivalence ratio and temperature of cells at crank angles of -6 , 2 , 10 , and 20 CAD for the injector with 3b nozzles and $SOI_{bio} = -16$ CAD and their comparison with NO_x and soot formation zones [51]. b) In-cylinder NO , NO_2 and $NO + NO_2$ formation.

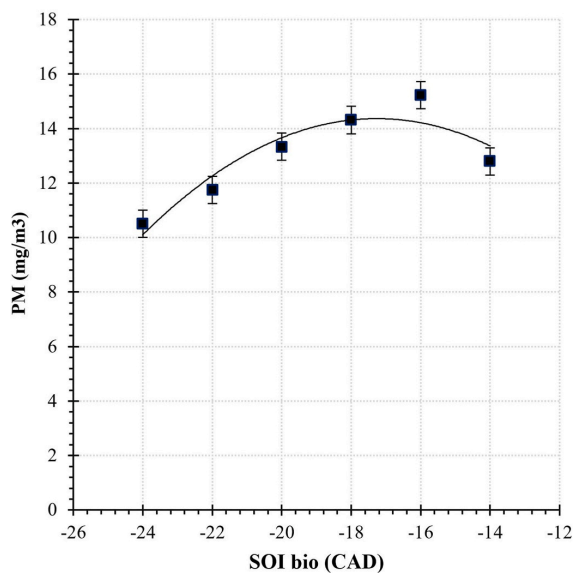


Fig. 13. Experimentally measured particulate matter emission for different biodiesel injection timings.

was measured at 115.0 ppm in SOI of -24 CAD. Subsequently, by retarding of biodiesel injection to -20 CAD, there was a slight increase to 139.6 ppm, which then remained constant for SOI of -14 CAD. Yousefi et al. [24] previously observed a similar trend for SOI of diesel and port injection of gaseous ammonia.

4. Conclusions

In this work, the single-cylinder diesel engine has been modified for direct injection of liquid ammonia with biodiesel. Biodiesel was used as a pilot fuel, which require a lower injected mass. However, the original biodiesel CR injector has six nozzles, leading to a relatively short injection timing. This could result in unstable injections and engine performance with high emissions. To address this, the number of holes in

the biodiesel injector was blocked in various configurations to improve the combustion of biodiesel with liquid ammonia, resulting in enhanced engine performance and reduced emissions. Furthermore, various biodiesel injection timings were tested, ranging from -24 to -14 CAD when AES is 50%. The research findings and conclusions can be summarized as follows.

- The number of biodiesel injector nozzles significantly impacts engine performance. By welding three nozzles from the original six-nozzle CR injector (3b nozzle), the highest pressure peak at 66.4 bar and the highest ITE of 39.7% were achieved, indicating the most effective combustion of liquid ammonia with biodiesel. Moreover, this also showed 5.9% reduction in ISFC compared to the original CR injector.
- Shifting SOI_{bio} from -24 to -14 CAD leads to 6 CAD increase in CA₁₀ and 3.2 CAD increase in CA₅₀. Hence, ignition delay and combustion duration times were reduced by 4 and 10.3 CAD, respectively.
- When ammonia energy share is 50%, blocking three nozzles of the original six-nozzle injector results in a remarkable 29.2% reduction in ammonia emissions compared to the original injector. It also reduces CO emission from 26.9 to 8.9 g/kWh.
- Decreasing CR injector nozzles reduced NO_x emissions from 4.1 g/kWh for the original injector to 2.0 g/kWh for the injector with two nozzles. The high number of nozzles leads to the formation of more local stoichiometric mixtures with high-temperature regions due to the combustion of biodiesel sprays. Additionally, the presence of NH_3 causes the thermal DeNO_x process.
- Retarding SOI_{bio} from -24 CAD to -16 CAD increased PM emissions, from 10.51 to 15.22 mg/m³, due to the formation of fuel-rich zones at high temperatures since the main combustion occurs near the TDC as a result of the late injection of both fuels. Also, the lowest CO was achieved at the latest SOI of biodiesel.
- Retarding SOI_{bio} also leads to a slight reduction in the NO_x emissions, decreasing from 3.1 at -24 CAD to 1.7 g/kWh at -14 CAD. This reduction is due to the injection of liquid ammonia at -10 CAD through cooling effects and the increase in equivalence ratio.
- The lowest N_2O emission of 115.0 ppm was measured at the earliest SOI_{bio} at -24 CAD. It then slightly increased to 139.6 ppm for SOI_{bio} of -20 CAD and then remained constant for late SOIs.

CRediT authorship contribution

Ebrahim Nadimi: Conceptualization, Methodology, Software, Validation, Investigation, Experiment, Data Curation, Visualization,

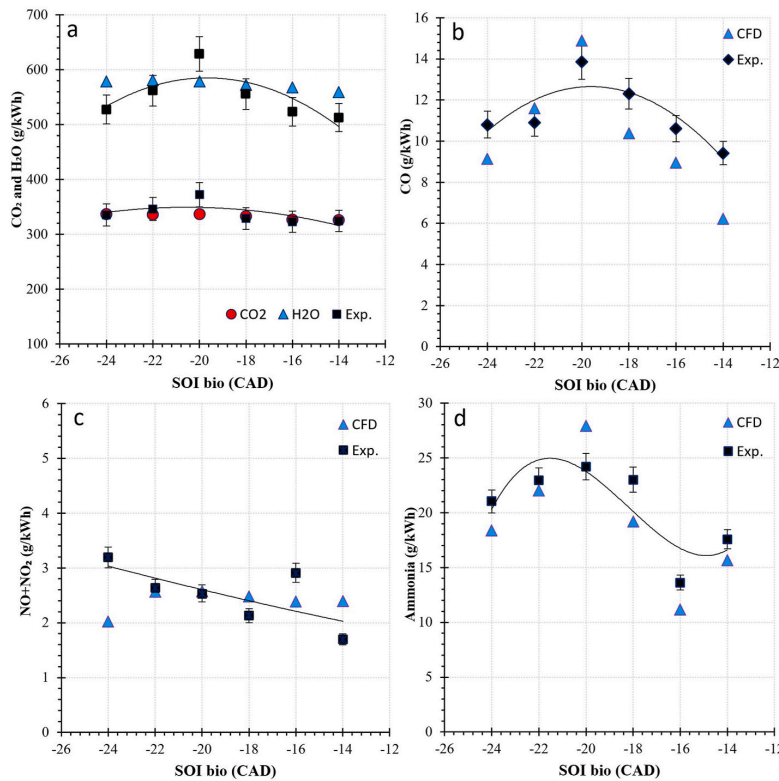


Fig. 14. Impacts of injection timing of biodiesel on experimental and CFD emissions: a) H₂O and CO₂, b) CO, c) NO_x, and d) ammonia emission.

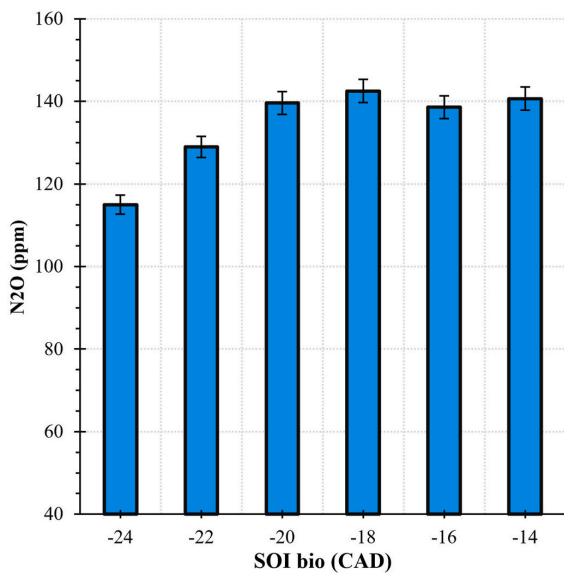


Fig. 15. N₂O emission for different biodiesel SOIs in the ammonia biodiesel engine with AES of 50%.

Original draft, Writing - review & editing. **Grzegorz Przybyła**: Conceptualization, Methodology, Investigation, Experiment, Supervision, Writing - review & editing, Funding acquisition. **Terese Lovås**: Writing - review & editing, Funding acquisition. **Wojciech Adamczyk**: Funding acquisition, Project administration Writing - review & editing.

Declaration of competing interest

The authors declare that they have no known competing financial interests or personal relationships that could have appeared to influence the work reported in this paper.

Acknowledgment

This study was funded by Norway and Poland grants in the ACTIVATE project “<https://ammoniaengine.org>” (Contract NO. NOR/POL-NOR/ACTIVATE/0046/2019-00).

The authors express their gratitude to CONVERGENT Science Inc. For providing the academic license.

References

- [1] R. Rehan, M. Nehdi, Carbon dioxide emissions and climate change: policy implications for the cement industry, *Environ. Sci. Pol.* 8 (2) (2005) 105–114.
- [2] Paris agreement. URL https://treaties.un.org/pages/ViewDetails.aspx?src=TREATY&mtsg_no=XXVII-7-d&chapter=27&clang=en.
- [3] G. Xu, W. Shan, Y. Yu, Y. Shan, X. Wu, Y. Wu, S. Zhang, L. He, S. Shuai, H. Pang, et al., Advances in emission control of diesel vehicles in China, *J. Environ. Sci.* 123 (2023) 15–29.
- [4] W. Zuo, Y. Zhang, E. Jiaqiang, J. Li, Q. Li, G. Zhang, Performance comparison between single s-channel and double s-channel cold plate for thermal management of a prismatic lifepo4 battery, *Renew. Energy* 192 (2022) 46–57.

E. Nadimi et al.

Journal of the Energy Institute 114 (2024) 101605

- [5] F. Li, W. Zuo, K. Zhou, Q. Li, Y. Huang, State of charge estimation of lithium-ion batteries based on pso-tcn-attention neural network, *J. Energy Storage* 84 (2024) 110806.
- [6] F. Li, W. Zuo, K. Zhou, Q. Li, Y. Huang, G. Zhang, State-of-charge estimation of lithium-ion battery based on second order resistor-capacitance circuit-pso-tcn model, *Energy* 289 (2024) 130025.
- [7] W. Zuo, Z. Wang, E. Jiaqiang, Q. Li, Q. Cheng, Y. Wu, K. Zhou, Numerical investigations on the performance of a hydrogen-fueled micro planar combustor with tube outlet for thermophotovoltaic applications, *Energy* 263 (2023) 125957.
- [8] W.S. Chai, Y. Bao, P. Jin, G. Tang, L. Zhou, A review on ammonia, ammonia-hydrogen and ammonia-methane fuels, *Renew. Sustain. Energy Rev.* 147 (2021) 111254.
- [9] C. Mounaïm-Rousselle, P. Bréquigny, A.V. Medina, E. Boulet, D. Emberson, T. Lovås, Ammonia as fuel for transportation to mitigate zero carbon impact, *Engines and Fuels for Future Transport* (2022) 257–279.
- [10] H. Xiao, S. Lai, A. Valera-Medina, J. Li, J. Liu, H. Fu, Study on counterflow premixed flames using high concentration ammonia mixed with methane, *Fuel* 275 (2020) 117902.
- [11] Y. Ishimoto, M. Voldsund, P. Nekså, S. Roussanaly, D. Berstad, S.O. Gardarsdottir, Large-scale production and transport of hydrogen from Norway to Europe and Japan: value chain analysis and comparison of liquid hydrogen and ammonia as energy carriers, *Int. J. Hydrogen Energy* 45 (58) (2020) 32865–32883.
- [12] A.J. Reiter, S.-C. Kong, Combustion and emissions characteristics of compression-ignition engine using dual ammonia-diesel fuel, *Fuel* 90 (1) (2011) 87–97.
- [13] A. Schönborn, Aqueous solution of ammonia as marine fuel, in: *Proceedings of the Institution of Mechanical Engineers, Part M: Journal of Engineering for the Maritime Environment*, vol. 235, 2021, pp. 142–151, 1.
- [14] Z. Liu, L. Zhou, H. Wei, Experimental investigation on the performance of pure ammonia engine based on reactivity controlled turbulent jet ignition, *Fuel* 335 (2023) 127116.
- [15] R. Pelé, P. Brequigny, J. Bellettre, C. Mounaïm-Rousselle, Performances and pollutant emissions of spark ignition engine using direct injection for blends of ethanol/ammonia and pure ammonia, *Int. J. Engine Res.* (2022) 14680874231170661.
- [16] K. Uddeen, Q. Tang, H. Shi, G. Magnotti, J. Turner, A novel multiple spark ignition strategy to achieve pure ammonia combustion in an optical spark-ignition engine, *Fuel* 349 (2023) 128741.
- [17] C. Mounaïm-Rousselle, P. Bréquigny, C. Dumand, S. Houillé, Operating limits for ammonia fuel spark-ignition engine, *Energies* 14 (14) (2021) 4141.
- [18] C. Lhuillier, P. Brequigny, F. Contino, C. Rousselle, Performance and emissions of an ammonia-fueled si engine with hydrogen enrichment, *Tech. rep.*, SAE Technical Paper (2019).
- [19] S. Oh, C. Park, S. Kim, Y. Kim, Y. Choi, C. Kim, Natural gas–ammonia dual-fuel combustion in spark-ignited engine with various air–fuel ratios and split ratios of ammonia under part load condition, *Fuel* 290 (2021) 120095.
- [20] B. Wang, H. Wang, D. Hu, C. Yang, B. Duan, Y. Wang, Study on the performance of premixed natural gas/ammonia engine with diesel ignition, *Energy* 271 (2023) 127056.
- [21] F. Salek, M. Babaie, A. Shakeri, S.V. Hosseini, T. Bodisco, A. Zare, Numerical study of engine performance and emissions for port injection of ammonia into a gasoline/ethanol dual-fuel spark ignition engine, *Appl. Sci.* 11 (4) (2021) 1441.
- [22] E. Nadimi, G. Przybyla, M. Lewandowski, W. Adamczyk, Effects of ammonia on combustion, emissions, and performance of the ammonia/diesel dual-fuel compression ignition engine, *J. Energy Inst.* (2022).
- [23] K.O.P. Bjørgen, D.R. Emberson, T. Lovås, Combustion of liquid ammonia and diesel in a compression ignition engine operated in high-pressure dual fuel mode, *Fuel* 360 (2024) 130269.
- [24] A. Yousefi, H. Guo, S. Dev, B. Liko, S. Lafrance, Effects of ammonia energy fraction and diesel injection timing on combustion and emissions of an ammonia/diesel dual-fuel engine, *Fuel* 314 (2022) 122723.
- [25] A. Yousefi, H. Guo, S. Dev, S. Lafrance, B. Liko, A study on split diesel injection on thermal efficiency and emissions of an ammonia/diesel dual-fuel engine, *Fuel* 316 (2022) 123412.
- [26] J. Shin, S. Park, Numerical analysis for optimizing combustion strategy in an ammonia-diesel dual-fuel engine, *Energy Convers. Manag.* 284 (2023) 116980.
- [27] X. Kan, L. Wei, X. Li, H. Li, D. Zhou, W. Yang, C.-H. Wang, Effects of the three dual-fuel strategies on performance and emissions of a biodiesel engine, *Appl. Energy* 262 (2020) 114542.
- [28] A. Doppalapudi, A. Azad, M. Khan, Advanced strategies to reduce harmful nitrogen-oxide emissions from biodiesel fueled engine, *Renew. Sustain. Energy Rev.* 174 (2023) 113123.
- [29] A. Azad, M. Rasul, M. Khan, S.C. Sharma, M. Mofijur, M. Bhuiya, Prospects, feedstocks and challenges of biodiesel production from beauty leaf oil and castor oil: a nonedible oil sources in Australia, *Renew. Sustain. Energy Rev.* 61 (2016) 302–318.
- [30] E. Nadimi, G. Przybyla, D. Emberson, T. Lovås, L. Ziolkowski, W. Adamczyk, Effects of using ammonia as a primary fuel on engine performance and emissions in an ammonia/biodiesel dual-fuel ci engine, *Int. J. Energy Res.* (2022).
- [31] R. Sivasubramanian, J. Sajin, G. Omanakuttan Pillai, Effect of ammonia to reduce emission from biodiesel fuelled diesel engine, *Int. J. Ambient Energy* (2019) 1–5.
- [32] A.J. Reiter, S.-C. Kong, Demonstration of compression-ignition engine combustion using ammonia in reducing greenhouse gas emissions, *Energy Fuels* 22 (5) (2008) 2963–2971.
- [33] M.-C. Chiong, C.T. Chong, J.-H. Ng, S. Mashruk, W.W.F. Chong, N.A. Samiran, G. R. Mong, A. Valera-Medina, Advancements of combustion technologies in the ammonia-fuelled engines, *Energy Convers. Manag.* 244 (2021) 114460.
- [34] E. Nadimi, G. Przybyla, T. Lovås, G. Peczkis, W. Adamczyk, Experimental and numerical study on direct injection of liquid ammonia and its injection timing in an ammonia-biodiesel dual injection engine, *Energy* 284 (2023) 129301.
- [35] K. Kuta, E. Nadimi, G. Przybyla, Z. Zmudka, W. Adamczyk, Ammonia ci engine aftertreatment systems design and flow simulation, *Combustion Engines* 61 (2022).
- [36] M. Proniewicz, K. Petela, A. Szlęk, G. Przybyla, E. Nadimi, Ł. Ziolkowski, T. Lovås, W. Adamczyk, et al., Energy and exergy assessments of a diesel-, biodiesel-, and ammonia-fueled compression ignition engine, *Int. J. Energy Res.* (2023).
- [37] W. Tutak, A. Jamrozik, K. Grab-Rogaliński, Evaluation of combustion stability and exhaust emissions of a stationary compression ignition engine powered by diesel/n-butanol and rme biodiesel/n-butanol blends, *Energies* 16 (4) (2023) 1717.
- [38] S.P. Richards, K. J. E. Pomraning, *Converge 3.0*, Convergent Science: Madison, WI, USA, 2023.
- [39] J.L. Brakora, A Comprehensive Combustion Model for Biodiesel-Fueled Engine Simulations, Ph. D. thesis, 2012.
- [40] J.L. Brakora, Y. Ra, R.D. Reitz, J. McFarlane, C.S. Daw, Development and validation of a reduced reaction mechanism for biodiesel-fueled engine simulations, *SAE International Journal of Fuels and Lubricants* 1 (1) (2009) 675–702.
- [41] A. Stagni, C. Cavallotti, S. Arunthanayothin, Y. Song, O. Herbinet, F. Battin-Leclerc, T. Faravelli, An experimental, theoretical and kinetic-modeling study of the gas-phase oxidation of ammonia, *React. Chem. Eng.* 5 (4) (2020) 696–711.
- [42] Y. Zhang, L. Xu, Y. Zhu, S. Xu, X.-S. Bai, Numerical study on liquid ammonia direct injection spray characteristics under engine-relevant conditions, *Appl. Energy* 334 (2023) 120680.
- [43] R.D. Reitz, Mechanism of breakup of round liquid jets, *Encyclopedia of fluid mechanics* 10 (1986).
- [44] D.P. Schmidt, C. Rutland, A new droplet collision algorithm, *J. Comput. Phys.* 164 (1) (2000) 62–80.
- [45] G. Faeth, Current status of droplet and liquid combustion, in: *Energy and Combustion Science*, Elsevier, 1979, pp. 149–182.
- [46] M.T. Lewandowski, M. Pasternak, M. Haugsvær, T. Lovås, Simulations of ammonia spray evaporation, cooling, mixture formation and combustion in a direct injection compression ignition engine, *Int. J. Hydrogen Energy* (2023).
- [47] A. Yousefi, H. Guo, M. Birouk, Effect of diesel injection timing on the combustion of natural gas/diesel dual-fuel engine at low-high load and low-high speed conditions, *Fuel* 235 (2019) 838–846.
- [48] K. Akihama, Y. Takatori, K. Inagaki, S. Sasaki, A.M. Dean, Mechanism of the smokeless rich diesel combustion by reducing temperature, *SAE Trans.* (2001) 648–662.
- [49] O. Mathieu, E.L. Petersen, Experimental and modeling study on the high-temperature oxidation of ammonia and related nox chemistry, *Combust. Flame* 162 (3) (2015) 554–570.
- [50] J. Joo, S. Lee, O. Kwon, Effects of ammonia substitution on combustion stability limits and nox emissions of premixed hydrogen–air flames, *Int. J. Hydrogen Energy* 37 (8) (2012) 6933–6941.
- [51] D.E. Nieman, A.B. Dempsey, R.D. Reitz, Heavy-duty rcci operation using natural gas and diesel, *SAE International Journal of Engines* 5 (2) (2012) 270–285.
- [52] R.K. Lyon, The nh3-no-o2 reaction, *Int. J. Chem. Kinet.* 8 (2) (1976) 315–318.
- [53] G.-W. Lee, B.-H. Shon, J.-G. Yoo, J.-H. Jung, K.-J. Oh, The influence of mixing between nh3 and no for a de-nox reaction in the snrc process, *J. Ind. Eng. Chem.* 14 (4) (2008) 457–467.
- [54] P. Tennison, R. Reitz, An experimental investigation of the effects of common-rail injection system parameters on emissions and performance in a high-speed direct-injection diesel engine, *J. Eng. Gas Turbines Power* 123 (1) (2001) 167–174.
- [55] P. Ye, A.L. Boehman, An investigation of the impact of injection strategy and biodiesel on engine nox and particulate matter emissions with a common-rail turbocharged di diesel engine, *Fuel* 97 (2012) 476–488.
- [56] Z. Zhang, W. Long, P. Dong, H. Tian, J. Tian, B. Li, Y. Wang, Performance characteristics of a two-stroke low speed engine applying ammonia/diesel dual direct injection strategy, *Fuel* 332 (2023) 126086.
- [57] H.G. How, H.H. Masjuki, M.A. Kalam, Y.H. Teoh, Influence of injection timing and split injection strategies on performance, emissions, and combustion characteristics of diesel engine fueled with biodiesel blended fuels, *Fuel* 213 (2018) 106–114.
- [58] S. Ghaffarzadeh, A.N. Toosi, V. Hosseini, An experimental study on low temperature combustion in a light duty engine fueled with diesel/cng and biodiesel/cng, *Fuel* 262 (2020) 116495.
- [59] H. Nakamura, S. Hasegawa, T. Tezuka, Kinetic modeling of ammonia/air weak flames in a micro flow reactor with a controlled temperature profile, *Combust. Flame* 185 (2017) 16–27.

